SIMULATOR INDEPENDENT EXACT ADJOINT SENSITIVITY ANALYSIS OF SELF-ADJOINT MICROWAVE STRUCTURES

By

Mohammad Sadegh Dadash, B. Sc. (Eng.)

A Thesis

Submitted to the School of Graduate Studies

in Partial Fulfillment of the Requirements

for the Degree

Master of Applied Science

McMaster University

© Copyright by Mohammad Sadegh Dadash, July 2011

MASTER OF APPLIED SCIENCE (2011) McMASTER UNIVERSITY
(Electrical and Computer Engineering) Hamilton, Ontario

TITLE: **Simulator Independent Exact Adjoint Sensitivity Analysis of Self-adjoint Microwave Structures**

AUTHOR: Mohammad Sadegh Dadash
B. Sc. (Electrical Engineering, Isfahan University of Technology)

SUPERVISOR: Natalia K. Nikolova, Professor,
Department of Electrical and Computer Engineering
Dipl.Eng. (Technical University of Varna)
Ph.D. (University of Electro-Communication)
P.Eng. (Province of Ontario)
Fellow, IEEE

CO-SUPERVISOR: John W. Bandler, Professor Emeritus,
Department of Electrical and Computer Engineering
B.Sc.(Eng), Ph.D., D.Sc.(Eng) (University of London)
D.I.C. (Imperial College)
P.Eng. (Province of Ontario)
C.Eng., FIEE (United Kingdom)
Fellow, IEEE
Fellow, Royal Society of Canada
Fellow, Engineering Institute of Canada
Fellow, Canadian Academy of Engineering

NUMBER OF PAGES: xv, 108

ABSTRACT

This thesis proposes a new analytical self-adjoint sensitivity analysis to calculate the Jacobian of the *S*-parameters for metallic shape parameters. This method is independent of the full-wave numerical analysis and the respective system matrix. The theory works for both volumetric and infinitesimally thin metallic shapes. It exploits the computational efficiency of the self-adjoint sensitivity analysis (SASA) approach where only one EM simulation suffices to obtain both the responses and their gradients in the designable parameter space.

There are three major advantages to this development: (1) the Jacobian computation for metallic structures is completely analytical and there is no approximation involved in the sensitivity analysis of shape parameters; (2) the implementation is straightforward and in the form of a post-processing algorithm operating on the exported field solutions on the surface or around the edge of the metallic structure; and (3) it provides the possibility for exact sensitivity analysis with all electromagnetic high-frequency simulators whose system matrices are not available to export or are not differentiable with respect to shape parameters, e.g., simulators based on the FDTD method and the MoM.

The method was verified in a number of examples using a commercial finite-element solver. The agreement between the results calculated with the proposed method and the reference self-adjoint sensitivity curves provided with the simulator are very promising.

Suggestions for future work are provided.

ACKNOWLEDGEMENTS

It is my pleasure to thank many people who made this thesis possible. First and foremost, I express my profound gratitude to my M.A.Sc. supervisor, Dr. Natalia K. Nikolova, who has supported me throughout my research with her patience and knowledge. Throughout my M.A.Sc program, she provided encouragement, sound advice, good company, and lots of novel ideas. Working with her has been a great privilege for me and her pedagogical personality will be a life-long inspiration for my future endeavors.

I would like to thank my co-supervisor Dr. John W. Bandler for his help and support during my studies. His truly scientist intuition exceptionally inspired my growth as a student. I also like to thank the members of my defense committee, Dr. Mohamed H. Bakr, Dr. John W. Bandler, and Dr. Ali Emadi for their precious time and valuable suggestions for the work done in this thesis.

Furthermore, I am deeply indebted to my colleagues at the Computational Electromagnetics Laboratory at McMaster University for sharing their experience in research as well as participating in stimulating team discussions. I was very lucky to have my wonderful colleagues and friends since they not only gave me

support but also made my long journey much more cheerful. My thanks go to all my friends including Kaveh Moussakhani, Ali Khalatpour, Dr. Reza Khalaj Amineh, Arthur Montazeri, Osman Ahmed, Mohamed Negm, and Yifan Zhang. Their co-operation and encouragement contribute to a pleasant environment of teamwork.

Last but not least, my deep love and appreciation goes to my family in Iran with whom I shared my childhood and whose love and support still sustain me today. To my mother who raised me with her caring and gentle love and my father who showed me the joy of intellectual pursuit.

CONTENTS

ABSTRACT iii

ACKNOWLEDGMENTS v

LIST OF FIGURES x

LIST OF TABLES xiv

LIST OF ACRONYMS xv

CHAPTER 1 INTRODUCTION 1

1.1 Motivation…… 12

1.2 Contribution……. 12

1.3 Outline of Thesis.……. 13

References……. 14

CHAPTER 2 METHODOLOGY OF THE SELF-ADJOINT SENSITIVITY ANALYSIS FOR METALLIC SHAPE PARAMETERS……..... 20

2.1 Introduction……... 20

2.2 Self-adjoint Sensitivity Analysis of Network Parameters ……... 23

2.3 Implementation of the FDFD-SASA Method for Metallic Shape Parameters…….. 26

2.3.1 Metallization……. 28
2.3.2 De-metallization…… 29

References……. 32

CHAPTER 3 SELF-ADJOINT SENSITIVITY ANALYSIS OF VOLUMETRIC METALLIC STRUCTURES…… 35

3.1 Introduction……. 35

3.2 Modal Magnitude Calculation……. 37

3.3 Exact Sensitivity Analysis of Volumetric Metallic Shape Parameters ……... 38

3.3.1 Contribution of the Tangential **E**-field Components……..…… 45

3.3.2 Contribution of the Normal **E**-field Component……..…….. 46

3.4 Implementation Example for Finite Conductivity Metallic Structures……... 55

3.5 Implementation Example for PEC Metallic Structures……..……..……... 59

3.5.1 Six-resonator H-plane Waveguide Filter…….…. 59

3.5.2 Two-section Impedance Transformer 69

References……. 76

CHAPTER 4 SELF-ADJOINT SENSITIVITY ANALYSIS OF INFINITESIMALLY THIN METALLIC STRUCTURES…… 78

4.1 Introduction……. 78

4.2 Field Singularity at the Edge of Metallic Sheet…….. 79

4.3 Sensitivity Formulation for Infinitesimally

Thin Metallic Structures…… 82

4.4 Implementation Example for Infinitesimally Thin Metallic Structure……. 86

References……. 93

CHAPTER 5 CONCLUSION……. 94

References……..……..... 96

COMPLETE REFERENCE LIST……. 97

LIST OF FIGURES

Figure 2.1 Illustration of the metallization of a metallic post for the shape parameter p_n: (a) locations (the black dots) where the double-curl operator C^2 is affected due to metallization at the white dots; $\bar{\mathbf{E}}_i$ is recorded at the white dots; (b) locations where $\bar{\mathbf{E}}_k$ is recorded and mapped to $\left(\bar{\mathbf{E}}_k\right)_n$ at the black dots of Figure 2.1 (a) 29

Figure 2.2 Illustration of the de-metallization of a metallic post for the shape parameter p_n: (a) locations (the black dots) where $\bar{\mathbf{G}}_j$ is affected due to de-metallization; $\bar{\mathbf{E}}_j$ is recorded at the white dots; (b) locations where $\bar{\mathbf{E}}_k$ is recorded and mapped to $\left(\bar{\mathbf{E}}_k\right)_n$ at the black dots of Figure 2.2 (a) 30

Figure 3.1 A metallic shape with the design parameter p_n. $\hat{\boldsymbol{\tau}}_1$ and $\hat{\boldsymbol{\tau}}_2$ are the tangential unit vectors and $\hat{\boldsymbol{\zeta}}$ is the normal unit vector to the perturbation surface S_Ω of the metallic shape 40

Figure 3.2 Finite difference representation of: (a) $\partial\sigma_g / \partial\zeta$ and (b) $\partial\sigma_g / \partial p_n$ at the interface between metal and air. White and black circles indicate inside and outside of the metal. Dash line indicates position is space where conductivity is evaluated. Δ is the step size in the FD approximation of the derivatives 43

Figure 3.3 The two-section waveguide impedance transformer. The width w_1 and the height h_1 of the first section are the parameters of interest 53

Figure 3.4 Sensitivity curves for the real part of S_{11} with respect to w_1 in the impedance-transformer example 55

Figure 3.5 Sensitivity curves for the imaginary part of S_{11} with respect to w_1 in the impedance-transformer example 55

Figure 3.6 Sensitivity curves for the real part of S_{11} with respect to h_1 in the impedance-transformer example 56

Figure 3.7 Sensitivity curves for the imaginary part of S_{11} with respect to h_1 in the impedance-transformer example 56

Figure 3.8 Sensitivity curves for the real part of S_{21} with respect to w_1 in the impedance-transformer example 57

Figure 3.9 Sensitivity curves for the imaginary part of S_{21} with respect to w_1 in the impedance-transformer example 57

Figure 3.10 Sensitivity curves for the real part of S_{21} with respect to h_1 in the impedance-transformer example 58

Figure 3.11 Sensitivity curves for the imaginary part of S_{21} with respect to h_1 in the impedance-transformer example 58

Figure 3.12 H-plane waveguide filter. The structure is symmetric along the width of the waveguide 60

Figure 3.13 Sensitivity curves for the real part of S_{11} with respect to w_3 in the H-plane filter example, calculated in the Field Calculator of the HFSS 63

Figure 3.14 Sensitivity curves for the imaginary part of S_{11} with respect to w_3 in the H-plane filter example, calculated in the Field Calculator of the HFSS 63

Figure 3.15 Sensitivity curves for the real part of S_{11} with respect to d_3 in the H-plane filter example, calculated in the Field Calculator of the HFSS 64

Figure 3.16 Sensitivity curves for the imaginary part of S_{11} with respect to d_3 in the H-plane filter example, calculated in the Field Calculator of the HFSS 64

Figure 3.17 Sensitivity curves for the real part of S_{11} with respect to w_3 in the H-plane filter example 65

Figure 3.18 Sensitivity curves for the imaginary part of S_{11} with respect to w_3 in the H-plane filter example 65

Figure 3.19 Sensitivity curves for the real part of S_{11} with respect to d_3 in the H-plane filter example 66

Figure 3.20 Sensitivity curves for the imaginary part of S_{11} with respect to d_3 in the H-plane filter example 66

Figure 3.21 Sensitivity curves for the real part of S_{21} with respect

to w_3 in the H-plane filter example 67

Figure 3.22 Sensitivity curves for the imaginary part of S_{21} with respect to w_3 in the H-plane filter example 67

Figure 3.23 Sensitivity curves for the real part of S_{21} with respect to d_3 in the H-plane filter example 68

Figure 3.24 Sensitivity curves for the imaginary part of S_{21} with respect to d_3 in the H-plane filter example 68

Figure 3.25 Sensitivity curves for the real part of S_{11} with respect to w_1 in the impedance-transformer example, calculated in the Field Calculator of the HFSS 70

Figure 3.26 Sensitivity curves for the imaginary part of S_{11} with respect to w_1 in the impedance-transformer example, calculated in the Field Calculator of the HFSS 70

Figure 3.27 Sensitivity curves for the real part of S_{11} with respect to h_1 in the impedance-transformer example, calculated in the Field Calculator of the HFSS 71

Figure 3.28 Sensitivity curves for the imaginary part of S_{11} with respect to h_1 in the impedance-transformer example, calculated in the Field Calculator of the HFSS 71

Figure 3.29 Sensitivity curves for the real part of S_{11} with respect to w_1 in the impedance-transformer example 72

Figure 3.30 Sensitivity curves for the imaginary part of S_{11} with respect to w_1 in the impedance-transformer example 72

Figure 3.31 Sensitivity curves for the real part of S_{11} with respect to h_1 in the impedance-transformer example 73

Figure 3.32 Sensitivity curves for the imaginary part of S_{11} with respect to h_1 in the impedance-transformer example 73

Figure 3.33 Sensitivity curves for the real part of S_{21} with respect to w_1 in the impedance-transformer example 74

Figure 3.34 Sensitivity curves for the imaginary part of S_{21} with respect to w_1 in the impedance-transformer example 74

Figure 3.35 Sensitivity curves for the real part of S_{21} with respect to h_1 in the impedance-transformer example 75

Figure 3.36 Sensitivity curves for the imaginary part of S_{21} with respect to h_1 in the impedance-transformer example 75

Figure 4.1 A two-dimensional wedge which is illuminated by an electric line source. ρ' and φ' determine the source location while ρ and φ show the observation location. *n* determines the wedge angle 80

Figure 4.2 The metallic sheet can be assumed to have a metallic cylinder attached to its end. ρ_n determines the radius of the cylinder 83

Figure 4.3 The field solutions are sampled a distance *d* away from the edge 85

Figure 4.4 The cylindrical waveguide filter. The parameters of interest are X_o, X_{o2}, Z_o, and Z_{o2}. Very fine mesh is created around the edges of the structure 87

Figure 4.5 Sensitivity curves for the real part of S_{11} with respect to X_o in the cylindrical waveguide filter example 89

Figure 4.6 Sensitivity curves for the imaginary part of S_{11} with respect to X_o in the cylindrical waveguide filter example 89

Figure 4.7 Sensitivity curves for the real part of S_{11} with respect to X_{o2} in the cylindrical waveguide filter example 90

Figure 4.8 Sensitivity curves for the imaginary part of S_{11} with respect to X_{o2} in the cylindrical waveguide filter example 90

Figure 4.9 Sensitivity curves for the real part of S_{11} with respect to Z_o in the cylindrical waveguide filter example 91

Figure 4.10 Sensitivity curves for the imaginary part of S_{11} with respect to Z_o in the cylindrical waveguide filter example 91

Figure 4.11 Sensitivity curves for the real part of S_{11} with respect to Z_{o2} in the cylindrical waveguide filter example 92

Figure 4.12 Sensitivity curves for the imaginary part of S_{11} with respect to Z_{o2} in the cylindrical waveguide filter example 92

LIST OF TABLES

TABLE 3.1 Nominal design parameter values of the two-section impedance transformer. (All dimensions are in mm.) 53

TABLE 3.2 Nominal parameter values of the H-plane waveguide filter. (All dimensions are in mm.) 61

TABLE 4.1 Nominal design parameter values of the cylindrical waveguide filter. (All dimensions are in cm.) 88

LIST OF ACRONYMS

CAD	Computer-aided-design
DSA	Design Sensitivity Analysis
RF	Radio Frequency
EM	Electromagnetics
FD	Finite difference
DDM	Direct Differentiation Method
HB	Harmonic Balance
AVM	Adjoint Variable Method
TLM	Transmission-line Method
FDTD	Finite-difference Time-domain
FEM	Finite Element Method
MoM	Method of Moments
SASA	Self-adjoint Sensitivity Analysis
FDFD	Finite-difference Frequency-domain
PEC	Perfect Electric Conductor
3-D	Three-dimensional
2-D	Two-dimensional
PDE	Partial Differential Equation

Chapter 1

INTRODUCTION

It was only after the advent of the first generation of computers in 1950s that computer-aided design (CAD) and analysis became a major branch of research in the area of engineering, microwave and millimetre-wave circuits and antennas. The modeling of radio-frequency (RF) and microwave structures started with the approximate representations of the complex electromagnetic (EM) environment with equivalent-circuit lumped elements and transmission lines. This method provides physical insight and high computational speed. It is still one of the major approaches used by the EM computational community. Thus, the first advances in the automated analysis and design of high-frequency structures were based on equivalent-circuit models.

As the power of the computing resources increased, computational electromagnetics emerged and various numerical methods were introduced for full-wave EM analysis. They calculate the complete field solution in the volume of the structure with superior accuracy compared to the circuit-based

representations as no approximations of the Maxwell equations are used. The main drawback of the full-wave EM analysis methods over the circuit modeling is the need for much greater computational resources, which often makes them prohibitively slow. Therefore, the integration of full-wave EM simulations into optimization precedures, which is usually referred to as simulation-based optimization, remains challenging.

Here, we are focusing on different approaches to design sensitivity analysis (DSA). The purpose of DSA is to calculate the gradients of the system responses in the design-parameter space. This information is widely used in engineering problems such as optimization, modeling, tolerance and yield analysis. For example, the response gradients are of particular importance in gradient-based optimization, which is a powerful optimization methodology featuring fast convergence.

In general, there are two major techniques to evaluate the system response sensitivities: (a) response level approximations using, for example, finite differences (FD) or response surface approximations, and (b) adjoint-based methods. The system response could be the given by the state variables such as voltage or current of a circuit or the field or current-density distribution in a high-frequency structure. These are known as distributed parameters. The responses can also be defined in terms of network parameters, e.g., *S*-parameters.

While the finite-difference method at the response level is easy to implement, it requires at least N+1 full-wave analyses per design iteration, where

N is the number of designable parameters. The simulator is invoked repeatedly for the perturbed values of the designable parameters. This significant computational toll motivates research for smarter DSA approaches. Furthermore, there is no robust way to setting the values of the perturbations of the designable parameters. Thus, FD gradient approximations are very susceptible to the numerical errors in the simulation results since the response function in the EM problem may exhibit highly nonlinear behaviour of the design-parameter space.

On the other hand, the adjoint-based methods are known to be the most efficient methods for sensitivity analysis, especially for problems of high complexity where the number of design parameters is large [1]-[3]. The adjoint-variable method yields the responses and their sensitivities with respect to all designable parameters through two system analyses: that of the original structure or circuit and that of the adjoint (auxiliary) structure or circuit which is built through some straightforward laws. The two system analyses are sufficient regardless of the number of designable parameters.

The first methodologies in the adjoint-based DSA of microwave structures have been formulated by Director and Rohrer [4], [5]. These are referred to as adjoint-network methods, which are based on Tellegen's theory and circuit concepts [6], [7]. An adjoint network is constructed and solved to calculate the adjoint voltages and currents, which then are substituted in the sensitivity expression. Mathematically, it is shown that the original problem can be related to the adjoint problem by transposing its system matrix [8], [9]. Hence, the analysis

of the adjoint problem can be accelerated through some mathematical operations on the original system matrix.

The adjoint network approach can be used for the sensitivity analysis of linear circuits and nonlinear time-domain circuits. However, it is not suitable for the sensitivity analysis of nonlinear circuits operating in the steady-state periodic or almost periodic conditions, since the analysis must be carried out until the transient response vanishes. Bandler *et al.* proposed a method to calculate the exact adjoint sensitivity information of linear and nonlinear circuits in the frequency domain [10]. This method is an extension to the harmonic balance (HB) method which is used to analyse the circuit in the frequency domain and only needs to solve a single adjoint system regardless of the number of parameters.

For certain classes of networks, it is inconvenient or even impossible to work with currents and voltages. For example, in the microwave region, a wave description of the network is preferable. In these cases, the theory of adjoint network analysis could be extended to calculate the sensitivity of network parameters directly in terms of wave variables [11].

The direct differentiation method (DDM) is another method, which can be applied to problems cast in the form of a system of linear or nonlinear equations [3], [12]. In the case of M state variables, this method permits the determination of the sensitivity of all M elements of the state-variable vector with respect to a single design parameter through M back-substitutions of the LU decomposition of

the system matrix. Thus, for N designable parameters, $N \times M$ back-substitutions are needed. Some implementation of this method is given in [36] and [37].

With further matrix manipulations, the DDM leads to an adjoint-based analysis approach, which is known in control theory, as the adjoint-variable method (AVM) [2], [3], or transpose-matrix method [12]. The AVM deals with the sensitivity of the response function as opposed to the DDM which calculates the sensitivity of the state-variable vector. Hence, it needs N back-substitutions of the LU decomposition of the system matrix [13] and it is M times faster than the DDM. Since in optimization problems we are mostly interested in the calculation of the sensitivity of the response function rather than the state variables, the AVM is the more computationally efficient alternative.

Both the DDM and the AVM need the derivatives of the system matrix with respect to the design parameters, which in the case of a non-analytical system matrix are often obtained through FD approximations. The latter need at least N system matrix refills. This overhead requires less time and memory than the N complete simulations required by a response-level FD response-gradient approximation. It is shown that the FD approximation at the level of the system matrix leads to better accuracy of the response derivative estimates than the FDs at the response level [13]. This is due to the fact that the dependence of the elements of the system matrix on the design parameters is closer to being linear than that of the final response function.

The theory of adjoint-sensitivity analysis can be extended to the full-wave EM analysis of high-frequency structures. As it was mentioned, the AVM could be applied to any linear or nonlinear system of equations, thus, it is also applicable to the system of equations arising in full-wave analysis. A variety of feasible AVM approaches to field-based EM analyses have been proposed, both in the time domain (the transmission-line method, TLM [14], and the finite-difference time-domain method, FDTD [15]) and in the frequency domain (the frequency-domain TLM [16], [17], finite-element-method (FEM), and the method of moments, MoM [18]).

The major difficulty here is the availability of the derivative of the system matrix with respect to the design parameters. These derivatives may be available analytically in circuit-based models but for most EM solvers, the analytical derivative of the system matrix with respect to the design parameters does not exist. This is because when the design parameter describes variations in the shape of an object, the system matrix elements depend on the solver's discretization mesh, the expansion and weighting functions, which in turn may be very complicated functions of the shape parameters. So, the finite-difference approximation of the system-matrix derivative is often used in the implementation of the AVM methods. Possible venues for this line of research could be the application of other computationally more efficient gradient approximation techniques to the estimation of the derivatives of the system matrix [19].

Similar to the adjoint network equivalent model, in field-based adjoint methods, a quasi-electromagnetic problem is created which constitutes the adjoint problem. The excitation sources of the adjoint problem are defined based on the differentiation of the volumetric response functions with respect to the field state variables. Excitations through the boundary conditions are also defined via differentiation of the surface response functions with respect to the field variables. The solution of the adjoint problem is referred to as the adjoint electric or magnetic field.

Since the adjoint simulation has response-dependent excitation, all traditional AVM approaches require modifications of the EM simulators to solve the adjoint problem. This is not feasible with most of the commercial CAD packages which prevents versatile applications. In 2000, Akel and Webb, for the first time, pointed out that, in the case of the FEM with tetrahedral edge elements, the sensitivities of the *S*-parameters can be derived directly from the field solutions needed to obtain the full scattering matrix, without the need for any adjoint simulation [20], [21].

FEM-based solvers also offer another advantage over other simulators. The elements of their system matrix are analytical functions of the mesh-node positions and hence have analytical (or exact) derivatives of the system matrix with respect to the shape design parameters [20]-[22]. This in turn leads to an accurate response derivative calculation (often referred to as ‘analytical’ or ‘exact’ sensitivity). Note that such calculation still depends on the local field

solution in the volume of interest and, therefore, its accuracy is determined by the numerical accuracy of the field solution. These two features give FEM solvers great advantage in implementing the adjoint sensitivities. In 2009, the sensitivity analysis of *S*-parameters was implemented for the first time in the FEM-based solvers of Ansoft HFSS [38], [39], and CST STUDIO SUITE [40].

In 2005, Bakr *et al.* proposed a technique for estimating adjoint *S*-parameter sensitivities with the time-domain TLM method. They show for the first time that for a lossless, homogeneous and isotropic structure, the TLM simulations utilized for the *S*-parameter calculations are sufficient to estimate their sensitivities as well [23].

In 2006, Nikolova *et al.* proposed a general approach, named self-adjoint sensitivity analysis (SASA), for the sensitivity analysis of microwave network parameters both in the frequency domain and in the time domain [24], [25]. The field solution in the time domain can be simply transformed into the frequency domain via Fourier transform. Contrary to the traditional AVM approaches, the adjoint simulation has been eliminated, so only one simulation is enough to yield both the responses and their sensitivities. It is shown that the EM field solution of the adjoint problem is related to the field solution in the original problem by a factor called self-adjoint coefficient, which is not dependent on the design parameters.

In order to implement this method as a post-processing toolbox, the EM simulator must have certain features [24]. First, it must be able to export the

system matrix and the field/current vector solution. Second, it must be able to allow some control over the mesh generation so that the mesh topology remains unchanged upon parameter perturbation. There are some difficulties involved with the first feature. Most commercial simulators do not provide access to their system matrix. Besides, even if the system matrix is accessible, it is typically very large, especially for practical high-frequency structures. Therefore, it takes too much time and memory to export the system matrix to the computer disk. As a result, the superior performance of the AVM is largely offset by the long time to write/read the system matrix to/from the disk.

The main drawback of all previous implementations of the adjoint-variable method is that they depend on the simulation tool generating the field solution. The main reason is the need for the derivatives of the system matrix with respect to the designable parameters. The system matrix describing the EM problem arises from the particular mathematical model and the discretization technique adopted by the simulation tool. So, there is a need to develop a more general method which is not dependent on the method of simulation.

Recently, a simulator-independent method has been proposed for the evaluation of the sensitivity analysis of *S*-parameters based on the finite-difference frequency-domain (FDFD) method, named finite-difference frequency-domain self-adjoint sensitivity analysis (FDFD-SASA) [27]-[30]. This new sensitivity solver is independent of the simulator's discretization method, grid and system equations. It relies on its own central-node finite-difference grid and a

sensitivity formula based on the FDFD equation for the electric field. The only requirement of the EM simulator is to perform the original system analysis and to export the field solution in particular locations referred to as the perturbation regions. Therefore, this method can be implemented as a post-processing plug-in with all commercial EM solvers. A note should be made here that the finite-difference grid does not imply the need for any new simulations.

While the proposed method provides an exact formulation for the sensitivity analysis of material parameters, e.g., permittivity, permeability, and conductivity, there is an approximation involved in the sensitivity analysis of the shape parameters [25], [30]. Since the structure is discretized on a finite-difference grid, the adjoint solution becomes parameter-dependent and needs to be calculated for different parameter perturbations. This implies the need to perform as many adjoint system analyses as the number of optimizable parameters which would completely offset the computational advantage of FDFD-SASA.

The need for more simulations is eliminated by using the field mapping technique of Bakr *et al.* [16], in which the required adjoint field solution in the perturbed structure is approximated with the adjoint solution in the original structure. The reason is that for a very small parameter perturbation, the field solution of the perturbed structure is not changing very much around the perturbed object; thus, it can be approximated by simply transferring the field

solution of the original structure in the direction of parameter change by one cell size.

Recently, a new algorithm has been proposed in which the adjoint variable method is applied with conformal boundary modeling exploiting rubber cells [31]. Using the idea of rubber cells introduced by Huilian *et al.* [31], the scattering matrix is expressed as an analytical function of both shape and material parameters which leads to exact sensitivity analysis with respect to all type of design parameters.

1.1 MOTIVATION

Although, there has been good progress in the implementation of the self-adjoint sensitivity analysis of the *S*-parameters of microwave structures, a general simulator-independent exact method for the shape parameters is still not available. The previously proposed FDFD-SASA algorithm [35][26]-[30] can provide the analytical derivatives with respect to material parameters only.

There is another possibility to calculate the exact sensitivity derivatives by the use of the analytic finite-element system matrix derivatives in conjunction with the field solution obtained by any valid electromagnetic analysis [33], [34], e.g., MoM or FDTD, since the field solution is unique for the given boundary conditions and excitation. In practice, however, such a hybrid approach is difficult to implement. First, finite-element meshing and discretization tools must be

available. Second, the excitation schemes differ between the various methods, making it difficult to adjust properly the self-adjoint constants.

The proposed sensitivity analysis method which uses the rubber cells [31] can calculate the exact sensitivity information with respect to shape parameters. However, it is not a simulator independent algorithm and still needs the system matrix information of the TLM method.

In this thesis, we aim at developing a method which is simulator-independent and can provide the exact sensitivities with respect to shape parameters. As a first step, we focus on metallic shape parameters, although the method is extendable to dielectric shape parameters.

1.2 CONTRIBUTIONS

Here, we present a method for self-adjoint sensitivity analysis of the scattering matrix with respect to the shape parameters of metallic components in microwave structures [35]. There is no need to obtain the system matrix or to know the discretization grid of the used simulator. The method is exact. It uses an analytical formulation based on Maxwell's equations alone. The derived self-adjoint sensitivity formula requires only the knowledge of the field (or the surface current density) at the surface of the metallic object of interest which makes it a good candidate to be used in solvers based on the MoM and the FDTD.

The author's contributions can be summarized as follows:

1) The development of an analytical sensitivity computation algorithm for shape parameters of volumetric metallic structures.
2) The development of an analytical sensitivity computation for shape parameters of infinitesimally thin metallic structures.
3) The implementation and validation of the method for volumetric and infinitesimally thin metallic structures with the commercial EM solver Ansoft HFSS® [39] and MATLAB® [41].

1.3 OUTLINE OF THESIS

Chapter 2 begins with the review of the FDFD-SASA formulation based on the **E**-field Helmholtz equation. The implementation of this method for metallic shape parameters is explained briefly.

Chapter 3 describes the methodology of the proposed analytical SASA method for volumetric metallic shape parameters and includes both formulations for finite-conductivity and infinit-conductivity metallic structures. The final formulation is validated by three examples and the results are compared with the reference derivatives provided with the EM solver Ansoft HFSS [39].

Chapter 4 is the extension of the theory for volumetric metallic structures described in chapter 3, to the infinitesimally thin metallic objects. The final formulation is validated by an example and the results are compared with the reference derivatives provided with the EM solver Ansoft HFSS.

The thesis concludes in Chapter 5 with suggestions for further research.

References

[1] D. G. Cacuci, *Sensitivity & Uncertainty Analysis, Volume 1: Theory*. Boca Raton, FL: Chaman & Hall/CRC, 2003.

[2] A. D. Belegundu and T. R. Chandrupatla, *Optimization Concepts and Applications in Engineering*. Upper Saddle River, NJ: Prentice-Hall, 1999.

[3] E. J. Haug, K. K. Choi, and V. Komkov, *Design Sensitivity Analysis of Structural Systems.* Orlando, FL: Academic, 1986.

[4] S. W. Director and R. A. Roher, "The generalized adjoint network and network sensitivities," *IEEE Trans. Circuit Theory*, vol. CT-16, pp. 318-323, Aug. 1969.

[5] S. W. Director and R. A. Rohrer, "Automated network design—The frequency-domain case," *IEEE Trans. Circuit Theory*, vol. CT-16, pp. 330-337, Aug. 1969.

[6] B. D. H. Tellegen, "A general network theorem with applications," *Philips Res. Rep.*, vol. 7, pp. 259-269, 1952.

[7] P. Penfield, Jr., R. Spence, and S. Duinker, "A generalized form of Tellegen's theorem," *IEEE Trans. Circuit Theory*, vol. CT-17, pp. 302-305, Aug. 1970.

[8] F. H. Branin, Jr., "Network sensitivity and noise analysis simplified," *IEEE Trans. Circuit Theory*, vol. CT-20, pp. 285-288, May 1973.

[9] S. W. Director, " *LU* factorization in network sensitivity computations," *IEEE Trans. Circuit Theory*, vol. CT-18, pp. 14-185 Jan. 1971.

[10] J. W. Bandler, Q. J. Zhang, and R. M. Biernacki, "A unified theory for frequency-domain simulation and sensitivity analysis of linear and nonlinear circuits, *IEEE Trans. Microwave Theory Tech*, vol. 36, pp. 1661-1669, Dec. 1988.

[11] J. W. Bandler and R. E. Seviora, "Wave sensitivities of networks, " *IEEE Trans. Microwave Theory Tech*, vol. 20, pp. 138-147, Feb. 1972.

[12] V. A. Monaco and P. Tiberio, "Computer-aided analysis of microwave circuits," *IEEE Trans. Microwave Theory Tech*, vol. 7, MTT-22, pp. 249-263, Mar. 1974.

[13] N. K. Georgieva, S. Glavic, M. H. Bakr, and J. W. Bandler, "Feasible adjoint sensitivity technique for EM design optimization," *IEEE Trans. Microwave Theory Tech*, vol. 50, pp. 2751-2758, Dec. 2002.

[14] M. H. Bakr and N. K. Nikolova, "An adjoint variable method for time domain TLM with wide-band Johns matrix boundaries," *IEEE Trans. Microwave Theory Tech.*, vol. 52, pp. 678-685, Feb. 2004.

[15] N. K. Nikolova, H. W. Tam, and M. H. Bakr, "Sensitivity analysis with the FDTD method on structured grids," *IEEE Trans. Microwave Theory Tech.*, vol. 52, pp. 1207-1216, Apr. 2004.

[16] M. H. Bakr and N. K. Nikolova, "An adjoint variable method for frequency domain TLM problems with conducting boundaries," *IEEE*

Microwave and Wireless Components Letters, vol. 13, pp. 408-410, Sep. 2003.

[17] S. M. Ali, N. K. Nikolova, and M. H. Bakr, "Central adjoint variable method for sensitivity analysis with structured grid electromagnetic solvers," *IEEE Trans. Magnetics,* vol. 40, pp. 1969-1971, Jul. 2004.

[18] N. K. Nikolova, J. Zhu, D. Li, M. Bakr, and J. Bandler, "Sensitivities analysis of network parameters with electromagnetic frequency domain simulators," *IEEE Trans. Microwave Theory Tech*., vol. 54, pp. 670-681, Feb. 2006.

[19] R. Safian, N. K. Nikolova, M. H. Bakr, and J.W. Bandler, "Feasible adjoint sensitivity technique for EM design exploiting Broyden's update," in *IEEE MTT-S Int. Microwave Symp. Dig.*, Philadelphia, PA, Jun. 2003, pp. 299-302.

[20] H. Akel and J. P. Webb, "Design sensitivities for scattering-matrix calculation with tetrahedral edge elements," *IEEE Trans. Magnetics*, vol. 36, pp. 1043-1046, Jul. 2000.

[21] J. P. Webb, "Design sensitivities using high-order tetrahedral vector elements," *IEEE. Trans. Magn*., vol 37, pp. 3600-3603, Sep. 2001.

[22] L. Vardapetyan, J. Manges, and Z. Cendes, "Sensitivity analysis of *S*-parameters including port variations using transfinite element method," *IEEE MTT-S Int. Microwave Symp. Dig.*, pp. 527-530, Jun. 2008.

[23] M. K. Bakr, N. K. Nikolova, and P. A. W. Basl, "Self-adjoint *S*-parameter

sensitivities for lossless homogeneous TLM problems, *Int. J. Numer. Modeling*, vol. 18, no. 6, pp. 441–455, Nov. 2005.

[24] N. K. Nikolova, Ying Li, Yan Li, and M. H. Bakr, "Sensitivity analysis of scattering parameters with electromagnetic time-domain simulators," *IEEE Trans. Microwave Theory Tech.*, vol. 54, pp. 1589-1610, Apr. 2006.

[25] N. K. Nikolova, X. Zhu, Y. Song, A. Hasib, and M. H. Bakr, "*S*-parameter sensitivities for electromagnetic optimization based on volume field solutions," *IEEE Trans. Microwave Theory Tech.*, vol. 57, pp. 1526-1538, Jun. 2009.

[26] X. Zhu, A. Hasib, N.K. Nikolova, and M.H. Bakr, "Efficient electromagnetic optimization using self-adjoint Jacobian computation based on a central-node FDFD method," in *IEEE MTT-S Int. Microw. Symp. Dig.*, Atlanta, GA, Jun. 2008, pp. 979-982.

[27] X. Zhu, A. Hasib, and N. K. Nikolova, "Electromagnetic sensitivity analysis of scattering parameters based on the FDFD method," in *Int. Signals, Syst., Electron. Symp.*, Montreal, QC, Canada, Jul.-Aug. 2007, pp. 165-168.

[28] N. K. Nikolova, A. Hasib, and X. Zhu, "Independent sensitivity solver based on the frequency domain finite difference method," *The 24th Int. Review of Progress in Applied Computational Electromagnetics (ACES 2008)*, pp. 1024-1029, Mar.-Apr. 2008.

[29] A. Hasib, *Sensitivity Analysis for Design Optimization of Metallic Microwave Structures with the Finite-difference Frequency-domain Method,* M.A.Sc., Dept. Elect. Comput. Eng., McMaster Univ, Hamilton, ON, Canada, 2008.

[30] X. Zhu, *Frequency-domain Self-adjoint S-parameter Sensitivity Analysis for Microwave Design*, M.A.Sc thesis, Dept. Elect. Comput. Eng., McMaster Univ., Hamilton, ON, Canada, 2008.

[31] P. A. W. Basl, M. H. Bakr, N. K. Nikolova, "Efficient TLM sensitivity analysis exploiting rubber cells, in *IEEE MTT-S Int. Microwave Symp. Dig.*, Jun. 2008, pp. 53-56.

[32] D. Huilian, S. Poman, and W. 1. R. Hoefer, "Cells with tensor properties for conformal TLM boundary modeling, *2006 IEEE MTT-S International Microwave Symposium,* San Francisco, CA, USA, 2006, vol. 11, pp. 157-160.

[33] Y. S. Chung, C. Cheon, I. H. Park, and S. Y. Hahn, "Optimal design method for microwave device using time domain method and design sensitivity analysis—Part I: FETD case," *IEEE Trans. Magn.*, vol. 37, pp. 3289-3293, Sep. 2001.

[34] , "Optimal design method for microwave device using time domain method and design sensitivity analysis—Part II: FDTD case," *IEEE Trans. Magn.*, vol. 37, pp. 3255-3259, Sep. 2001.

[35] M. S. Dadash, K. Moussakhani, N. K. Nikolova, and L. Liu, " New

method for exact self-adjoint sensitivity analysis of metallic shapes, presented at the *IEEE MTT-S Int. Microwave Symp.*, Jun. 2011.

[36] S. Amari, "Sensitivity analysis of coupled resonator filters," *IEEE Trans. Circuits Syst. II*, vol. 47, pp. 1017-1022, Oct. 2000.

[37] P. Harscher, S. Amari, and R. Vahldieck, "A fast finite-element-based field optimizer using analytically alculated gradients," *IEEE Trans. Microwave Theory Tech.*, vol. 50, pp. 433-439, Feb. 2002.

[38] Ansoft HFSS ver. 12.1, Ansoft Corporation, 225 West Station Square Drive, Suite 200, Pittsburgh, PA 15219, USA, 2010, www.ansoft.com.

[39] Ansoft HFSS ver. 13, Ansoft Corporation, 225 West Station Square Drive, Suite 200, Pittsburgh, PA 15219, USA, 2011, www.ansoft.com.

[40] CST Studio Suite ver. 2010.06, Computer Simulation Technology, Bad Nauheimer Str. 19, 64289 Darmstadt, Germany, www.cst.com.

[41] Matlab, ver. 7.1, The MathWorks Inc., USA, 2010, www.mathworks.com.

Chapter 2

METHODOLOGY OF THE SELF-ADJOINT SENSITIVITY ANALYSIS FOR METALLIC SHAPE PARAMETERS

2.1 Introduction

Design sensitivity analysis (DSA) aims at finding the derivatives of the system responses in the design-parameter space. This information is widely used in engineering problems such as optimization, modeling, tolerance and yield analyses. If sensitivities are required, a simple but inefficient finite-difference (FD) approximation at the response level is usually carried out, which requires at least one additional system analysis for each designable parameter. Furthermore, FD gradient approximations are very susceptible to the numerical errors in the simulation results since the response function in the EM problem is only accurate

to a level determined by the mesh convergences error. In addition, the EM responses may exhibit highly nonlinear behaviour in the design-parameter space.

On the other hand, the adjoint-based methods are known to be the most efficient methods for sensitivity analysis, especially for problems of high complexity where the number of design variables is large [1]-[3]. The adjoint-variable method yields the responses and their sensitivities with respect to all designable parameters through two system analyses, namely the original structure and the adjoint (auxiliary) structure, where the latter is built through some straightforward rules.

A variety of feasible AVM approaches for field-based EM analyses have been proposed, both in the time domain (the transmission-line method, TLM [4], and the finite-difference time-domain method, FDTD [5]) and in the frequency domain (the frequency-domain TLM [6], [7], finite-element-method (FEM), and the method of moments, MoM [8]). Since the adjoint simulation has response-dependent excitation, all traditional AVM approaches require modifications of the EM simulators to solve the adjoint problem. This makes them difficult to implement.

In 2005, Bakr *et al.* proposed a technique for estimating adjoint *S*-parameter sensitivities with the time-domain TLM method. They show for the first time that for a lossless, homogeneous and isotropic structure, the TLM simulations utilized for *S*-parameter calculations are sufficient to estimate their sensitivities as well [9].

Nikolova *et al.* proposed a general approach, named self-adjoint sensitivity analysis (SASA), for the sensitivity analysis of microwave network parameters both in the frequency domain and in the time domain [10], [11]. Contrary to the traditional AVM approaches, the self-adjoint sensitivity analysis exploits the nature of the linear problem and eliminates the adjoint system analysis for certain objective functions, i.e., network parameters [8], [10]. While there is no need for the adjoint simulation, this method still employs approximations in the case of shape parameters and it depends on the method of simulation.

Recently, a simulator-independent method has been proposed for the evaluation of the sensitivity analysis of *S*-parameters based on the finite-difference frequency-domain (FDFD) method, named finite-difference frequency-domain self-adjoint sensitivity analysis (FDFD-SASA) [13]-[15]. This new sensitivity solver is independent of the simulator's discretization method, grid and system equations. The only requirement of the EM simulator is to perform the original system analysis and to export the field solution in particular locations referred to as the perturbation regions. The proposed method can provide exact sensitivity derivatives with respect to material parameters. However, there is still an approximation involved in the sensitivity analysis with respect to shape parameters.

In this chapter, the methodology of FDFD-SASA method is briefly reviewed. Since metallic shape parameters are the focus of this thesis, the

implementation of the FDFD-SASA method for metallic shape parameters is reviewed in detail.

2.2 Self-adjoint Sensitivity Analysis of Network Parameters [11]

In this work, we focus on the *S*-parameter sensitivity analysis based on the volume **E**-field solution in the frequency domain such as that produced by the finite-element method (FEM). To obtain the full scattering matrix of an *N*-port structure, *N* simulations are carried out with one of the ports being excited while the rest of the ports are matched. If the *j*th port is excited, the S_{kj} parameters are defined as [17]

$$S_{kj} = \frac{\iint_{S_k} \left(\bar{\mathbf{E}}_j \times \mathbf{h}_k^{(\nu)} \right) \cdot ds}{\iint_{S_j} \left(\bar{\mathbf{E}}_j^{inc} \times \mathbf{h}_j^{(\nu)} \right) \cdot ds} - \delta_{kj}, \qquad j \text{ and } k = 1, \ldots, N,$$
$$\delta_{kj} = \begin{cases} 1, & k = j \\ 0, & k \neq j \end{cases} \tag{2.1}$$

where ν denotes the desired EM mode, $\mathbf{h}_\xi^{(\nu)}$ (ξ = j, k) is the magnetic modal vector, $\bar{\mathbf{E}}_j$ is the electric field solution in the volume of the structure when port j is excited and all other ports are matched, and $\bar{\mathbf{E}}_j^{inc}$ is the incident-field vector at the *j*th port cross-section. In the definition of (2.1), only the **E**-field components that are tangential to the port surfaces contribute to the integral. The distribution of the tangential **E**-field of the mode ν at port ξ is described by the electric modal

vector $\mathbf{e}_{\xi}^{(\nu)}$, which relates to $\mathbf{h}_{\xi}^{(\nu)}$ through Maxwell equations. In the case of isotropic loss-free ports, the modal vectors are real valued [17].

The general self-adjoint sensitivity formulation for the scattering parameters of a multi-port electromagnetic structure is derived in [11]. This formulation is based on the **E**-field vector Helmholtz equation and has no dependence on the numerical technique which is used for the analysis of the structure. It only needs the field solution in the volume of the structure and hence can be applied with any EM simulator providing volume field solution.

The sensitivity formula of the scattering parameters with respect to the design parameter p_n, for any desired EM mode, can be written as

$$\frac{\partial S_{kj}}{\partial p_n} = \kappa_{kj} \iiint_{\Omega} \bar{\mathbf{E}}_k \cdot \frac{\partial R\left(\bar{\mathbf{E}}_j\right)}{\partial p_n} d\Omega, \qquad j \text{ and } k = 1, \cdots, N. \tag{2.2}$$

Here, Ω is the computational volume and κ_{kj} is the self-adjoint coefficient, which is independent of the design parameter. It is defined as

$$\kappa_{kj} = \frac{1}{2V_k V_j \left(j\omega\mu_0\right)} \tag{2.3}$$

where V_j and V_k are the modal magnitudes of the incident waves at ports j and k, respectively, ω is the angular frequency, and μ_0 is the permeability of vacuum.

The important term in (2.2) is the residual derivative $\partial R(\overline{\mathbf{E}}_j)/\partial p_n$ which involves the respective derivatives of the coefficients in the **E**-field Helmholtz wave equation:

$$\frac{\partial R\left(\overline{\mathbf{E}}_j\right)}{\partial p_n} = \frac{\partial C^2\left(\overline{\mathbf{E}}_j\right)}{\partial p_n} + \frac{\partial \alpha}{\partial p_n}\overline{\mathbf{E}}_j - \frac{\partial \overline{\mathbf{G}}^i}{\partial p_n}, \tag{2.4}$$

where

$$\begin{aligned} C^2 &= -\nabla \times \mu_r^{-1} \nabla \times \\ \alpha &= k_0^2\left[\varepsilon_r\left(1 - j\tan\delta_d\right) - j\sigma\left(\omega\varepsilon_0\right)^{-1}\right] \\ \overline{\mathbf{G}}^i &= j\omega\mu_0\overline{\mathbf{J}}^i. \end{aligned} \tag{2.5}$$

In (2.5), ε_0, ε_r, $\tan\delta_d$, and σ are the permittivity of vacuum, the relative permittivity, the loss tangent, and the conductivity of the medium, respectively. The vacuum wave number is k_0. $\overline{\mathbf{J}}^i$ represents the imposed current sources in the volume of the structure.

A note should be made here about the parameter p_n. In the derivation of (2.2), it is assumed that the geometry of the port cross-section is not affected by the change in the parameter p_n [8]. Therefore, this theory is valid for problems in which the ports geometry is independent of the design parameter. This is the usual case in practice and this assumption does not limit significantly the applicability of the method.

2.3 Implementation of the FDFD-SASA Method for Metallic Shape Parameters [11], [15]-[16]

The drawback of the FDFD-SASA is that the sensitivity formula is not exact in the case of shape parameters since a finite-difference grid is used. The shape parameters are constrained to values that are integer multiples of the grid step size, i.e., $\Delta p_n = \pm\Delta x$, or $\pm\Delta y$, or $\pm\Delta z$. Thus, the system coefficients are not analytical derivatives with respect to the shape parameters.

When central finite differences are applied to the **E**-field Helmholtz equation, the finite-difference equation

$$C^2\mathbf{E} + \alpha\mathbf{E} = \mathbf{G}^i \tag{2.6}$$

is obtained, where

$$\begin{aligned} &C^2 \approx -\Delta h^2 \nabla \times \mu_r^{-1} \nabla, \\ &\alpha = k_0^2 \left[\varepsilon_r \left(1 - j\tan\delta_d\right) - j\sigma\left(\omega\varepsilon_0\right)^{-1} \right], \\ &\mathbf{G}^i = j\omega\mu_0 \mathbf{J}^i. \end{aligned} \tag{2.7}$$

Here, ε_0, ε_r, $\tan\delta_d$, σ, k_0 and $\mathbf{J}^i$ were defined already at equation (2.5). For the case of metallic structures, $\mathbf{G}^i$ arises from the induced currents at metallic objects. $\Delta h = \min\left(\Delta x, \Delta y, \Delta z\right)$ denotes the smallest discretization step of the finite-difference mesh. C^2 is the central finite-difference approximation of the double curl operator.

Similarly to (2.2), a second-order formula can be developed for the shape sensitivity analysis of *S*-parameters as

$$\frac{\partial S_{kj}}{\partial p_n} \approx \frac{1}{2V_k V_j \left(j\omega\mu_0\right)\Delta h^2} \cdot \iiint_{\Omega} \left(\bar{\mathbf{E}}_k\right)_n \cdot \frac{\Delta_n R(\bar{\mathbf{E}}_j)}{\Delta p_n} d\Omega \quad n = 1, 2, \ldots, N, \qquad (2.8)$$

where Δ_n denotes a change due to the perturbation of p_n and $\left(\bar{\mathbf{E}}_k\right)_n$ refers to the field solution in the nth perturbed state. The difference residual term $\Delta_n R(\mathbf{E}_j) / \Delta p_n$ is defined as

$$\frac{\Delta_n R(\bar{\mathbf{E}}_j)}{\Delta p_n} = \frac{\Delta_n C^2 \bar{\mathbf{E}}_j}{\Delta p_n} + \frac{\Delta_n \alpha}{\Delta p_n} \cdot \bar{\mathbf{E}}_j - \frac{\Delta_n \bar{\mathbf{G}}_j}{\Delta p_n}. \qquad (2.9)$$

The field $\left(\bar{\mathbf{E}}_k\right)_n$, $n = 1, \ldots, N$, in (2.8) is formally dependent on the parameter perturbation Δp_n because for each shape parameter there is a different adjoint field. However, all these field solutions can be derived from the field solution of the nominal (unperturbed) structure $\bar{\mathbf{E}}_k$ by a simple coordinate translation by one discretization step (Δx, Δy, or Δz) in the direction of the assumed perturbation [18]. Thus, only one system analysis is sufficient to obtain all necessary information for the sensitivity analysis.

With (2.8)-(2.9), the FDFD-SASA becomes independent from the simulator's grid, system equations and discretization method. It uses its own FD grid and FDFD system equations. The only requirement of the simulator is to export the field solution at the perturbation grid points and at the corresponding excitation ports (to compute the self-adjoint constant). The perturbation region is the region where the system coefficients change due to the perturbation of the designable parameters.

The implementation of (2.8) for metallization and de-metallization problem is different which is explained in the following two sub-sections.

2.2.1 Metallization

In the case of metallization, the assumed perturbation Δp_n implies a change of grid cell adjacent to the metallic object from dielectric (e.g. air) to metal. As an example, a cross-sectional view of a metallic object is shown in Figure 2.1 on a finite-difference grid whose step size equals Δx. The object in the nominal state is shown in dark gray while in the *n*th perturbed state it is longer and includes the light-gray cells. The light-gray cells are thus "metallized" as a result of the perturbation. In the nominal state, the field components in this cell are not zero, while in the *n*th perturbed state, they must be set to zero. This change affects the C^2 system coefficients at all neighbouring points [marked with black circles in Figure 2.1].

Since in the *n*th perturbed state, the field solution of the white dots is zero, the respective cells don not have contribution to the sensitivity integral. Thus, only the **E**-field solution at the black circles is exported and used in the calculation. In this case, the system residual derivative $\Delta_n R(\bar{\mathbf{E}}_j) / \Delta p_n$ reduces to

$$\frac{\Delta_n R(\bar{\mathbf{E}}_j)}{\Delta p_n} = \frac{\Delta_n C^2 \bar{\mathbf{E}}_j}{\Delta p_n}. \tag{2.10}$$

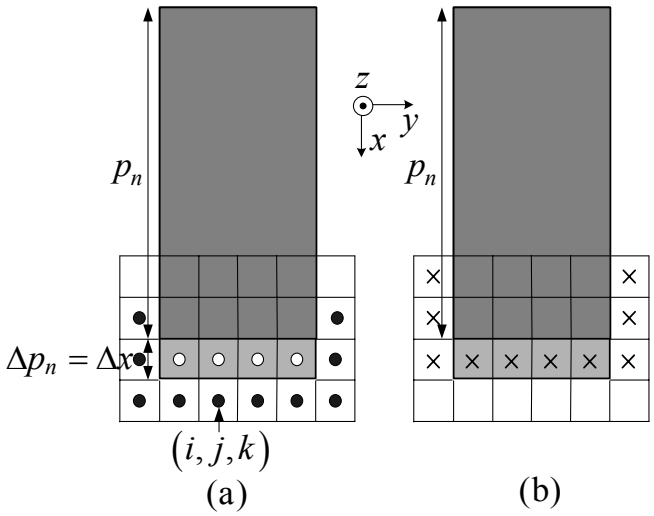

Figure 2.1 Illustration of the metallization of a metallic post for the shape parameter p_n: (a) locations (the black dots) where the double-curl operator C^2 is affected due to metallization at the white dots; $\bar{\mathbf{E}}_j$ is recorded at the white dots; (b) locations where $\bar{\mathbf{E}}_k$ is recorded and mapped to $\left(\bar{\mathbf{E}}_k\right)_n$ at the black dots of Figure 2.1 (a).

The values of $\left(\bar{\mathbf{E}}_k\right)_n$ at the black dots are obtained through the field mapping by exporting the field solution of the nominal structure at the points designated with crosses as shown in Figure 2.1 (b).

2.2.2 De-metallization

In the case of de-metallization, the assumed perturbation Δp_n implies that boundary cells of the metallic object are changing into dielectric (e.g. air). The

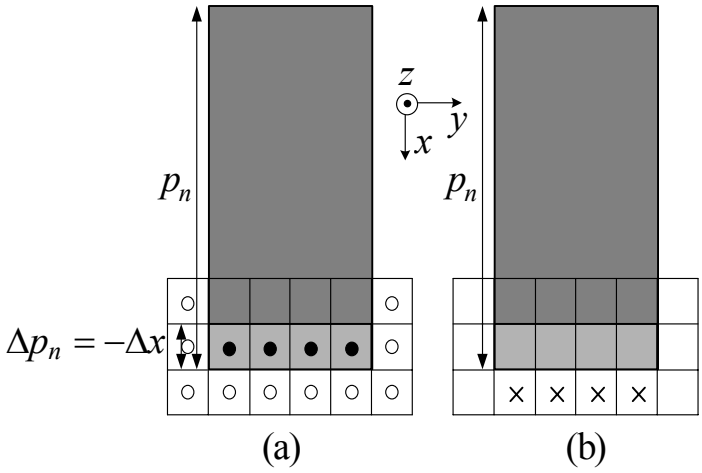

Figure 2.2 Illustration of the de-metallization of a metallic post for the shape parameter p_n: (a) locations (the black dots) where $\bar{\mathbf{G}}_j$ is affected due to de-metallization; $\bar{\mathbf{E}}_j$ is recorded at the white dots; (b) locations where $\bar{\mathbf{E}}_k$ is recorded and mapped to $\left(\bar{\mathbf{E}}_k\right)_n$ at the black dots of Figure 2.2 (a).

analysis of (2.9) shows that the term $\Delta_n C^2 \bar{\mathbf{E}}$ at the "demetallized" cells is always zero due to zero values of $\bar{\mathbf{E}}$ [light-gray cells in Figure 2.2 (a)]. However, due to the changes in the induced current densities at the metallic surfaces, the $\Delta_n \bar{\mathbf{G}}$ terms are non-zero at these points. In this case, the system residual derivative $\Delta_n R(\bar{\mathbf{E}}_j) / \Delta p_n$ reduces to

$$\frac{\Delta_n R(\bar{\mathbf{E}}_j)}{\Delta p_n} = -\frac{\Delta_n \bar{\mathbf{G}}_j}{\Delta p_n}. \tag{2.11}$$

It can be shown that

$$\Delta_n \bar{\mathbf{G}}_j = \Delta_n C^2 \bar{\mathbf{E}}_j. \tag{2.12}$$

The term $\Delta_n C^2 \bar{\bar{\mathbf{E}}}_j$ is non zero at both white and black dots but the original field $\bar{\bar{\mathbf{E}}}_j$ at the black dots is zero. $\left(\bar{\bar{\mathbf{E}}}_k\right)_n$ at the black dots is also needed and it is obtained from $\bar{\bar{\mathbf{E}}}_k$ of the nominal structure through the field mapping where $\bar{\bar{\mathbf{E}}}_k$ at the points denoted with the crosses in Figure 2.2 (b) is made equal to $\left(\bar{\bar{\mathbf{E}}}_k\right)_n$ at the black dots.

References

[1] D. G. Cacuci, *Sensitivity & Uncertainty Analysis, Volume 1: Theory*. Boca Raton, FL: Chaman & Hall/CRC, 2003.

[2] A. D. Belegundu and T. R. Chandrupatla, *Optimization Concepts and Applications in Engineering*. Upper Saddle River, NJ: Prentice-Hall, 1999.

[3] E. J. Haug, K. K. Choi, and V. Komkov, *Design Sensitivity Analysis of Structural Systems.* Orlando, FL: Academic, 1986.

[4] M. H. Bakr and N. K. Nikolova, "An adjoint variable method for time domain TLM with wide-band Johns matrix boundaries," *IEEE Trans. Microwave Theory Tech.,* vol. 52, pp. 678-685, Feb. 2004.

[5] N. K. Nikolova, H. W. Tam, and M. H. Bakr, "Sensitivity analysis with the FDTD method on structured grids," *IEEE Trans. Microwave Theory Tech.,* vol. 52, pp. 1207-1216, Apr. 2004.

[6] M. H. Bakr and N. K. Nikolova, "An adjoint variable method for frequency domain TLM problems with conducting boundaries," *IEEE Microwave and Wireless Components Letters*, vol. 13, pp. 408-410, Sep. 2003.

[7] S. M. Ali, N. K. Nikolova, and M. H. Bakr, "Central adjoint variable method for sensitivity analysis with structured grid electromagnetic solvers," *IEEE Trans. Magnetics,* vol. 40, pp. 1969-1971, Jul. 2004.

[8] N. K. Nikolova, J. Zhu, D. Li, M. Bakr, and J. W. Bandler, "Sensitivities analysis of network parameters with electromagnetic frequency domain simulators," *IEEE Trans. Microwave Theory Tech*., vol. 54, pp. 670-681, Feb. 2006.

[9] M. K. Bakr, N. K. Nikolova, and P. A. W. Basl, "Self-adjoint *S*-parameter sensitivities for lossless homogeneous TLM problems, *Int. J. Numer. Modeling*, vol. 18, no. 6, pp. 441–455, Nov. 2005.

[10] N. K. Nikolova, Ying Li, Yan Li, and M. H. Bakr, "Sensitivity analysis of scattering parameters with electromagnetic time-domain simulators," *IEEE Trans. Microwave Theory Tech.*, vol. 54, pp. 1589-1610, Apr. 2006.

[11] N. K. Nikolova, X. Zhu, Y. Song, A. Hasib, and M. H. Bakr, "*S*-parameter sensitivities for electromagnetic optimization based on volume field solutions," *IEEE Trans. Microwave Theory Tech.*, vol. 57, pp. 1526-1538, Jun. 2009.

[12] X. Zhu, A. Hasib, N.K. Nikolova, and M. H. Bakr, "Efficient electromagnetic optimization using self-adjoint Jacobian computation based on a central-node FDFD method," in *IEEE MTT-S Int. Microw. Symp. Dig*., Atlanta, GA, Jun. 2008, pp. 979-982.

[13] X. Zhu, A. Hasib, and N. K. Nikolova, "Electromagnetic sensitivity analysis of scattering parameters based on the FDFD method," in *Int. Signals, Syst., Electron. Symp*., Montreal, QC, Canada, Jul.-Aug. 2007, pp. 165-168.

[14] N. K. Nikolova, A. Hasib, and X. Zhu, "Independent sensitivity solver based on the frequency domain finite difference method," *The 24th Int. Review of Progress in Applied Computational Electromagnetics (ACES 2008)*, pp. 1024-1029, Mar.-Apr. 2008.

[15] A. Hasib, *Sensitivity Analysis for Design Optimization of Metallic Microwave Structures with the Finite-difference Frequency-domain Method*, M.A.Sc., Dept. Elect. Comput. Eng., McMaster Univ, Hamilton, ON, Canada, 2008.

[16] X. Zhu, *Frequency-domain Self-adjoint S-parameter Sensitivity Analysis for Microwave Design*, M.A.Sc thesis, Dept. Elect. Comput. Eng., McMaster Univ., Hamilton, ON, Canada, 2008.

[17] M. Salazar-Palma, T. K. Sarkar, L.-E. García-Castillo, T. Roy, and A. Djordjevic, *Iterative and Self-Adaptive Finite-Elements in Electro-magnetic Modeling*. Norwood, MA: Artech House, 1998, pp. 462–463, 465–466.

[18] M. H. Bakr and N. K. Nikolova, "An adjoint variable method for time domain TLM with fixed structured grids," *IEEE Trans. Microwave Theory Tech*., vol. 52, pp. 554-559, Feb. 2004.

Chapter 3

SELF-ADJOINT SENSITIVITY ANALYSIS OF VOLUMETRIC METALLIC STRUCTURES

3.1 Introduction

Recently, significant progress has been made toward the development of electromagnetic sensitivity-analysis tools. The traditional response-level gradient approximations for the scattering parameters have been already replaced in some commercial finite-element analysis packages [1][2] by efficient and accurate self-adjoint sensitivity computations. The theoretical basis for the self-adjoint sensitivity analysis of network parameters of high-frequency structures can be found in [3] along with implementations on finite-difference grids.

The advantage of the finite-element based sensitivity analysis over the finite-difference implementations is that the finite-element system matrix is an analytical function of the mesh node positions [4][5] thereby allowing for

analytical (or exact) derivatives of the system matrix with respect to shape parameters. Note that such calculation still depends on the local field solution in the volume of the shapes of interest and, therefore, its accuracy is determined by the numerical accuracy of the field solution.

The system matrices arising in methods employing finite-difference grids are not analytically differentiable with respect to shape parameters and approximations of the derivatives of the system coefficients are needed [3][6]. Similar problem arises in a number of method-of-moment (MoM) discretization techniques. The sensitivity calculation could utilize the analytic finite-element system matrix derivatives in conjunction with the field solution obtained by any valid electromagnetic analysis [7], e.g., MoM or FDTD, since the field solution is unique for the given boundary conditions and excitation. In practice, however, such hybrid approach is difficult to implement. First, finite-element meshing and discretization tools must be available. Second, the excitation schemes differ between the various methods, making it difficult to adjust properly the self-adjoint constants [3].

In this thesis, we present a method for self-adjoint sensitivity analysis of the scattering matrix with respect to the shape parameters of metallic components in microwave structures. This method is exact. It uses an analytical formulation based on Maxwell's equations alone. There is no need for the system matrix or discretization grid information of the field-analysis method. The derived self-

adjoint sensitivity formula requires only the knowledge of the field (or the surface current density) at the surface of the metallic object of interest.

The theoretical outline of the proposed method is explained for volumetric metallic structures in section 3.3. In section 3.4, the implementation of the proposed method for finite-conductivity metallic structures is presented together with a two-section impedance-transformer example [10]. Section 3.5 presents the implementation of this method in two examples: an H-plane waveguide filter [9] and a two-section impedance transformer where the metal is set to PEC [10].

3.2 Modal Magnitude Calculation

The field solution in any electromagnetic problem can be viewed as the superposition of modal vector fields of the particular structure:

$$\begin{aligned} \bar{\mathbf{E}} &= \sum_{\nu} V_{\nu} \mathbf{e}^{(\nu)}, \\ \bar{\mathbf{H}} &= \sum_{\nu} V_{\nu} \mathbf{h}^{(\nu)}. \end{aligned} \tag{3.1}$$

Here, $\mathbf{e}^{(\nu)}$ and $\mathbf{h}^{(\nu)}$ are the electric and magnetic modal vectors of the mode ν and the weighting coefficient V_{ν} is the modal magnitude.

The pairs of modal vectors form a bi-orthogonal set and have to be suitably normalized. The common bi-orthonormal relationship is

$$\iint_{S_j} \mathbf{e}^{(\nu)} \times \mathbf{h}^{(\nu')} \cdot d\boldsymbol{s} = \begin{cases} 1, & \text{if } \nu = \nu' \\ 0, & \text{if } \nu \neq \nu' \end{cases}, \tag{3.2}$$

where S_j is the jth port cross-section.

Using the Poynting theorem together with (3.2) leads to a relation between the excitation power at the *j*th port and the modal magnitudes of the excited field as

$$P_{j\text{-port}} = \iint_{S_j} \left(\frac{1}{2} \bar{\mathbf{E}}^{inc} \times \bar{\mathbf{H}}^{inc} \right) \cdot d\boldsymbol{s} = \frac{1}{2} \sum_{\nu} |V_\nu|^2 . \tag{3.3}$$

We use Ansoft HFSS® [1] for our simulation examples and the excitation is done through wave ports. By default, the excitation power at a wave port is set to 1 W. So, if only one mode, e.g. mode ν, is excited then the modal magnitude of the incident field V_ν can be calculated as

$$P_{j\text{-port}} = \frac{V_\nu^{\,2}}{2} = 1 \quad \Rightarrow \quad V_\nu = \sqrt{2}. \tag{3.4}$$

3.3 Exact Sensitivity Analysis of Volumetric Metallic Shape Parameters [12]

In any electromagnetic problem, the change in the shape parameter can be viewed as a change in the material parameters of the region which is affected by the shape-parameter perturbation. This helps find a way to deal with material parameters instead of shape parameters. The advantage of this approach is that the Helmholtz equation coefficients are analytically differentiable with respect to the material parameters while this is not the case with shape parameters.

The starting point is the sensitivity expression of the scattering parameters explained in chapter 2. This expression is repeated here for the sake of easy referencing:

$$\frac{\partial S_{kj}}{\partial p_n} = \kappa_{kj} \iiint_{\Omega} \bar{\mathbf{E}}_k \cdot \frac{\partial R\left(\bar{\mathbf{E}}_j\right)}{\partial p_n} d\Omega, \qquad j \text{ and } k = 1, \cdots, N, \tag{3.5}$$

where

$$\kappa_{kj} = \frac{1}{2V_k V_j \left(j\omega\mu_0\right)}, \tag{3.6}$$

$$\frac{\partial R\left(\bar{\mathbf{E}}_j\right)}{\partial p_n} = \frac{\partial C^2\left(\bar{\mathbf{E}}_j\right)}{\partial p_n} + \frac{\partial \alpha}{\partial p_n}\bar{\mathbf{E}}_j - \frac{\partial \bar{\mathbf{G}}^i}{\partial p_n}, \tag{3.7}$$

and

$$\begin{aligned} C^2 &= -\nabla \times \mu_r^{-1} \nabla \times \\ \alpha &= k_0^2 \left[\varepsilon_r \left(1 - j\tan\delta_d\right) - j\sigma\left(\omega\varepsilon_0\right)^{-1} \right] \\ \bar{\mathbf{G}}^i &= j\omega\mu_0 \bar{\mathbf{J}}^i. \end{aligned} \tag{3.8}$$

By applying the chain rule, the residual derivative $\partial R(\bar{\mathbf{E}}_j)/\partial p_n$ in (3.7) can be expanded via the constitutive parameters as

$$\frac{\partial R\left(\bar{\mathbf{E}}_j\right)}{\partial p_n} = \frac{\partial R\left(\bar{\mathbf{E}}_j\right)}{\partial \varepsilon_r} \cdot \frac{\partial \varepsilon_r}{\partial p_n} + \frac{\partial R\left(\bar{\mathbf{E}}_j\right)}{\partial \mu_r} \cdot \frac{\partial \mu_r}{\partial p_n} + \frac{\partial R\left(\bar{\mathbf{E}}_j\right)}{\partial \sigma} \cdot \frac{\partial \sigma}{\partial p_n}. \tag{3.9}$$

In the above expression, each of the constitutive parameters, ε_r, μ_r, and σ, should be considered as diagonal tensors since they are not the same in the different directions. For example, the last term in (3.9) can be expanded further as

$$\frac{\partial R\left(\bar{\mathbf{E}}_j\right)}{\partial \sigma} \cdot \frac{\partial \sigma}{\partial p_n} = \frac{\partial R\left(\bar{\mathbf{E}}_j\right)}{\partial \sigma_{\tau_1}} \cdot \frac{\partial \sigma_{\tau_1}}{\partial p_n} + \frac{\partial R\left(\bar{\mathbf{E}}_j\right)}{\partial \sigma_{\tau_2}} \cdot \frac{\partial \sigma_{\tau_2}}{\partial p_n} + \frac{\partial R\left(\bar{\mathbf{E}}_j\right)}{\partial \sigma_{\zeta}} \cdot \frac{\partial \sigma_{\zeta}}{\partial p_n} \tag{3.10}$$

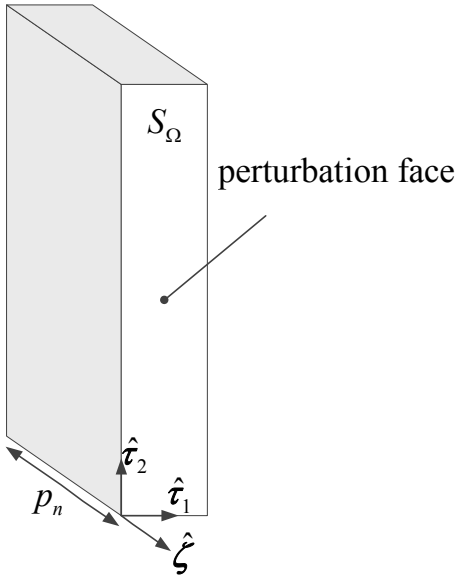

Figure 3.1 A metallic shape with the design parameter p_n. $\hat{\tau}_1$ and $\hat{\tau}_2$ are the tangential unit vectors and $\hat{\zeta}$ is the normal unit vector to the perturbation surface S_Ω of the metallic shape.

where τ_1, and τ_2 denote the two tangential directions and ζ is the normal direction on the surface of the metal as shown in Figure 3.1.

The term of $\partial R(\bar{\mathbf{E}}_j)/\partial p_n$ in (3.5) assumes analytical derivatives which exist only with respect to the constitutive parameters of the medium as per (3.7)-(3.8). The first term in the right-hand side of (3.7) depends on the relative permeability while the second term depends on both the relative permittivity and the conductivity of the medium. Since in most microwave simulations the imposed magnetic and electric sources exist on the surface of the ports rather than in the volume of the simulation, the last term in (3.7) does not have any contribution in our development and is set to zero.

In the case of using non-magnetic metallic objects, the values of ε_r and μ_r are equal to one. If the surrounding medium is vacuum, then the values of these two parameters are not changing between the metallic structure and the vacuum. Therefore, the residual derivatives with respect to ε_r and μ_r are zero and only the residual derivative with respect to the conductivity remains. Thus,

$$\frac{\partial \varepsilon_r}{\partial p_n} = \frac{\partial \mu_r}{\partial p_n} = 0. \tag{3.11}$$

The expression for $\partial R(\bar{\mathbf{E}}_j) / \partial p_n$ can be further reduced bearing in mind its terms as shown in (3.8). The only part which has dependence on the conductivity is the second term. Therefore, $\partial R(\bar{\mathbf{E}}_j) / \partial p_n$ reduces to

$$\frac{\partial R\left(\bar{\mathbf{E}}_j\right)}{\partial p_n} = \frac{\partial R\left(\bar{\mathbf{E}}_j\right)}{\partial \sigma} \cdot \frac{\partial \sigma}{\partial p_n} = \left(\frac{\partial \alpha}{\partial \sigma} \bar{\mathbf{E}}_j\right) \cdot \frac{\partial \sigma}{\partial p_n}. \tag{3.12}$$

For a metallic object, the conductivity is constant inside and outside of the object. The only place where it changes abruptly is on the surface of the metallic object, which is called the perturbation surface [see Figure 3.1]. If we assign a constant value σ_m to the conductivity of the metallic medium, then the directional derivative of the conductivity in the $\hat{\zeta}$ direction is

$$\frac{\partial \sigma_\vartheta}{\partial \zeta} = -\sigma_m \delta(\zeta), \quad \vartheta = \tau_1, \tau_2, \zeta \tag{3.13}$$

where ϑ denotes different directions on the surface of the metal and $\delta(\zeta)$ is the Dirac delta function.

In (3.12), we are interested in the derivative with respect to p_n rather than the directional derivative in the $\hat{\zeta}$ direction. The relationship between these two derivatives can be explained through the finite-difference approximation shown in Figure 3.2. The derivative with respect to the spatial variable ζ can be approximated as

$$\frac{\partial \sigma_{\vartheta}}{\partial \zeta} \approx \frac{\sigma_{\text{air}} - \sigma_m}{2\Delta}. \tag{3.14}$$

On the other hand, the derivative of the conductivity with respect to the shape parameter p_n is approximated as

$$\frac{\partial \sigma_{\vartheta}}{\partial p_n} \approx \frac{\sigma_m - \sigma_{\text{air}}}{2\Delta}. \tag{3.15}$$

Thus, $\partial \sigma_{\vartheta} / \partial p_n = -\partial \sigma_{\vartheta} / \partial \zeta$. Also,

$$\frac{\partial \sigma_{\vartheta}}{\partial p_n} = \sigma_m \delta(\zeta), \quad \vartheta = \tau_1, \tau_2, \zeta. \tag{3.16}$$

The next step in (3.12) is to calculate the term $(\partial \alpha / \partial \sigma)\bar{\mathbf{E}}_j$. From the definition in (3.8) it follows that in metals $\alpha = k_0^2 \left[1 - j\sigma (\omega \varepsilon_0)^{-1} \right]$. Then, the derivative of α with respect to the conductivity is

$$\frac{\partial \alpha}{\partial \sigma} = -j\omega\mu_0. \tag{3.17}$$

However, the multiplication of (3.17) with $\bar{\mathbf{E}}_j$ causes some ambiguity which does not allow for the same treatment of both tangential and normal components. This is explained below.

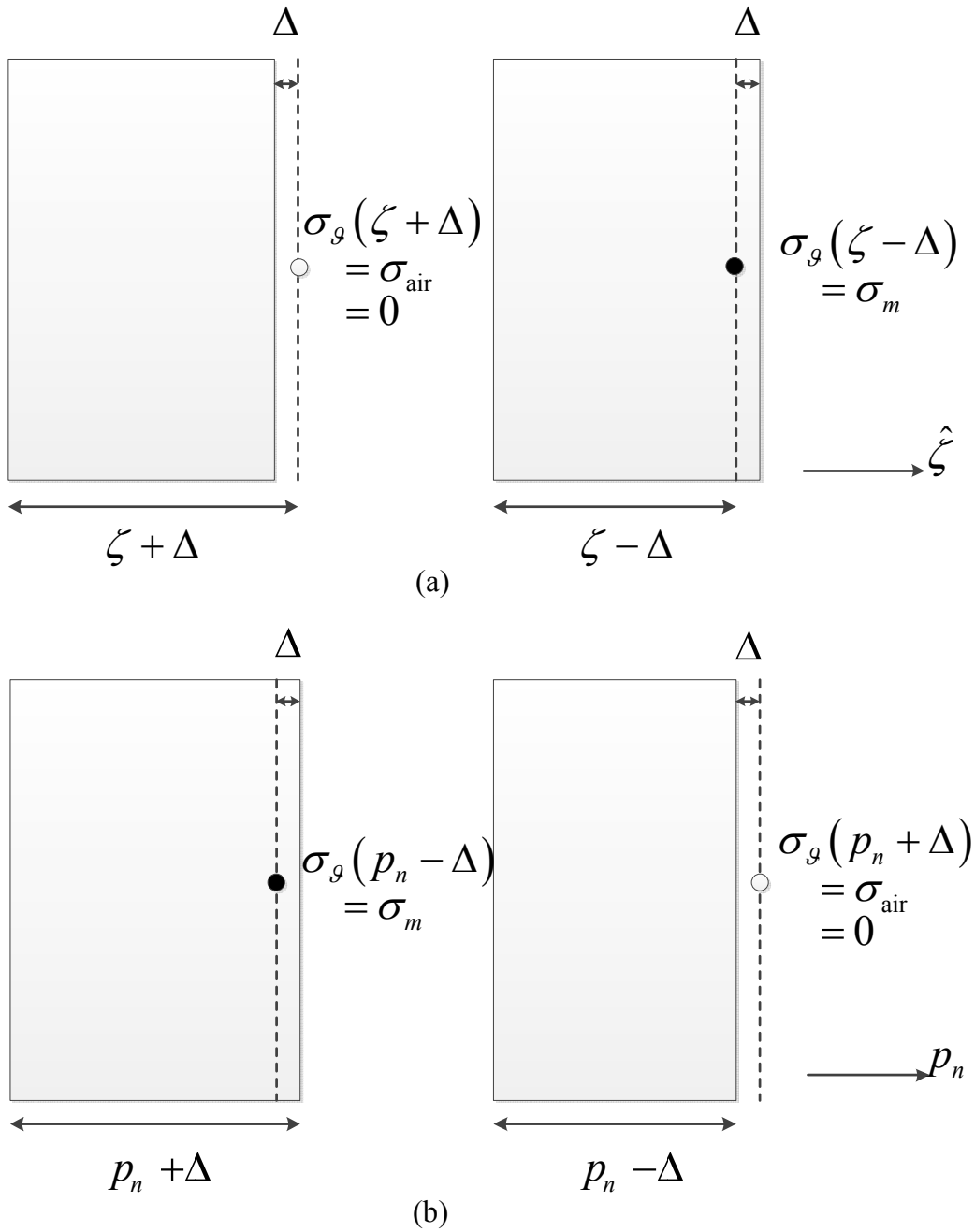

Figure 3.2 Finite-difference (FD) representation of: (a) $\partial\sigma_\vartheta/\partial\zeta$ and (b) $\partial\sigma_\vartheta/\partial p_n$, at the interface between metal and air. White and black circles indicate the inside and the outside of the metal. The dash line indicates the position in space where the conductivity is evaluated. Δ is the step size in the FD approximation of the derivatives.

As is known from the electromagnetic boundary conditions, the normal component of the electric field is not continuous on the surface of the metal while the tangential component is continuous because there are no magnetic sources, $\bar{\mathbf{M}}^i = 0$. The boundary conditions are stated below:

$$\begin{aligned} &\hat{\zeta} \times \left(\bar{\mathbf{E}}^{air} - \bar{\mathbf{E}}^{metal} \right) = -\bar{\mathbf{M}}^i \quad \overset{\mathbf{M}^i = 0}{\Rightarrow} \quad \bar{\mathbf{E}}_\tau^{air} = \bar{\mathbf{E}}_\tau^{metal}, \\ &\hat{\zeta} \cdot \left(\bar{\mathbf{E}}^{air} - \bar{\mathbf{E}}^{metal} \right) = \frac{\rho_s}{\varepsilon_0}. \end{aligned} \tag{3.18}$$

If we try to find $\left(\partial\alpha / \partial\sigma\right)\bar{\mathbf{E}}_j$ in two cases, first, approaching the surface from the air (right limit), and then approaching the surface from the metal (left limit), the expressions for the normal and tangential field components are:

$$\begin{aligned} &\lim_{\zeta \to 0^+} \left(\frac{\partial \alpha_\zeta}{\partial \sigma} \bar{\mathrm{E}}_{j,\zeta} \right) \cdot \frac{\partial \sigma_\zeta}{\partial p_n} = -\sigma_m j\omega\mu_0 \bar{\mathrm{E}}_{j,\zeta}^{air} \delta(\zeta), \\ &\lim_{\zeta \to 0^-} \left(\frac{\partial \alpha_\zeta}{\partial \sigma} \bar{\mathrm{E}}_{j,\zeta} \right) \cdot \frac{\partial \sigma_\zeta}{\partial p_n} = -\sigma_m j\omega\mu_0 \bar{\mathrm{E}}_{j,\zeta}^{metal} \delta(\zeta), \\ &\lim_{\zeta \to 0^\pm} \left(\frac{\partial \alpha_\tau}{\partial \sigma} \bar{\mathbf{E}}_{j,\tau} \right) \cdot \frac{\partial \sigma_\tau}{\partial p_n} = -\sigma_m j\omega\mu_0 \bar{\mathbf{E}}_{j,\tau}^{air} \delta(\zeta). \end{aligned} \tag{3.19}$$

While the tangential part gives the same answer for the two limits, the normal part gives different answers, thus causing ambiguity. Therefore, the two contributions require different treatment which is investigated in the next two sub-sections.

3.3.1 Contribution of the Tangential E-field Components

In this sub-section, the metallic structures are divided into two categories: of finite conductivity and perfectly conducting structures. The contribution of the

tangential **E**-field components in the sensitivity formula is then found for both categories.

a) Finite Conductivity Metallic Structures

Using (3.16) and (3.17) in (3.12), the residual-derivative expression for the tangential **E**-field components is

$$\frac{\partial R\left(\overline{\mathbf{E}}_{j,\tau}\right)}{\partial p_n} = -\sigma_m j\omega\mu_0 \overline{\mathbf{E}}_{j,\tau}^{air}\delta\left(\zeta\right). \tag{3.20}$$

Thus, the tangential part of the sensitivity formulation in (3.5) is

$$I_\tau = \left(-j\omega\mu_0\kappa_{kj}\right)\sigma_m \iiint_{\Omega} \overline{\mathbf{E}}_{k,\tau}\cdot\overline{\mathbf{E}}_{j,\tau}\delta\left(\zeta\right)d\Omega. \tag{3.21}$$

Due to the presence of the Dirac delta function in (3.21), the volume integral reduces to the surface integral on the perturbation face of the metallic object, i.e.,

$$I_\tau = \left(-j\omega\mu_0\kappa_{kj}\right)\sigma_m \iint_{S_\Omega} \overline{\mathbf{E}}_{k,\tau}\cdot\overline{\mathbf{E}}_{j,\tau}ds. \tag{3.22}$$

b) Perfectly Conducting Metallic Structures

The expression in (3.22) is only applicable for metallic structures with finite conductivity. To develop this theory in the case of perfect electric conductor (PEC) structures, the limit of (3.22) as σ_m goes to infinity must be found.

As the metal conductivity goes to infinity, the tangential **E**-field components tend to zero. This leads to multiplication of the infinite conductivity with the zero electric field. This ambiguity can be solved by using the surface

impedance concept to relate the tangential **E**-field components to the surface current density $\overline{\mathbf{J}}_j^s$. The surface impedance boundary condition is

$$\overline{\mathbf{E}}_{j,\tau} = Z_s \overline{\mathbf{J}}_j^s, \tag{3.23}$$

where

$$Z_s = \frac{1+j}{\sigma_m \delta_s} \quad \text{and} \quad \delta_s = \frac{1}{\sqrt{\pi f \mu_0 \sigma_m}}. \tag{3.24}$$

Here, f is the frequency, Z_s is the surface impedance of the metal, and δ_s is the skin depth.

Using (3.23) and (3.24), the contribution of the tangential **E**-field components in the sensitivity integral of (3.21) for a shape parameter of a PEC structure is obtained as

$$I_\tau = \kappa_{kj} \left(\omega \mu_0\right)^2 \iint_{S_\Omega} \overline{\mathbf{J}}_k^s \cdot \overline{\mathbf{J}}_j^s ds. \tag{3.25}$$

3.3.2 Contribution of the Normal E-field Component

The normal component of the residual derivative in (3.12) can be expanded as

$$\frac{\partial R\left(\overline{E}_{j,\zeta}\right)}{\partial p_n} = \frac{\partial \alpha}{\partial p_n} \overline{E}_{j,\zeta} = \frac{\partial}{\partial p_n}\left(\alpha \overline{E}_{j,\zeta}\right) - \alpha \frac{\partial \overline{E}_{j,\zeta}}{\partial p_n}. \tag{3.26}$$

According to (3.8), in metals $\alpha = -j\omega\mu_0\left(j\omega\varepsilon_0 + \sigma\right)$. This helps to relate the expression for the term $\alpha \overline{E}_{j,\zeta}$ to the normal component of the current density $\overline{J}_{j,\zeta}$ which includes both displacement and conduction current density terms:

$$\alpha \bar{E}_{j,\zeta} = -j\omega\mu_0 \bar{J}_{j,\zeta}. \tag{3.27}$$

So, the first term in the right-hand side of (3.26) can then be related to the derivative of the $\bar{J}_{j,\zeta}$ with respect to p_n, and (3.26) is rewritten as

$$\frac{\partial R\left(\bar{E}_{j,\zeta}\right)}{\partial p_n} = -j\omega\mu_0 \frac{\partial \bar{J}_{j,\zeta}}{\partial p_n} - \alpha \frac{\partial \bar{E}_{j,\zeta}}{\partial p_n}. \tag{3.28}$$

The derivative $\partial \bar{E}_{j,\zeta} / \partial p_n$ in (3.28) can be related to $\partial \bar{E}_{j,\zeta} / \partial \zeta$ through the procedure summarized by (3.14)-(3.15):

$$\frac{\partial \bar{E}_{j,\zeta}}{\partial p_n} = -\frac{\partial \bar{E}_{j,\zeta}}{\partial \zeta}, \qquad \frac{\partial \bar{J}_{j,\zeta}}{\partial p_n} = -\frac{\partial \bar{J}_{j,\zeta}}{\partial \zeta}. \tag{3.29}$$

In order to find $\partial \bar{E}_{j,\zeta} / \partial \zeta$, we use the Gauss law,

$$\nabla \cdot \bar{\mathbf{E}} = \frac{\rho_v}{\varepsilon_0}, \tag{3.30}$$

where ρ_v is the volume charge density.

The three-dimensional (3-D) divergence operator can be broken down into the normal derivative ($\partial / \partial \zeta$), and the tangential operator ∇_τ as

$$\frac{\partial \bar{E}_{j,\zeta}}{\partial \zeta} + \nabla_\tau \cdot \bar{\mathbf{E}}_{j,\tau} = \frac{\rho_v}{\varepsilon_0}, \tag{3.31}$$

where

$$\nabla_\tau = \left(\frac{\partial}{\partial \tau_1} \hat{\tau}_1 + \frac{\partial}{\partial \tau_2} \hat{\tau}_2 \right). \tag{3.32}$$

Next, the continuity equation can be used to calculate $\partial \bar{J}_{j,\zeta} / \partial \zeta$. It is written as

$$\nabla \cdot \overline{\mathbf{J}} = -j\omega\rho_v, \tag{3.33}$$

which can also be expressed as

$$\frac{\partial \overline{J}_{j,\zeta}}{\partial \zeta} + \nabla_\tau \cdot \overline{\mathbf{J}}_{j,\tau} = -j\omega\rho_v. \tag{3.34}$$

Substituting (3.29), (3.31) and (3.34) in (3.28), we obtain

$$\begin{aligned} \frac{\partial R\left(\overline{E}_{j,\zeta}\right)}{\partial p_n} &= j\omega\mu_0\left(-j\omega\rho_v - \nabla_\tau \cdot \overline{\mathbf{J}}_{j,\tau}\right) + \alpha\left(\frac{\rho_v}{\varepsilon_0} - \nabla_\tau \cdot \overline{\mathbf{E}}_{j,\tau}\right) \\ &= \left(\omega^2\mu_0 + \frac{\alpha}{\varepsilon_0}\right)\rho_v - j\omega\mu_0\nabla_\tau \cdot \overline{\mathbf{J}}_{j,\tau} - \alpha\nabla_\tau \cdot \overline{\mathbf{E}}_{j,\tau}. \end{aligned} \tag{3.35}$$

With the use of (3.27), the last two terms in the right-hand side of (3.35) cancel. Since $\alpha = -j\omega\mu_0\left(j\omega\varepsilon_0 + \sigma\right)$, we can write

$$\frac{\partial R\left(\overline{E}_{j,\zeta}\right)}{\partial p_n} = \left(2\omega^2\mu_0 - \frac{j\omega\mu_0}{\varepsilon_0}\sigma_m\right)\rho_v. \tag{3.36}$$

From now on, we can treat the problem as if the current and charge densities have uniform volume distribution inside one skin depth of the metal rather than having surface distribution on the surface of the metal. This is a very good approximation for good conductors. Furthermore, we will find the limit when the conductivity goes to infinity by reducing the skin depth to zero. All field quantities, e.g., **E**-field, **H**-field, $\mathbf{J}^s$, and ρ_v, are assumed to be nonzero and to have uniform distribution in one skin depth inside the metallic object.

Assuming a uniform volume charge density distribution inside one skin depth of the metal and using the Gauss law, the relationship between ρ_v and the normal **E**-field at the surface of the metal inside the air $\bar{E}^{\text{air}}_{j,\zeta}$ can be obtained as

$$\rho_v(\zeta) = \frac{\varepsilon_0 \bar{E}^{\text{air}}_{j,\zeta}}{\delta_s}. \tag{3.37}$$

Substituting (3.37) in (3.36), the expression for $\partial R\left(\bar{\mathrm{E}}_{j,\zeta}\right)/\partial p_n$ can be written as

$$\frac{\partial R\left(\bar{E}_{j,\zeta}\right)}{\partial p_n} = \left(2\omega^2\mu_0 - \frac{j\omega\mu_0}{\varepsilon_0}\sigma_m\right)\frac{\varepsilon_0 \bar{E}^{\text{air}}_{j,\zeta}}{\delta_s}. \tag{3.38}$$

The integration for the contribution of the normal field component in the sensitivity integral in (3.5) should be done in the metal. At the same time, we have access to **E**-field solution on the surface of the metal. So, the boundary condition for the normal **E**-field component at the surface for a finite σ_m is used.

$$\bar{E}^{\text{met}}_{j,\zeta} = \frac{1}{1 - j\dfrac{\sigma_m}{\omega\varepsilon_0}}\bar{E}^{\text{air}}_{j,\zeta}, \tag{3.39}$$

where $\bar{E}^{\text{met}}_{j,\zeta}$ is the normal **E**-field component inside the metal at the interface. This is done through the use of the continuity of the normal component of the electric flux density $\bar{D}_{j,\zeta}$ since there is no surface charge when σ_m is finite.

Using (3.38)-(3.39), the contribution of the normal component of the **E**-field in the sensitivity integral of (3.5) is obtained as

$$I_\zeta = \kappa_{kj} \iiint_\Omega \left(\frac{2\omega^2 \mu_0 - \frac{j\omega\mu_0}{\varepsilon_0}\sigma_m}{1 - j\frac{\sigma_m}{\omega\varepsilon_0}} \frac{\varepsilon_0}{\delta_s} \right) \bar{E}^{\text{air}}_{j,\zeta} \cdot \bar{E}^{\text{air}}_{j,\zeta} d\Omega \tag{3.40}$$

Since, everything is constant in the depth of δ_s, the volume integration of (3.40) is reduced to the surface integrate:

$$I_\zeta = \kappa_{kj} \iint_{S_p} \left(\varepsilon_0 \frac{2\omega^2 \mu_0 - \frac{j\omega\mu_0}{\varepsilon_0}\sigma_m}{1 - j\frac{\sigma_m}{\omega\varepsilon_0}} \right) \bar{E}^{\text{air}}_{j,\zeta} \cdot \bar{E}^{\text{air}}_{j,\zeta} ds \tag{3.41}$$

By taking the limit of I_ζ as σ_m goes to infinity, the final expression for the contribution of the normal field component to the sensitivity integral of (3.5) is obtained as

$$I_\zeta = \kappa_{kj} \omega^2 \mu_0 \varepsilon_0 \iint_{S_p} \bar{E}^{\text{air}}_{j,\zeta} \cdot \bar{E}^{\text{air}}_{j,\zeta} ds \tag{3.42}$$

Hereafter, the superscript 'air' is omitted and $\bar{E}_{k,\zeta}$ and $\bar{E}_{j,\zeta}$ denote the normal **E**-field components at the surface of the metal.

Using (3.22), and (3.42), the exact self-adjoint sensitivity expression for the shape parameters of finite-conductivity metallic structures is obtained as

$$\frac{\partial S_{kj}}{\partial p_n} = \frac{-j\omega}{2V_j V_k} \iint_{S_\Omega} \left(\frac{\sigma_m}{j\omega} \bar{\mathbf{E}}_{k,\tau} \cdot \bar{\mathbf{E}}_{j,\tau} + \varepsilon_0 \bar{E}_{k,\zeta} \cdot \bar{E}_{j,\zeta} \right) ds. \tag{3.43}$$

With the use of (3.25), and (3.42), the exact self-adjoint sensitivity expression for shape parameters of PEC structures is obtained as

$$\frac{\partial S_{kj}}{\partial p_n} = \frac{-j\omega}{2V_j V_k} \iint_{S_\Omega} \left(\mu_0 \bar{\mathbf{J}}^s_{k,\tau} \cdot \bar{\mathbf{J}}^s_{j,\tau} + \varepsilon_0 \bar{E}_{k,\zeta} \cdot \bar{E}_{j,\zeta} \right) ds. \tag{3.44}$$

The sensitivity formula (3.44) can also be written as a function of the tangential magnetic field $\bar{\mathbf{H}}_{j,\tau}$ instead of the surface current density. This can be done through the use of the boundary condition,

$$\bar{\mathbf{J}}^s_{j,\boldsymbol{\tau}} = \hat{\zeta} \times \bar{\mathbf{H}}_{j,\boldsymbol{\tau}}, \tag{3.45}$$

where $\hat{\zeta}$ is the unit normal at the surface of the metal. The self-adjoint sensitivity expression then becomes

$$\frac{\partial S_{kj}}{\partial p_n} = \frac{-j\omega}{2V_j V_k} \iint_{S_\Omega} \left(\mu_0 \bar{\mathbf{H}}_{j,\tau} \cdot \bar{\mathbf{H}}_{k,\tau} + \varepsilon_0 \bar{E}_{k,\zeta} \cdot \bar{E}_{j,\zeta} \right) ds. \tag{3.46}$$

A note should be made here about the field components in (3.46). As can be seen in Figure 3.1, the direction of the perturbation is assumed to be along $\hat{\zeta}$, and $\hat{\tau}_1$ and $\hat{\tau}_2$ are tangential to the surface of perturbation. So, we need the normal **E**-field and the tangential **H**-field components associated with the perturbation face for the parameter p_n.

3.4 Implementation Example for Finite Conductivity Metallic Structures

In this section, a two-section impedance-transformer example is presented to verify the new sensitivity formula (3.43) proposed for finite conductivity metallic structures. The material of the metal as set to copper with the value of

conductivity of 5.8×10^7 S/m. The simulations are performed with the commercial finite-element solver, Ansoft HFSS [1]. It can provide the *S*-parameters as well as the field solution at the surface of the perturbation faces. The field solution at the desired shape surfaces is exported using the post-processing tool. Moreover, HFSS can provide reference sensitivity curves as it has a sensitivity-analysis capability.

The proposed self-adjoint sensitivity analysis formula of (3.43) is implemented in MATLAB® [8]. The results are compared with the reference self-adjoint sensitivities provided by HFSS. The reference plots are exact since the simulator is using the analytical derivatives of the FEM system matrix.

The waveguide two-section impedance transformer [10] example is shown in Figure 3.3. The rectangular cross-sections of ports 1 and 2 are 36.4×10.2 mm^2 and 36×7 mm^2, respectively. The nominal design parameter values of the two-section impedance transformer are given in Table 3.1

The waveguide is excited using wave ports with the dominant TE_{10} mode. The mesh convergence error for the *S*-parameters is set as 0.005.

The proposed method is used to calculate the derivatives of S_{11} and S_{21} with respect to two shape parameters: the width w and the height h of the first transformer section in the frequency range from 5 to 7 GHz. Very fine mesh is imposed on the perturbation faces for the respective parameters, w_1 and h_1, to make the field solutions as accurate as possible.

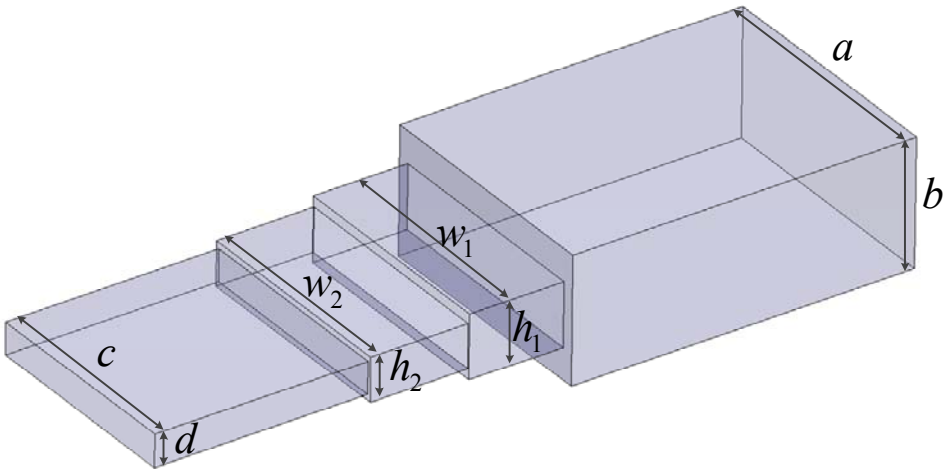

Figure 3.3 The two-section waveguide impedance transformer. The width w_1 and the height h_1 of the first section are the parameters of interest.

Table 3.1 Nominal design parameter values of the two-section impedance transformer.

Parameter	Value (mm)
a	40.4
b	20.2
c	34.8
d	5.1
W_1	36.4
W_2	36
h_1	10.2
h_2	7

Figure 3.4 to Figure 3.7 show the derivatives of the S_{11} with respect to the parameters w_1 and h_1 in which the integrations are done in the MATLAB®. Here, the agreement between the derivatives calculated by the proposed method and the reference curves is very good.

The derivatives of S_{21} with respect to the parameters w_1 and h_1 calculated in the MATLAB® are shown in Figure 3.8 to Figure 3.11. The results for the parameter h_1 show minor disagreement with the reference sensitivity curves. This disagreement can be explained with inaccuracies in the numerical field solution and the inaccuracy of the numerical integration over the perturbation face.

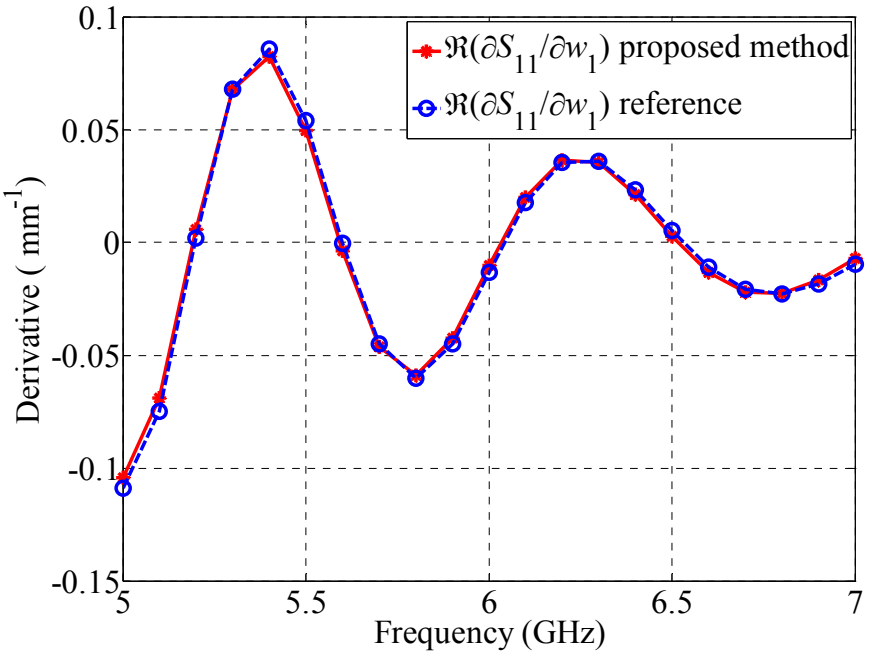

Figure 3.4 Sensitivity curves for the real part of S_{11} with respect to w_1 in the impedance-transformer example.

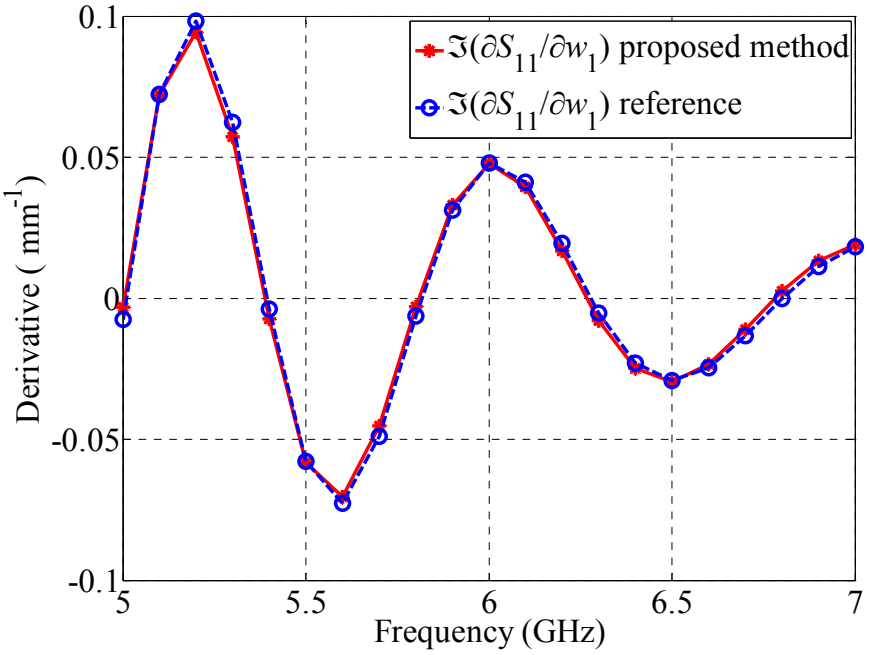

Figure 3.5 Sensitivity curves for the imaginary part of S_{11} with respect to w_1 in the impedance-transformer example.

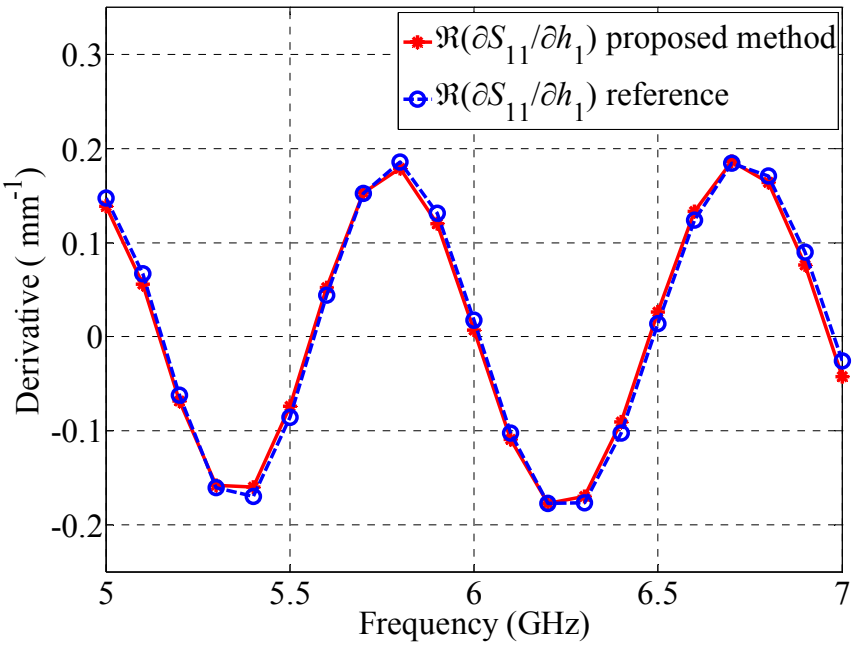

Figure 3.6 Sensitivity curves for the real part of S_{11} with respect to h_1 in the impedance-transformer example.

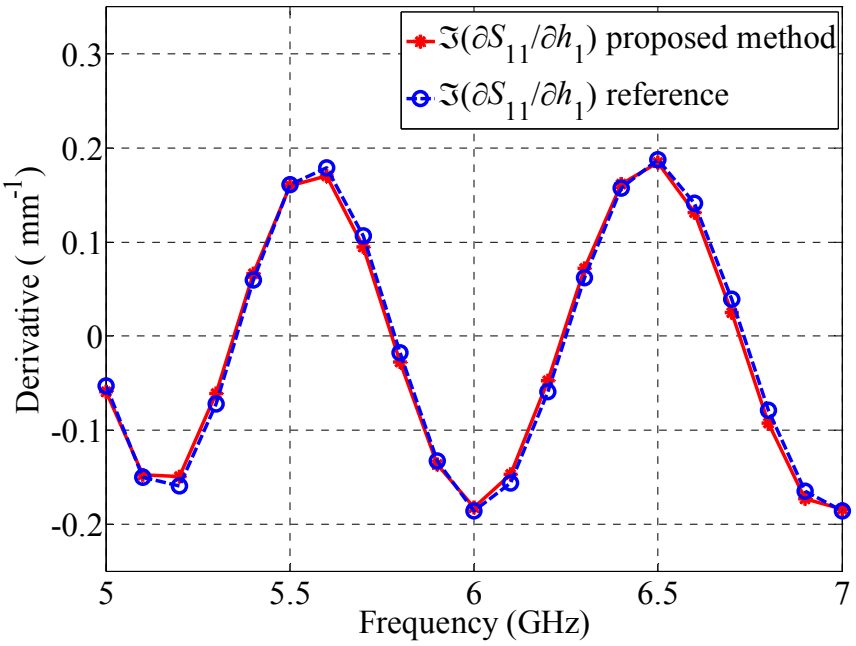

Figure 3.7 Sensitivity curves for the imaginary part of S_{11} with respect to h_1 in the impedance-transformer example.

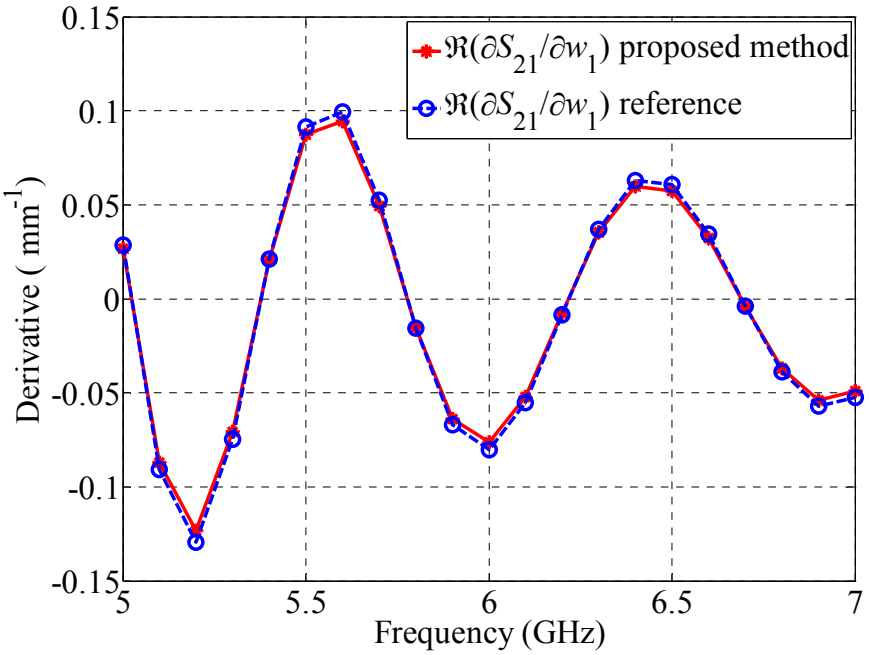

Figure 3.8 Sensitivity curves for the real part of S_{21} with respect to w_1 in the impedance-transformer example.

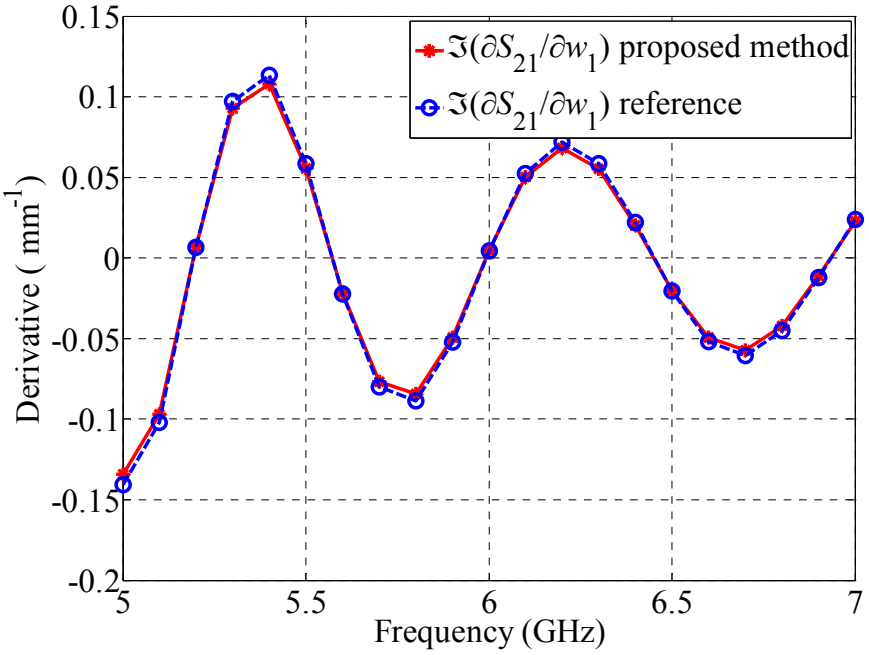

Figure 3.9 Sensitivity curves for the imaginary part of S_{21} with respect to w_1 in the impedance-transformer example.

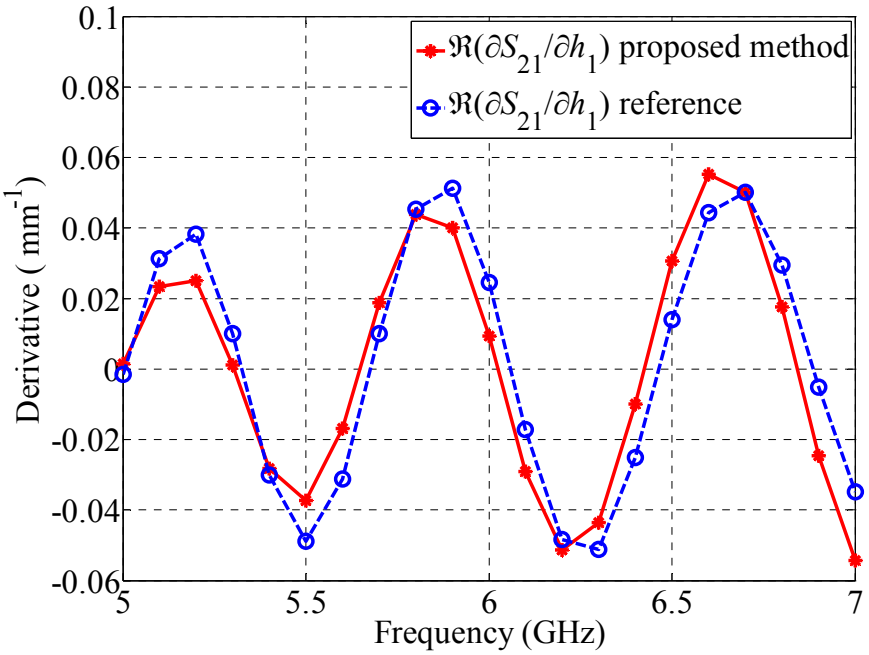

Figure 3.10 Sensitivity curves for the real part of S_{21} with respect to h_1 in the impedance-transformer example.

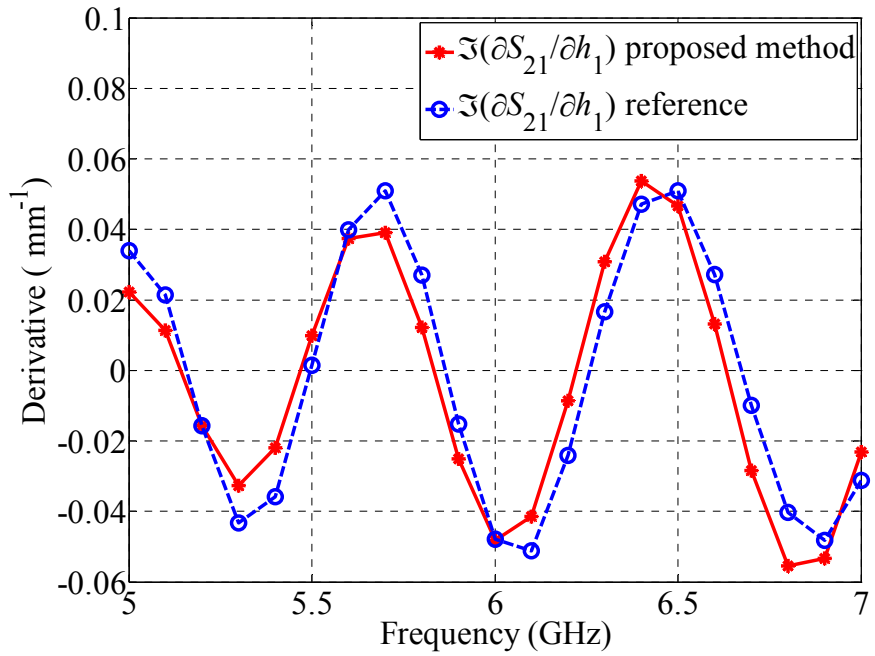

Figure 3.11 Sensitivity curves for the imaginary part of S_{21} with respect to h_1 in the impedance-transformer example.

3.5 Implementation Examples for PEC Metallic Structures

In this section, two examples are presented to verify the new sensitivity formula (3.46) proposed for PEC metallic structures. These include an H-plane waveguide filter and two-section impedance transformer in which PEC is set as the material for the metal. The simulations are performed with the commercial finite-element solver, Ansoft HFSS [1]. It can provide the *S*-parameters as well as the field solution at the surface of the perturbation faces. The field solution at the desired shape surfaces is exported using the post-processing tool. Moreover, the reference sensitivity curves are provided by the HFSS.

3.5.1 Six-resonator H-plane Waveguide Filter

The six-resonator H-plane filter [9] is shown in Figure 3.12. The rectangular waveguide is of width $2a = 34.8488$ mm and height $b = 15.7988$ mm. The nominal parameter values of the this structure is given in Table 3.2. The six resonators are separated by seven septa of finite thickness $\delta = 0.6223$ mm. The material of the metal is set as PEC.

The waveguide is excited using wave ports in a way that only the dominant TE_{10} mode propagates. The mesh convergence error for the *S*-parameters is set to 0.005.

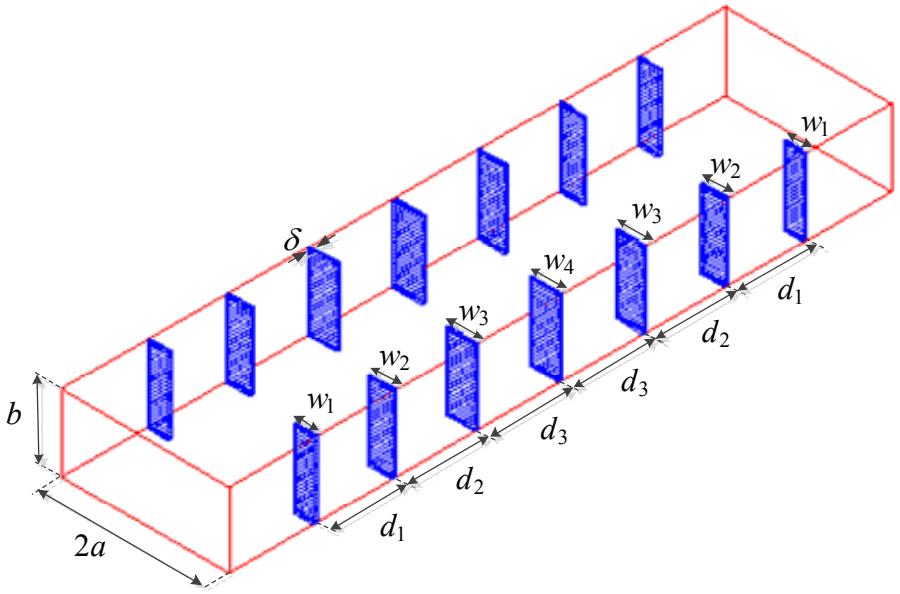

Figure 3.12 H-plane waveguide filter. The structure is symmetric along the width of the waveguide.

One design parameter of interest is the width of the four septa w_3 located symmetrically about the mid-length of the waveguide. To obtain an accurate field solution, a very fine mesh is imposed on the perturbation faces of interest. The other design parameter of interest is d_3 which determines the location of the four septa of width w_3 [see Figure 3.12]. The proposed sensitivity formula is used to calculate the derivatives of S_{11} and S_{21} with respect to w_3 and d_3 in the frequency range from 4 to 7 GHz.

The field solution is exported using the Field Calculator in the Post-processing Toolbox of HFSS. This toolbox also allows to perform mathematical operations on the EM field quantities in the structure when only one port is

Table 3.2 Nominal parameter values of the H-plane waveguide filter.

Parameter	Value (mm)
a	17.4244
b	15.7988
δ	0.62230
w_1	4.35610
w_2	5.60070
w_3	6.22300
w_4	6.22300
d_1	16.1798
d_2	16.1798
d_3	16.8021

excited. This information of the S_{21}, because it needs both the field solution of ports 1 and 2. Therefore, the integrations for sensitivity analysis of the S_{21} are done in the MATLAB®.

Figure 3.13 to Figure 3.16 show the derivatives of the S_{11} with respect to parameters calculated in the Field Calculator of HFSS. While the agreement between the derivatives calculated by the proposed method and the reference curves calculated by HFSS is very good, there is a slight difference between them.

The same derivatives are shown in Figure 3.17 to Figure 3.22 in which the integrations are done in the MATLAB®. While the calculated $\partial S_{11} / \partial w_3$ shows better agreement with the reference sensitivity curves, there is some discrepancy for $\partial S_{11} / \partial d_3$ around the frequency of 4.5 GHz. This should be the effect of the imperfect sampling of the numerical field solution and the numerical integration.

The derivatives of S_{21} with respect to parameters w_3 and d_3 calculated in MATLAB®, are shown in Figure 3.21 to Figure 3.24. The results show a very good agreement with the reference sensitivity curves.

A very fine mesh is needed at the perturbation faces for the respective parameters to make the field solutions as accurate as possible. Without defining a fine mesh, the calculated sensitivities are very different from the reference plots.

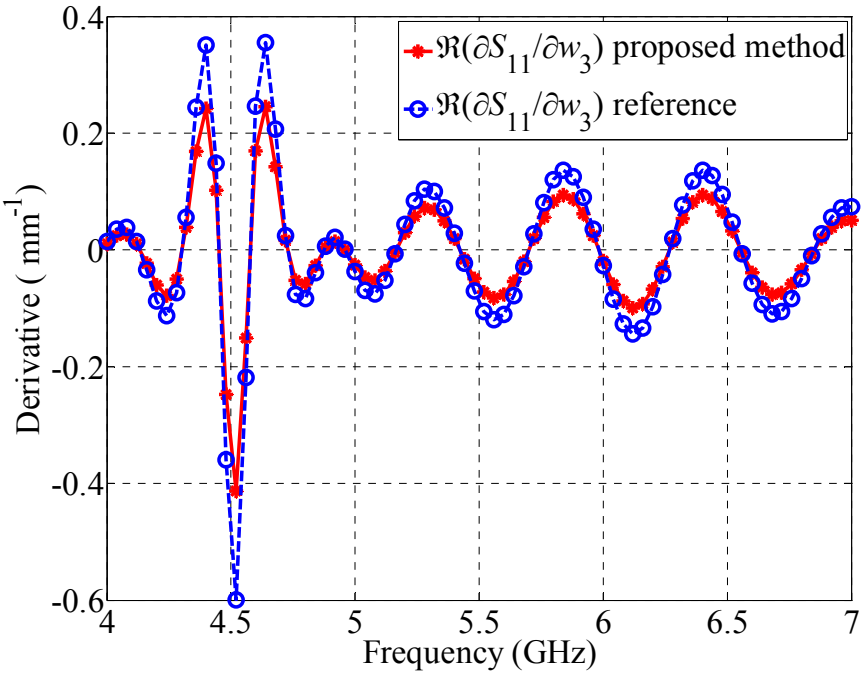

Figure 3.13 Sensitivity curves for the real part of S_{11} with respect to w_3 in the H-plane filter example, calculated in the Field Calculator of HFSS.

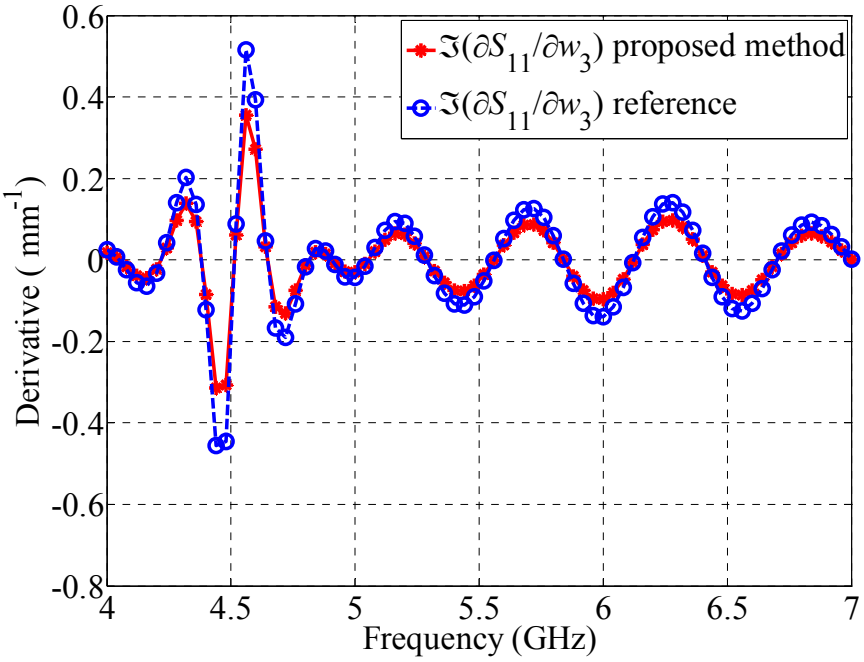

Figure 3.14 Sensitivity curves for the imaginary part of S_{11} with respect to w_3 in the H-plane filter example, calculated in the Field Calculator of HFSS.

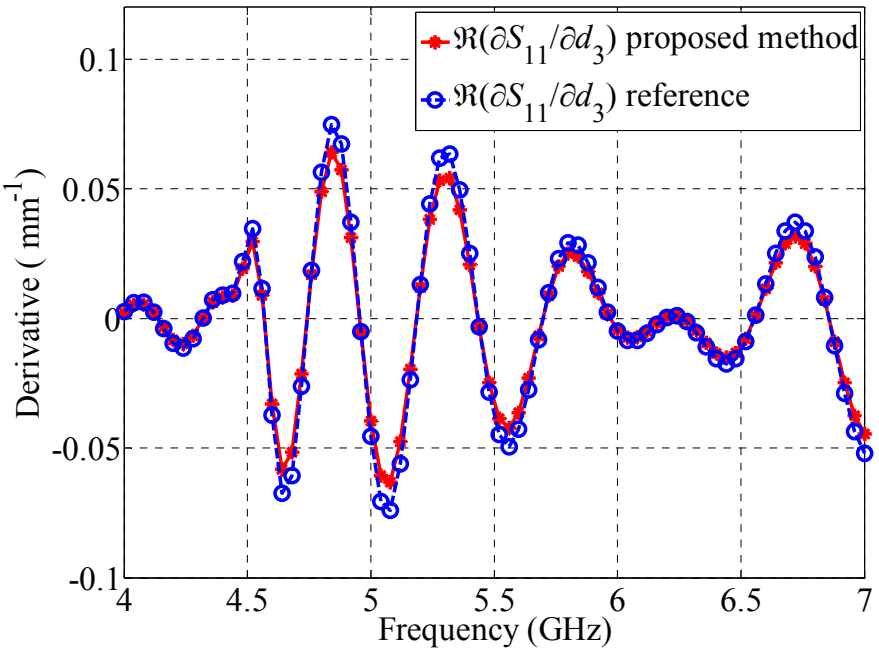

Figure 3.15 Sensitivity curves for the real part of S_{11} with respect to d_3 in the H-plane filter example, calculated in the Field Calculator of HFSS.

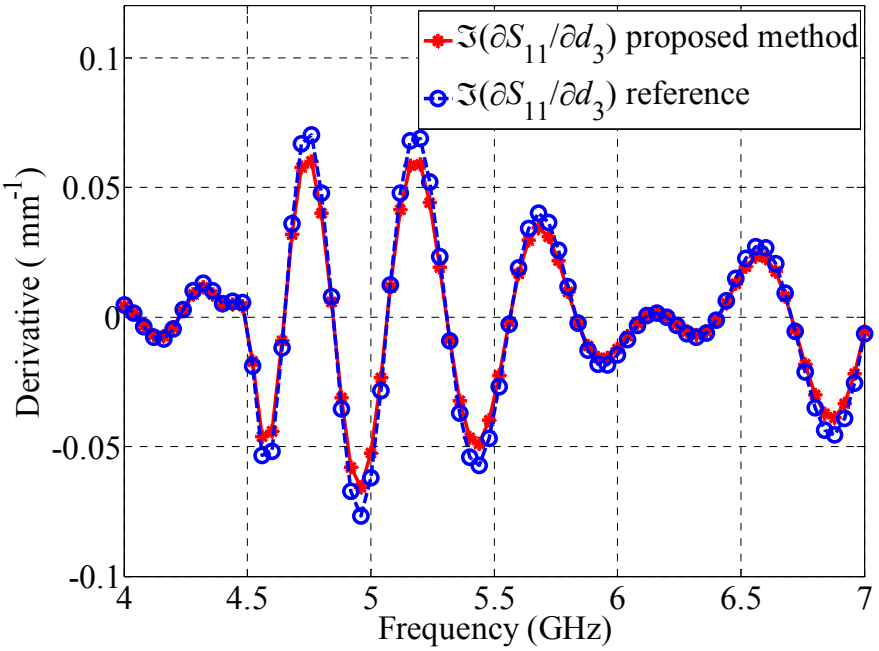

Figure 3.16 Sensitivity curves for the imaginary part of S_{11} with respect to d_3 in the H-plane filter example, calculated in the Field Calculator of HFSS.

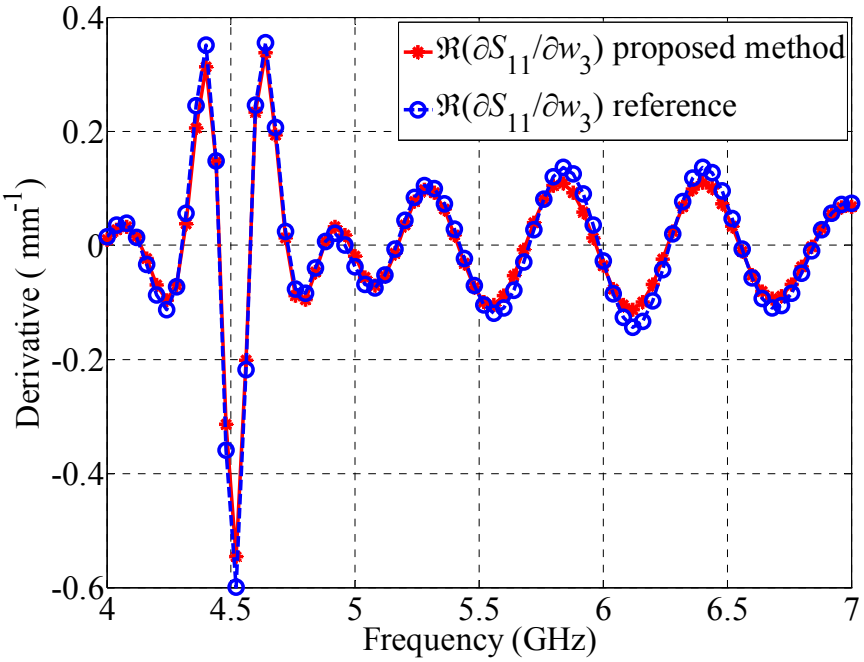

Figure 3.17 Sensitivity curves for the real part of S_{11} with respect to w_3 in the H-plane filter example.

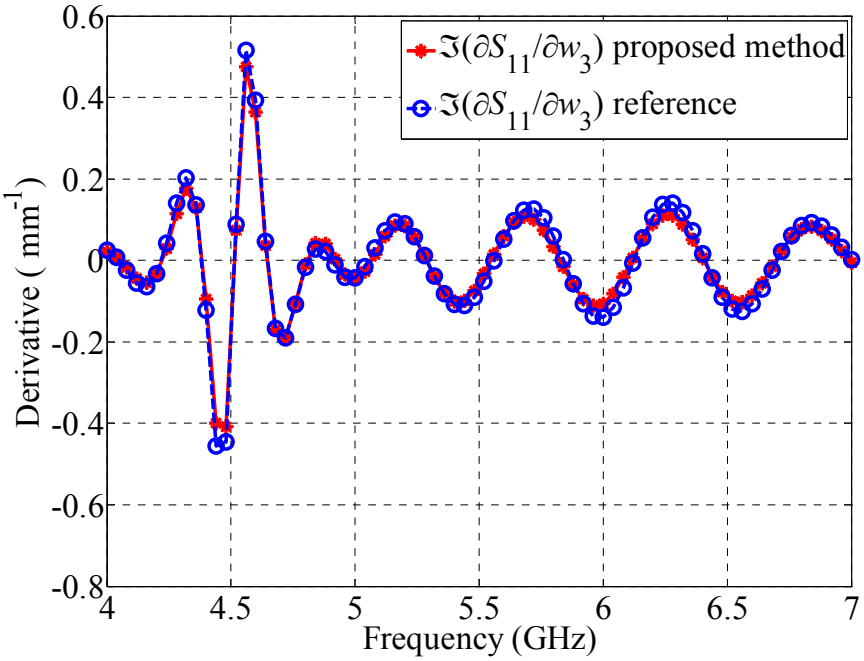

Figure 3.18 Sensitivity curves for the imaginary part of S_{11} with respect to w_3 in the H-plane filter example.

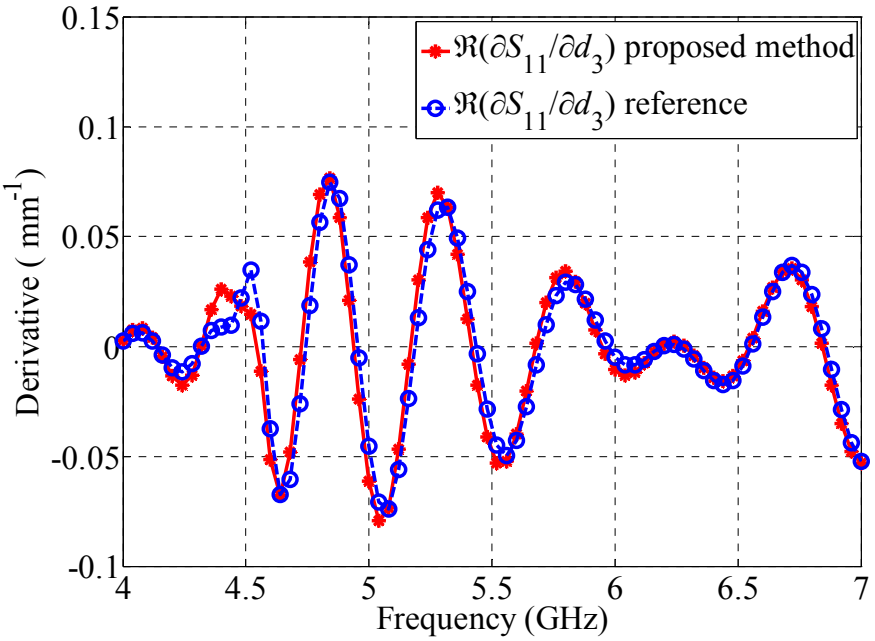

Figure 3.19 Sensitivity curves for the real part of S_{11} with respect to d_3 in the H-plane filter example.

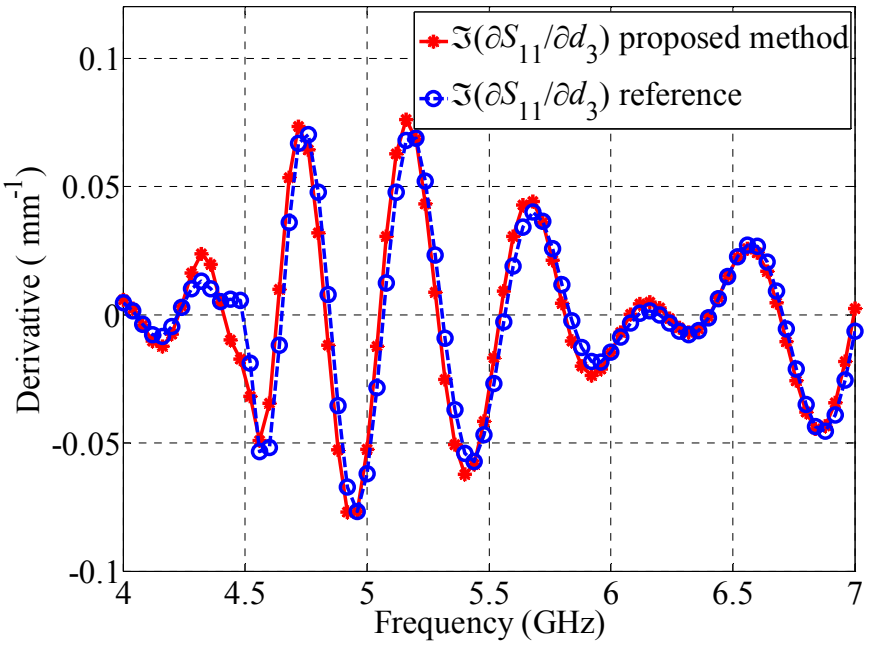

Figure 3.20 Sensitivity curves for the imaginary part of S_{11} with respect to d_3 in the H-plane filter example.

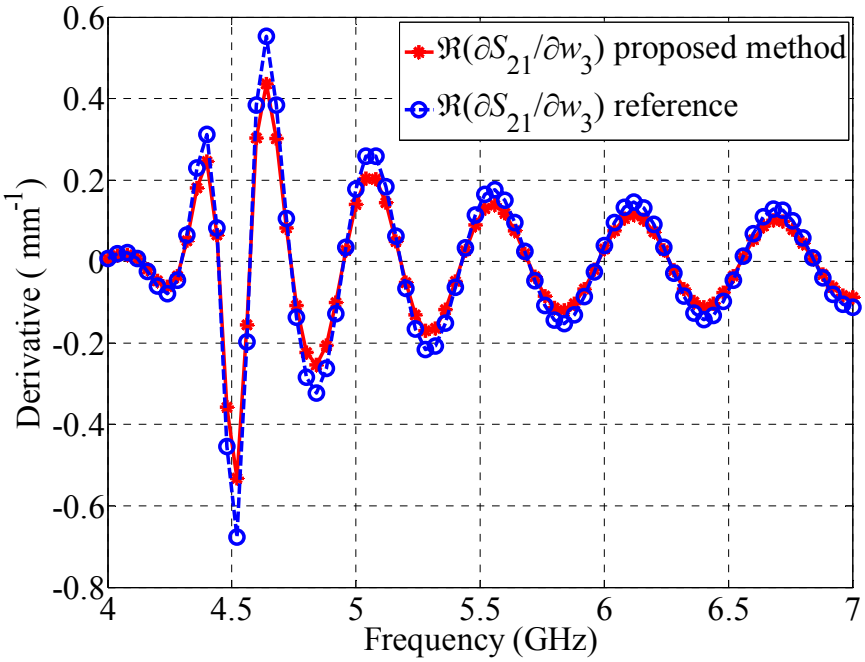

Figure 3.21 Sensitivity curves for the real part of S_{21} with respect to w_3 in the H-plane filter example.

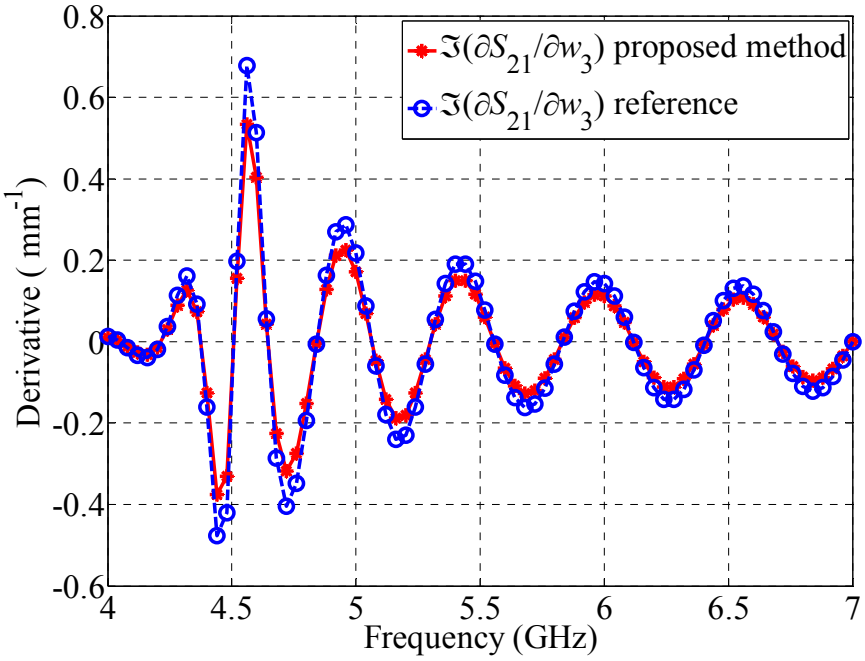

Figure 3.22 Sensitivity curves for the imaginary part of S_{21} with respect to w_3 in the H-plane filter example.

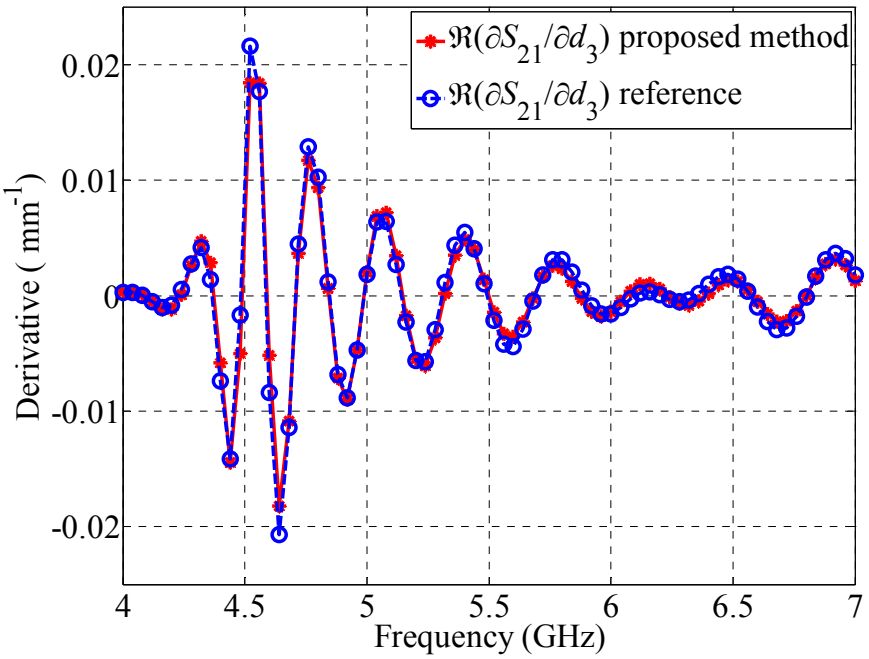

Figure 3.23 Sensitivity curves for the real part of S_{21} with respect to d_3 in the H-plane filter example.

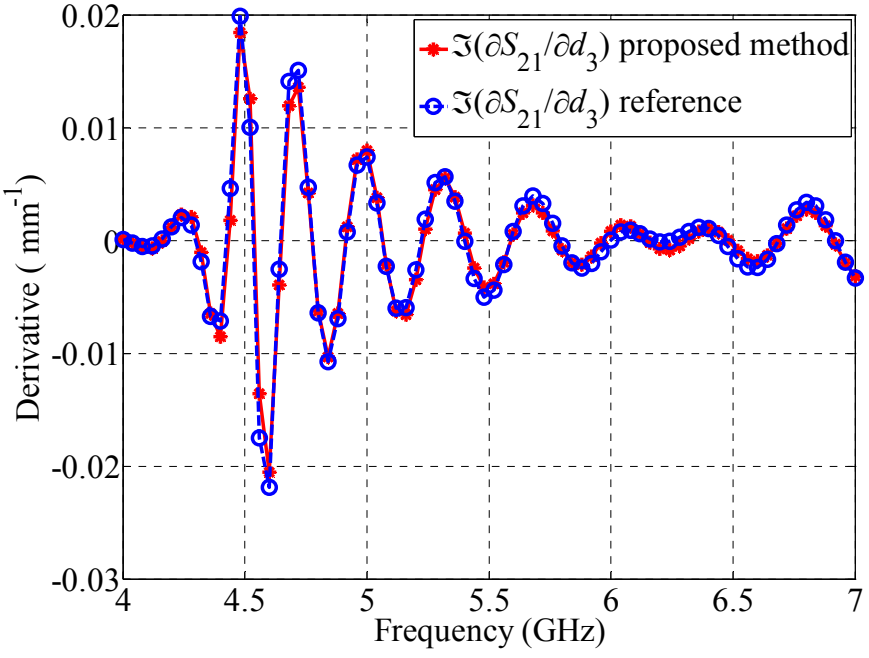

Figure 3.24 Sensitivity curves for the imaginary part of S_{21} with respect to d_3 in the H-plane filter example.

3.5.2 Two-section Impedance Transformer

The second example is a waveguide two-section impedance transformer [10] which is shown in Figure 3.3. Here the metal is set as PEC.

The waveguide is excited using wave-ports with the dominant TE_{10} mode. The mesh convergence error for the *S*-parameters is set as 0.005.

The proposed method is used to calculate the derivatives of S_{11} and S_{21} with respect to two shape parameters: the width w and the height h of the first transformer section in the frequency range from 5 to 7 GHz. Very fine mesh is imposed on the perturbation faces for the respective parameters, w_1 and h_1, to make the field solutions as accurate as possible.

Figure 3.25 to Figure 3.28 show the derivatives of the S_{11} with respect to parameters w_1 and h_1 calculated in the Field Calculator of HFSS. The same derivatives are plotted in Figure 3.29 to Figure 3.32 in which the integrations are done in the MATLAB®. Here, the agreement between the derivatives calculated either in the Field Calculator of HFSS or in the MATLAB®, and the reference curves is very good.

The derivatives of S_{21} with respect to parameters w_1 and h_1 calculated in the MATLAB®, are shown in Figure 3.33 to Figure 3.36. The results for parameter h_1 shows some discrepancy with the reference sensitivity curves which should be the effect of numerical imperfect field sampling and integration.

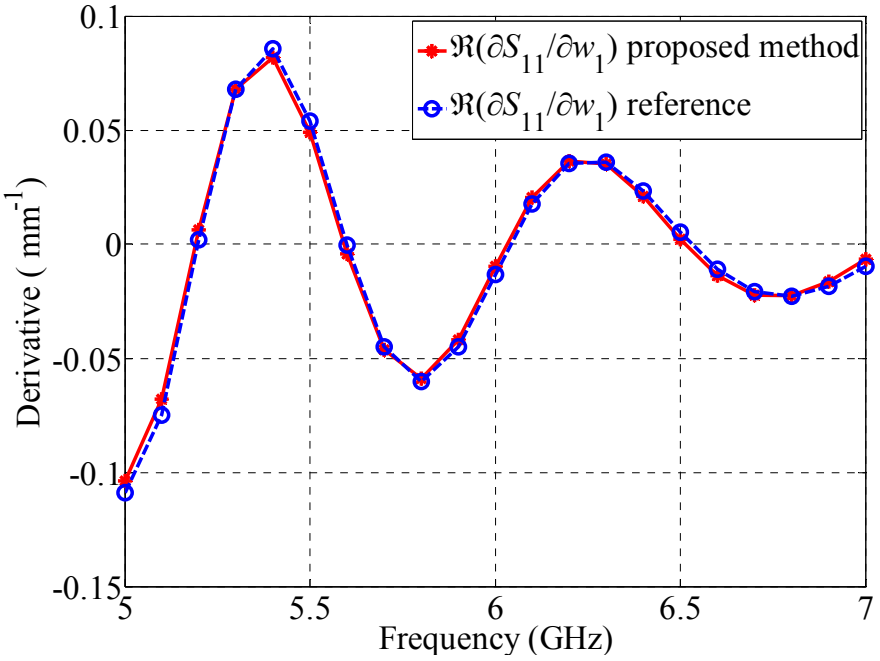

Figure 3.25 Sensitivity curves for the real part of S_{11} with respect to w_1 in the impedance-transformer example, calculated in the Field Calculator of HFSS.

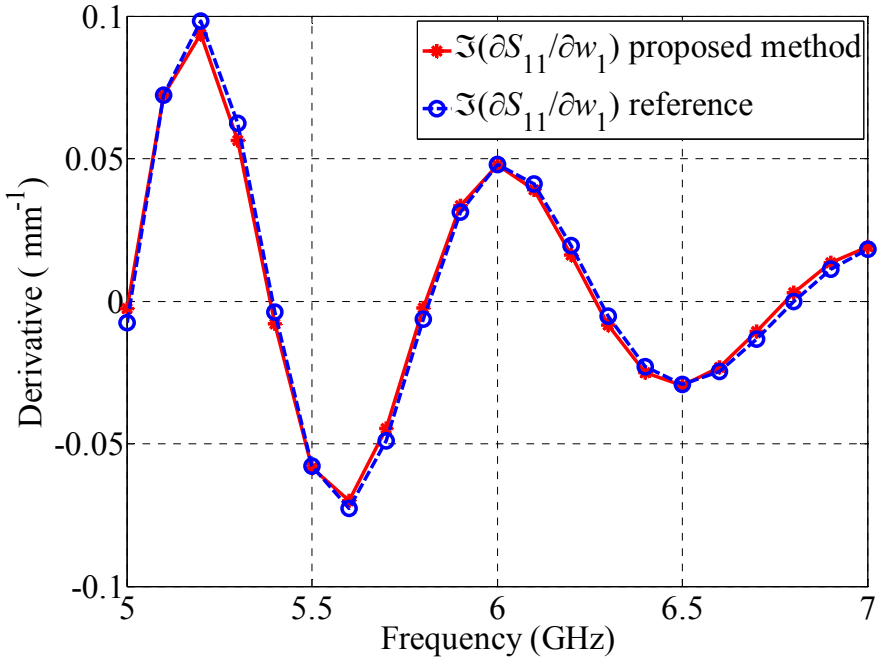

Figure 3.26 Sensitivity curves for the imaginary part of S_{11} with respect to w_1 in the impedance-transformer example, calculated in the Field Calculator of HFSS.

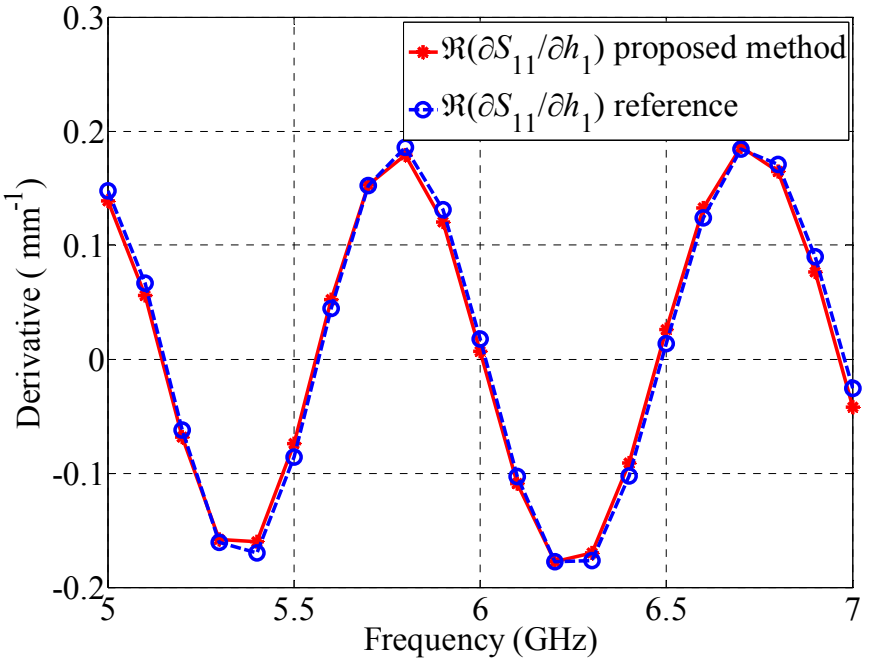

Figure 3.27 Sensitivity curves for the real part of S_{11} with respect to h_1 in the impedance-transformer example, calculated in the Field Calculator of HFSS.

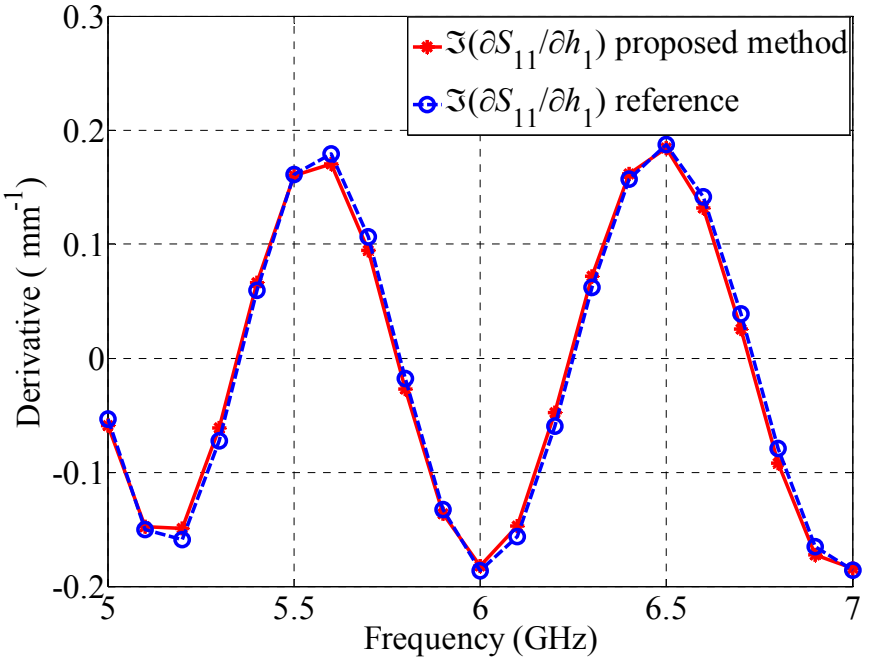

Figure 3.28 Sensitivity curves for the imaginary part of S_{11} with respect to h_1 in the impedance-transformer example, calculated in the Field Calculator of HFSS.

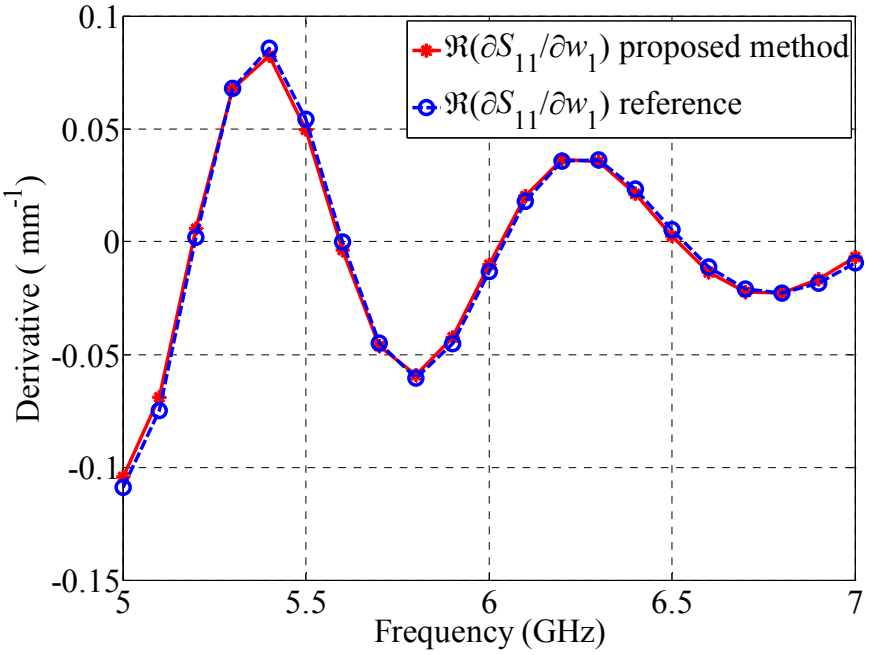

Figure 3.29 Sensitivity curves for the real part of S_{11} with respect to w_1 in the impedance-transformer example.

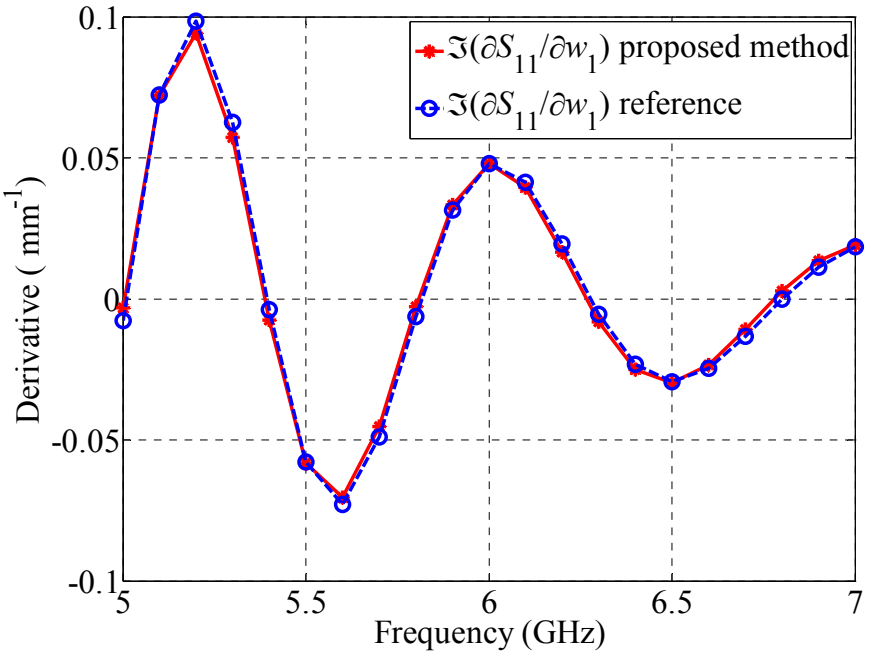

Figure 3.30 Sensitivity curves for the imaginary part of S_{11} with respect to w_1 in the impedance-transformer example.

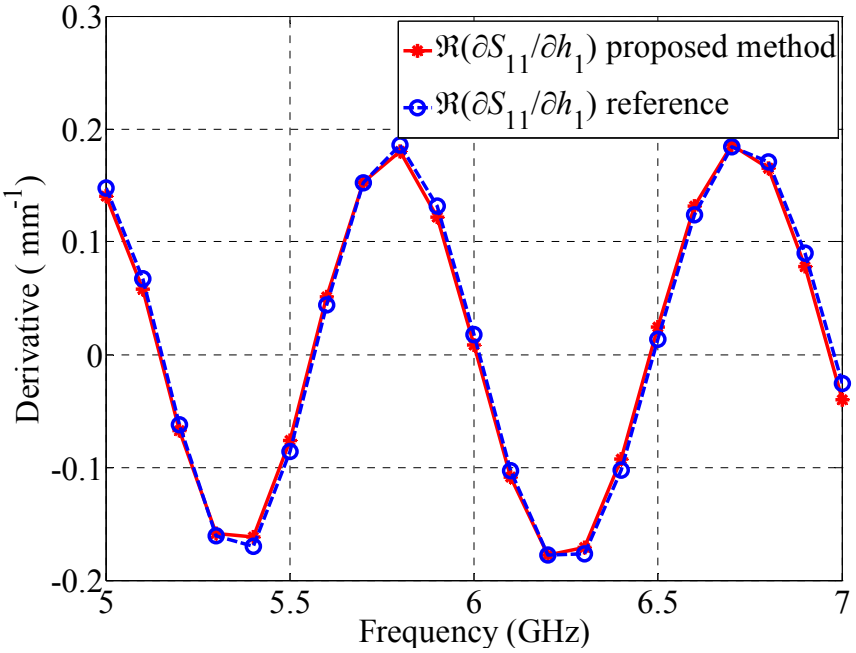

Figure 3.31 Sensitivity curves for the real part of S_{11} with respect to h_1 in the impedance-transformer example.

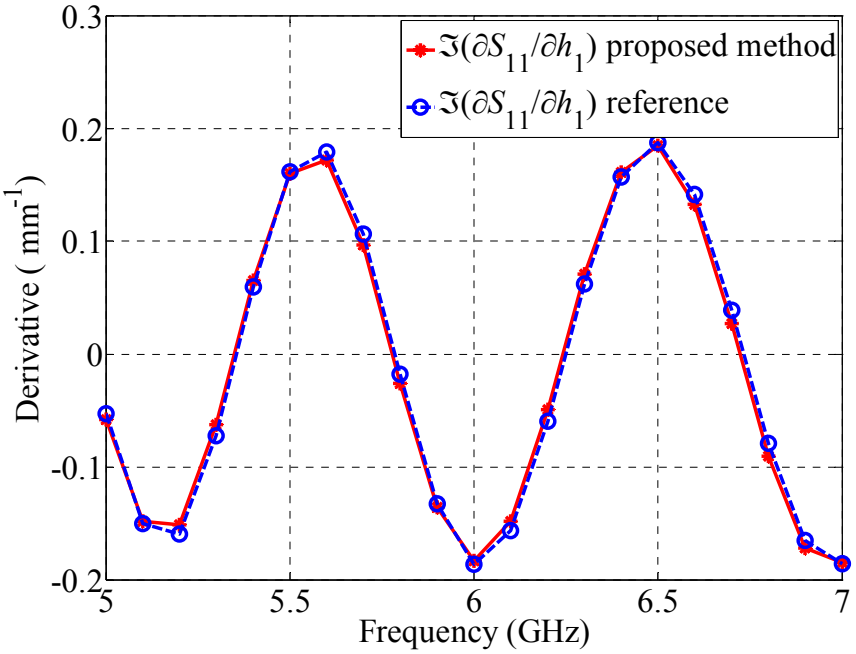

Figure 3.32 Sensitivity curves for the imaginary part of S_{11} with respect to h_1 in the impedance-transformer example.

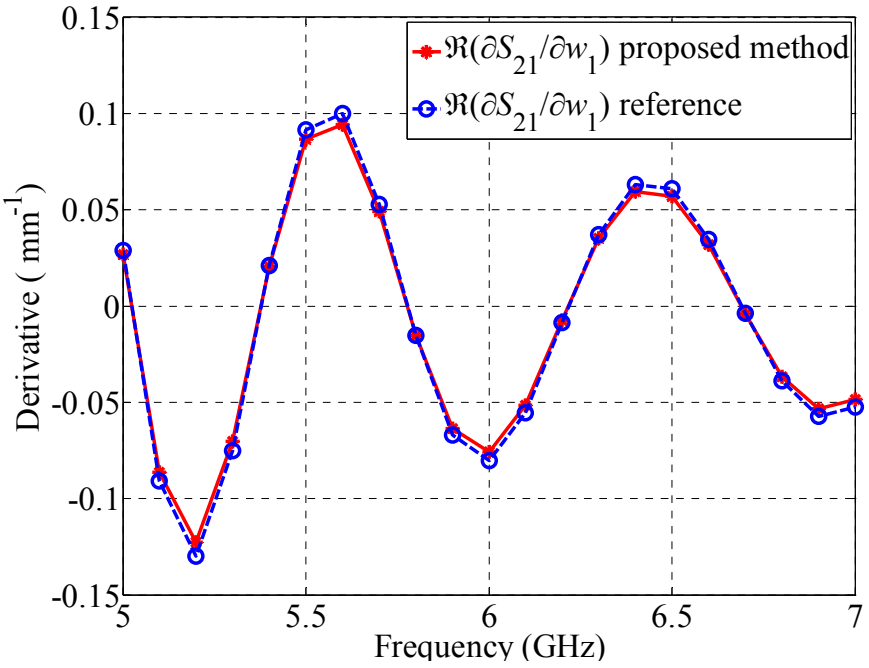

Figure 3.33 Sensitivity curves for the real part of S_{21} with respect to w_1 in the impedance-transformer example.

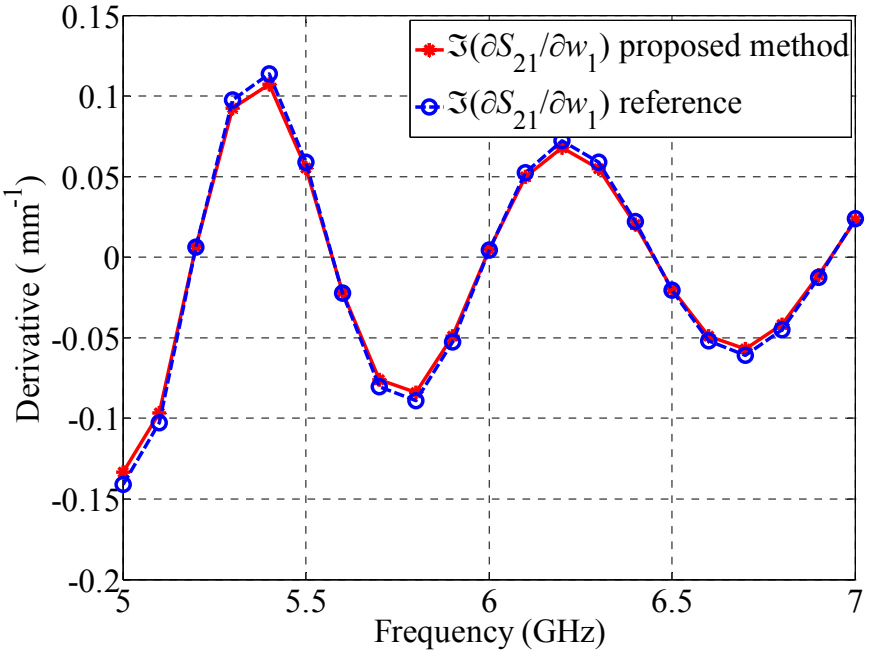

Figure 3.34 Sensitivity curves for the imaginary part of S_{21} with respect to w_1 in the impedance-transformer example.

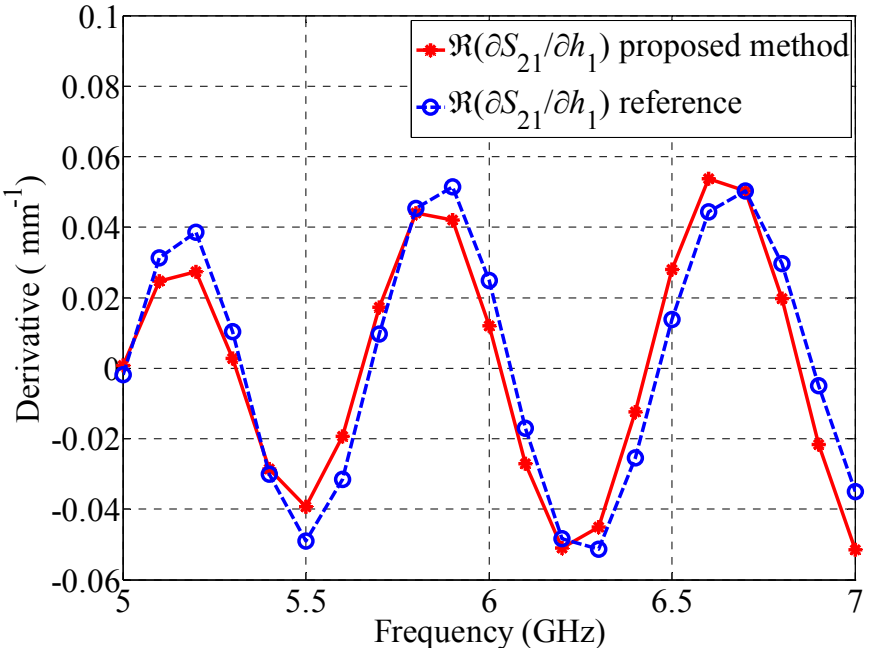

Figure 3.35 Sensitivity curves for the real part of S_{21} with respect to h_1 in the impedance-transformer example.

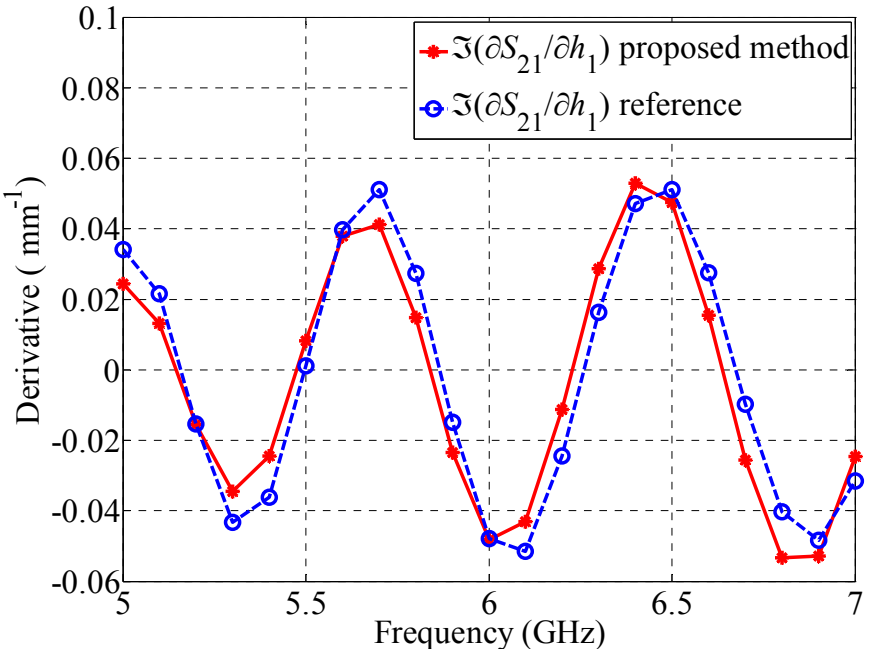

Figure 3.36 Sensitivity curves for the imaginary part of S_{21} with respect to h_1 in the impedance-transformer example.

References

[1] Ansoft HFSS ver. 13, Ansoft Corporation, 225 West Station Square Drive, Suite 200, Pittsburgh, PA 15219, USA, 2011, www.ansoft.com.

[2] CST Studio Suite ver. 2010.06, Computer Simulation Technology, Bad Nauheimer Str. 19, 64289 Darmstadt, Germany, www.cst.com.

[3] N. K. Nikolova, X. Zhu, Y. Song, A. Hasib, and M. H. Bakr, "*S*-parameter sensitivities for electromagnetic optimization based on volume field solutions," *IEEE Trans. Microw. Theory Tech.*, vol. 57, pp. 1526–1538, Jun. 2009.

[4] H. Akel and J.P. Webb, "Design sensitivities for scattering-matrix calculation with tetrahedral edge elements," *IEEE Trans. Magnetics*, vol. 36, pp. 1043–1046, Jul. 2000.

[5] L. Vardapetyan, J. Manges, and Z. Cendes, "Sensitivity analysis of *S*-parameters including port variations using transfinite element method," *IEEE MTT-S Int. Microwave Symp. Dig.*, pp. 527–530, Jun. 2008.

[6] N. K. Nikolova, H. W. Tam, and M. H. Bakr, "Sensitivity analysis with the FDTD method on structured grids," *IEEE Trans. Microw. Theory Tech.*, vol. 52, pp. 1207–1216, Apr. 2004.

[7] Y. S. Chung, C. Cheon, I. H. Park, and S. Y. Hahn, "Optimal shape design of microwave device using FDTD and design sensitivity analysis," *IEEE Trans. Microw. Theory Tech.*, vol. 48, pp. 2289–2296, Dec. 2000.

[8] Matlab, ver. 7.1, The MathWorks Inc., Natick, MA, USA, 2010, www.mathworks.com.

[9] G. Matthaei, L. Young, and E. M. T. Jones, *Microwave Filters, Impedance-Matching Networks, and Coupling Structures*. Norwood, MA: Artech House, 1980, pp. 545–547.

[10] L. Young, "Inhomogeneous quarter-wave transformers of two sections," *IRE Trans. Microwave Theory Tech.*, vol. MTT-8, pp. 645–649, Nov. 1960.

[11] N. K. Nikolova, J. Zhu, D. Li, M. Bakr, and J. W. Bandler, "Sensitivities analysis of network parameters with electromagnetic frequency domain simulators," *IEEE Trans. Microwave Theory Tech.*, vol. 54, pp. 670-681, Feb. 2006.

[12] M. S. Dadash, K. Moussakhani, N. K. Nikolova, and L. Liu, " New method for exact self-adjoint sensitivity analysis of metallic shapes, presented at the *IEEE MTT-S Int. Microwave Symp.*, Jun. 2011.

Chapter 4

SELF-ADJOINT SENSITIVITY ANALYSIS OF INFINITESIMALLY THIN METALLIC STRUCTURES

4.1 Introduction

Metallic sheet is a special case of the volumetric metallic structure which is infinitesimally thin. The shape has two dimensions, but the sensitivity calculations with respect to the designable parameters involve field solution in three dimensions. Similarly to the case of volumetric metallic structures, a theory should be developed for these kind of parameters.

We start from the same formulation obtained for the volumetric metallic structures and then with the use of EM field singularity at the edge of metallic sheet, the new formulation would be developed.

The singular behaviour of EM fields at the edge of metallic sheet is explained in section 4.2. In section 4.3, the theory for sensitivity analysis of infinitesimally thin metallic shape parameters will be explained. The final

formulation is validated in section 4.4 in the cylindrical waveguide filter example [1].

4.2 Field Singularity at the Edge of Metallic Sheet [2], [3]

To understand the behaviour of the electromagnetic wave at, or around, the edge of a metallic sheet, the scattering problem of a two-dimensional (2-D) conducting wedge should be investigated first, as shown in Figure 4.1. The canonical problem of a 2-D conducting wedge can be used to represent locally (near the edge) the scattering of a metallic sheet by reducing the wedge angle, 2α, to zero.

First, the modal solution for the scattering of the two EM polarizations TE_z and TM_z are explained. This solution helps to understand the behaviour of an arbitrary EM field since it is a superposition of these two polarizations.

a) TE_z Polarization

For the TE_z polarization, we can assume that the wedge is illuminated by an electric line source I_e , as shown in Figure 4.1. For the case of a plane wave excitation, this line source is placed very far from the structure which is done by setting ρ' as infinity. The final field solutions in this case can be written as:

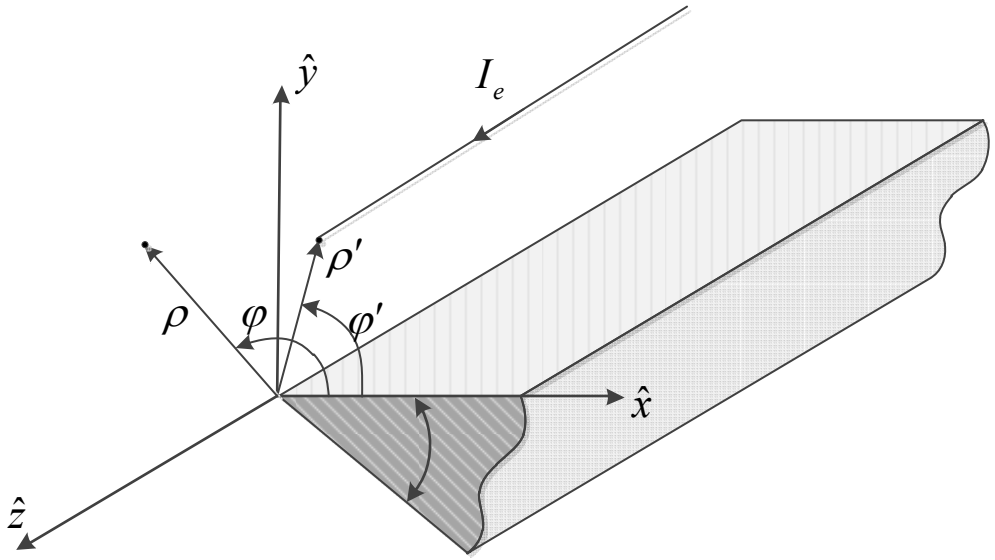

Figure 4.1 A two-dimensional wedge which is illuminated by an electric line source. ρ' and φ' determine the source location while ρ and φ show the observation location. n determines the wedge angle.

$$\mathrm{H}_z = H_0 \sum_{m=0,1,\ldots}^{\infty} j^{\frac{m}{n}} P_m J_{m/n}(\beta\rho)\left[\cos\left(\frac{m}{n}(\psi-\psi')\right)+\cos\left(\frac{m}{n}(\psi+\psi')\right)\right],$$

$$\begin{aligned}\mathrm{E}_\rho &= \frac{1}{j\omega\varepsilon_0}\frac{1}{\rho}\frac{\partial \mathrm{H}_z}{\partial\psi}\\ &= -\frac{H_0}{j\omega\varepsilon_0}\frac{1}{\rho}\sum_{m=0,1,\ldots}^{\infty}\frac{m}{n}j^{\frac{m}{n}}P_m J_{m/n}(\beta\rho)\left[\sin\left(\frac{m}{n}(\psi-\psi')\right)+\sin\left(\frac{m}{n}(\psi+\psi')\right)\right],\end{aligned} \tag{4.1}$$

$$\begin{aligned}\mathrm{E}_\varphi &= \frac{1}{j\omega\varepsilon_0}\frac{1}{\rho}\frac{\partial \mathrm{H}_z}{\partial\rho}\\ &= -\frac{H_0}{j\omega\varepsilon_0}\sum_{m=0,1,\ldots}^{\infty}\frac{m}{n}j^{\frac{m}{n}}P_m\left[-\beta J_{m/n+1}(\beta\rho)+\frac{m}{n}\frac{1}{\rho}J_{m/n}(\beta\rho)\right]\cdot\\ &\quad\left[\cos\left(\frac{m}{n}(\psi-\psi')\right)+\cos\left(\frac{m}{n}(\psi+\psi')\right)\right],\end{aligned}$$

where

$$P_m = \begin{cases} 1, & m = 0 \\ 2, & m \neq 0 \end{cases}, \tag{4.2}$$

β is the propagation constant of the EM wave in vacuum, H_0 is the coefficient, which relates to the excitation source, and $J_p(x)$ is the Bessel function of the first kind of order *p*, which is defined as

$$J_p(x) = \sum_{k=0}^{\infty} \frac{(-1)^k (x/2)^{2k+p}}{k!(k+p)!}. \tag{4.3}$$

Here, we are interested in infinitesimally thin structures, so the wedge angle is set to zero by choosing the value of 2 for *n*. As it can be seen from (4.1) and (4.3), the only field components which are singular with respect to ρ are E_ρ^t, and E_φ^t. This singularity happens for the terms in the summation where $0 < m/n < 1$, i.e., when $n = 2$, the only term which causes singularity is $m = 1$.

Thus, only the terms with $m = 1$ exhibit singularity. This singularity can be written as,

$$\mathrm{E}_\rho \propto \frac{1}{\sqrt{\rho}}, \quad \mathrm{E}_\varphi \propto \frac{1}{\sqrt{\rho}}. \tag{4.4}$$

Note that, in the TE_z polarization, H_z is not singular.

b) TM_z Polarization

Contrary to the TE_z polarization, the wedge in this case is illuminated by a magnetic line source I_m. For a plane wave excitation, the line source could be

placed in the far distance by setting ρ' to infinity. The final field solution for this polarization is

$$\begin{aligned}
\mathrm{E}_z &= E_0 \sum_{m=0,1,\ldots}^{\infty} j^{\frac{m}{n}} J_{m/n}(\beta\rho)\left[\cos\left(\frac{m}{n}(\psi-\psi')\right)-\cos\left(\frac{m}{n}(\psi+\psi')\right)\right], \\
\mathrm{H}_\rho &= \frac{1}{j\omega\mu_0}\frac{1}{\rho}\frac{\partial \mathrm{E}_z}{\partial\psi} \\
&= \frac{E_0}{j\omega\mu_0}\frac{1}{\rho}\sum_{m=0,1,\ldots}^{\infty}\frac{m}{n}j^{\frac{m}{n}}J_{m/n}(\beta\rho)\left[\sin\left(\frac{m}{n}(\psi-\psi')\right)-\sin\left(\frac{m}{n}(\psi+\psi')\right)\right], \\
\mathrm{H}_\varphi &= \frac{1}{j\omega\mu_0}\frac{\partial \mathrm{E}_z}{\partial\rho} \\
&= \frac{E_0}{j\omega\mu_0}\sum_{m=0,1,\ldots}^{\infty} j^{\frac{m}{n}}\left[-\beta J_{m/n+1}(\beta\rho)+\frac{m}{n}\frac{1}{\rho}J_{m/n}(\beta\rho)\right]\cdot \\
&\quad \left[\cos\left(\frac{m}{n}(\psi-\psi')\right)-\cos\left(\frac{m}{n}(\psi+\psi')\right)\right],
\end{aligned} \tag{4.5}$$

where E_0 is the coefficient which relates to the excitation source.

Similarly to the TE$_z$ polarization, only the two field components H_ρ and H_φ have singularity near the edge. They are proportional to $\sqrt{\rho}$:

$$\mathrm{H}_\rho \propto \frac{1}{\sqrt{\rho}}, \quad \mathrm{H}_\varphi \propto \frac{1}{\sqrt{\rho}}. \tag{4.6}$$

4.3 Sensitivity Formulation for Infinitesimally Thin Metallic Structures

The starting point is the sensitivity formula for the volumetric metallic shape parameters (3.46), explained completely in chapter 3. There, we need to perform a surface integration over a perturbation face, which collapses into a line

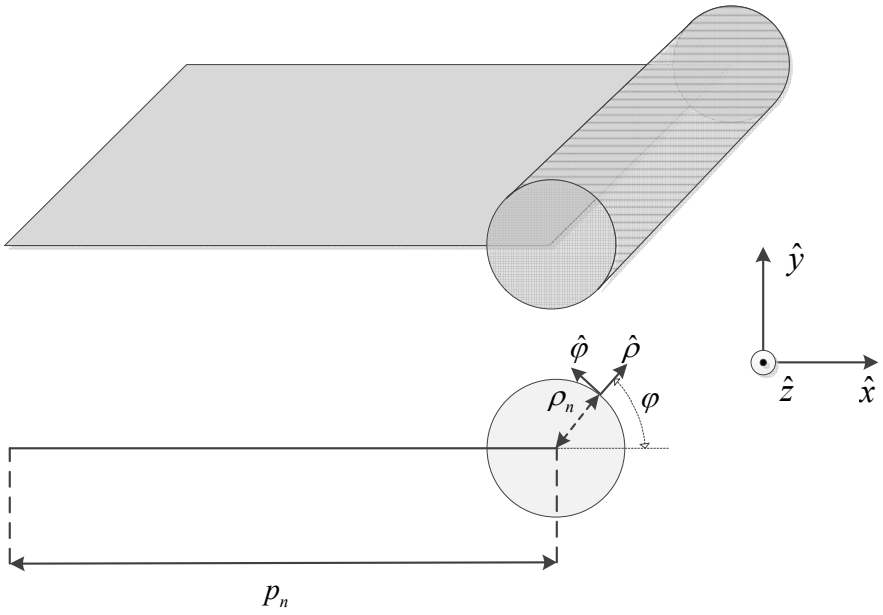

Figure 4.2 The metallic sheet can be assumed to have a metallic cylinder attached to its end. ρ_n determines the radius of the cylinder.

in the case of an infinitesimally thin structure. We can overcome this problem by a simple assumption that a metallic cylinder is connected to the end of the metallic sheet so that its axis coincides with the edge, as shown in Figure 4.2. By reducing the radius of the cylinder to zero, we obtain the infinitesimally thin structure. Thus, we can consider the asymptotic behavior of the field around the cylinder when its radius tends to zero.

Furthermore, we can relate the parameter of interest form p_n to ρ_n, the radius of the cylinder. This is true since a very small increase Δ in each of these parameters has the same effect of increasing the length of the metallic sheet by Δ. Now that we are working with ρ_n, we can use the formulation for the volumetric

objects and assume that the tangential components of the **H**-field are in the $\hat{\varphi}$ and $\hat{z}$ directions and the normal component of the **E**-field is in the $\hat{\rho}$ direction.

For the cylinder, the perturbation face is its outer surface S_c. On this surface, the sensitivity formula can be written as

$$\frac{\partial S_{kj}}{\partial \rho_n} = \frac{-j\omega\mu_0}{4} \lim_{\rho_n \to 0} \iint_{S_c} \left[\mu_0 \bar{\mathbf{H}}_{k,\tau} \cdot \bar{\mathbf{H}}_{j,\tau} + \varepsilon_0 \bar{\mathrm{E}}_{k,\rho} \cdot \bar{\mathrm{E}}_{j,\rho} \right] \rho_n d\varphi dz. \tag{4.7}$$

Since $\bar{\mathrm{H}}_z$ does not have singularity with respect to ρ, the limit of its integral on the vanishing surface of S_c is zero. So, only $\bar{\mathrm{H}}_\varphi$ and $\bar{\mathrm{E}}_\rho$ terms remain in (4.7):

$$\frac{\partial S_{kj}}{\partial \rho_n} = \frac{-j\omega\mu_0}{4} \lim_{\rho_n \to 0} \iint_{S_c} \left[\mu_0 \bar{\mathrm{H}}_{k,\varphi} \cdot \bar{\mathrm{H}}_{j,\varphi} + \varepsilon_0 \bar{\mathrm{E}}_{k,\rho} \cdot \bar{\mathrm{E}}_{j,\rho} \right] \rho_n d\varphi dz. \tag{4.8}$$

Using the singularity expressions in (4.4) and (4.6), the field solution on the metallic cylinder (at $\rho = \rho_n$), can be related to the field sampled a distance *d* away from the surface of the cylinder in the air (at $\rho = \rho_n + \Delta$), as shown in Figure 4.3:

$$\begin{aligned} \bar{\mathrm{H}}_\varphi(\rho_n) &= \frac{\bar{\mathrm{H}}_\varphi(\rho_n + d)}{\sqrt{\rho_n}} \sqrt{\rho_n + d}, \\ \bar{\mathrm{E}}_\rho(\rho_n) &= \frac{\bar{\mathrm{E}}_\rho(\rho_n + d)}{\sqrt{\rho_n}} \sqrt{\rho_n + d}. \end{aligned} \tag{4.9}$$

Substituting (4.9) in the surface integral in (4.8), we have the following two terms:

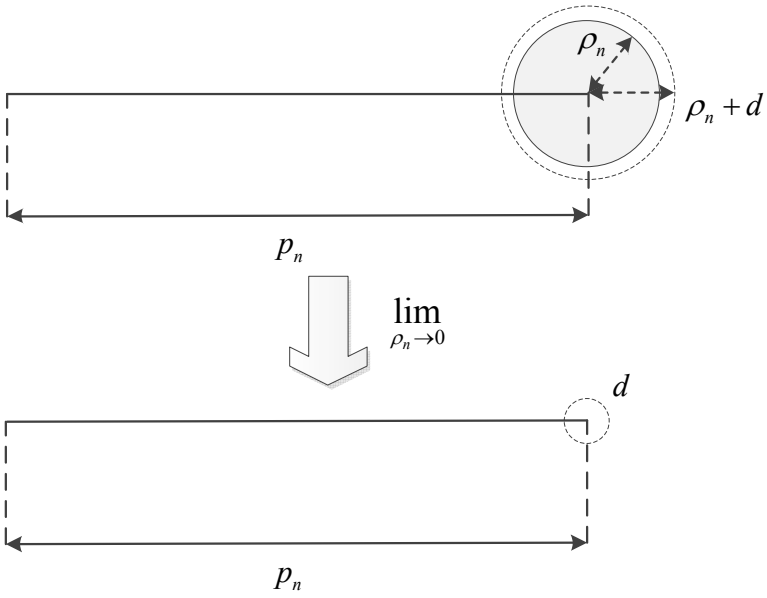

Figure 4.3 The field solutions are sampled a distance d away from the edge.

$$
\begin{aligned}
I_1 &= \lim_{\rho_n \to 0} \iint_{S_c} \bar{\mathrm{H}}_{k,\varphi} \cdot \bar{\mathrm{H}}_{j,\varphi} \rho_n d\varphi dz \\
&= \lim_{\rho_n \to 0} \iint_{S_c} \frac{\bar{\mathrm{H}}_{k,\varphi}\left(\rho_n + d\right)}{\sqrt{\rho_n}} \cdot \frac{\bar{\mathrm{H}}_{j,\varphi}\left(\rho_n + d\right)}{\sqrt{\rho_n}} \left(\rho_n + d\right) \rho_n d\varphi dz \\
&= \lim_{\rho_n \to 0} \iint_{S_c} \left[\bar{\mathrm{H}}_{k,\varphi}\left(\rho_n + d\right) \cdot \bar{\mathrm{H}}_{j,\varphi}\left(\rho_n + d\right) \right] \left(\rho_n + d\right) d\varphi dz \\
&= d \iint_{S_c} \bar{\mathrm{H}}_{k,\varphi}\left(d\right) \cdot \bar{\mathrm{H}}_{j,\varphi}\left(d\right) d\varphi dz
\end{aligned}
\tag{4.10}
$$

and, similarly,

$$
\begin{aligned}
I_2 &= \lim_{\rho_n \to 0} \iint_{S_c} \bar{\mathrm{E}}_{k,\rho} \cdot \bar{\mathrm{E}}_{j,\rho} \rho_n d\varphi dz \\
&= d \iint_{S_c} \bar{\mathrm{E}}_{k,\rho}\left(d\right) \cdot \bar{\mathrm{E}}_{j,\rho}\left(d\right) d\varphi dz.
\end{aligned}
\tag{4.11}
$$

The final sensitivity formula for an infinitesimally thin metallic structures can thus be written as

$$\begin{aligned}\frac{\partial S_{kj}}{\partial \rho_n} &= \frac{-j\omega\mu_0}{4}\left[\mu_0 I_1 + \varepsilon_0 I_2\right] \\ &= \frac{-j\omega\mu_0}{4} d \iint_{S_c} \left[\mu_0 \bar{\mathrm{H}}_{k,\varphi}(d)\cdot \bar{\mathrm{H}}_{j,\varphi}(d) + \varepsilon_0 \bar{\mathrm{E}}_{k,\rho}(d)\cdot \bar{\mathrm{E}}_{j,\rho}(d)\right] d\varphi dz.\end{aligned} \tag{4.12}$$

This formula implies surface integration of the respective field components around the edge of the metallic sheet over a cylinder with radius *d*.

4.4 Implementation Example for Infinitesimally Thin Metallic Structure

The last example is a cylindrical waveguide filter [1][1], which is shown in Figure 4.4. The rectangular cross-sections of ports 1 and 2 are 36.4×10.2 mm^2 and 36×7 mm^2, respectively. The material of the metal is set as PEC.

The waveguide is excited using wave-ports in a way that only the dominant TE_{10} mode. The mesh convergence error for the *S*-parameters is set as 0.005.

The proposed method is used to calculate the derivatives of S_{11} and S_{21} with respect to four shape parameters of the aperture: X_o, Z_o, X_{o2}, and Z_{o2}, in the frequency range from 13 to 14 GHz.

The expression in (4.12) is used to calculate the derivatives of S_{11} with respect to the design parameters. The integration is done around the edge on a cylindrical surface. Since the cylindrical integration is difficult to implement in the Field Calculator of HFSS, all the calculations are done outside in the MATLAB®. Very fine mesh is created around the edges of the middle aperture as

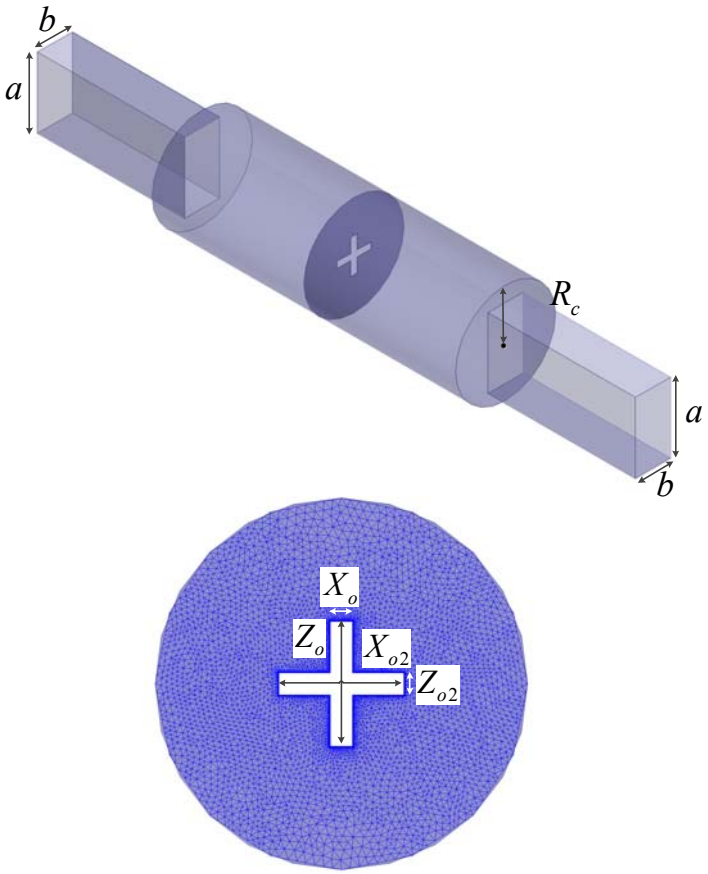

Figure 4.4 The cylindrical waveguide filter. The parameters of interest are X_o, X_{o2}, Z_o, and Z_{o2}. Very fine mesh is created around the edges of the structure.

shown in Figure 4.4. The field components are exported using the Field Calculator export capability.

The derivative of S_{11} with respect to X_o, X_{o2}, Z_o, and Z_{o2} are shown in Figure 4.5 to Figure 4.12. The derivative results calculated with the proposed method are in a very good agreement with the reference sensitivity curves calculated in the HFSS.

Since the structure is symmetric and the place of field sampling is in the equal distance from port 1 and port 2, the derivatives of S_{21} with respect to design

Table 4.1 Nominal design parameter values of the cylindrical waveguide filter.

Parameter	Value (mm)
a	1.905
b	0.9525
R_c	1.3589
X_o	0.1651
X_{o2}	0.9144
Z_o	0.9144
Z_{o2}	0.1651

parameters of interest are the same as the derivatives of S_{11}. Therefore, there is no need to calculate the sensitivity of the S_{21}.

Figure 4.5 to Figure 4.12 show the derivative of S_{11} with respect to design parameters X_o, X_{o2}, Z_o and Z_{o2} respectively. The results show a good agreement between the obtained derivatives using the proposed method and the reference sensitivity curves of the HFSS.

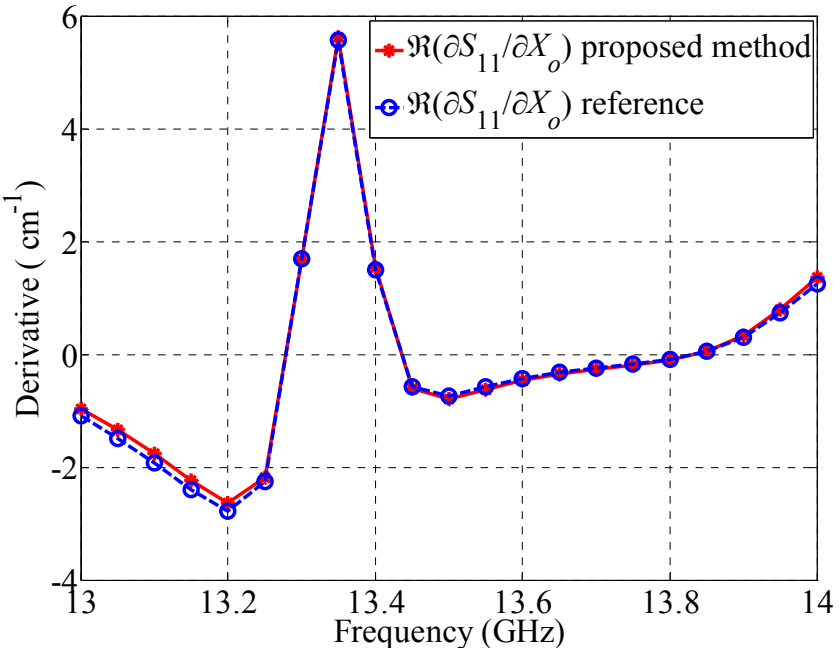

Figure 4.5 Sensitivity curves for the real part of S_{11} with respect to X_o in the cylindrical waveguide filter example.

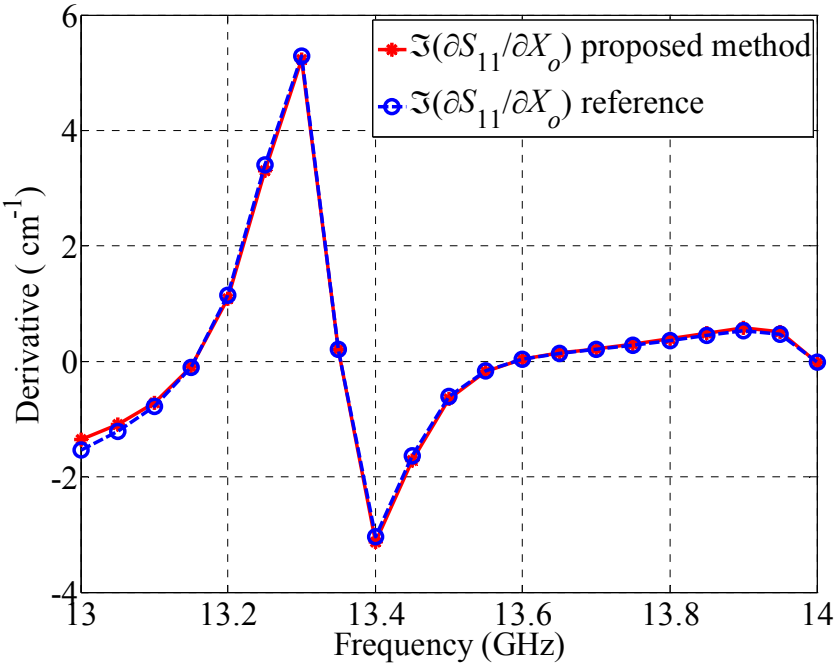

Figure 4.6 Sensitivity curves for the imaginary part of S_{11} with respect to X_o in the cylindrical waveguide filter example.

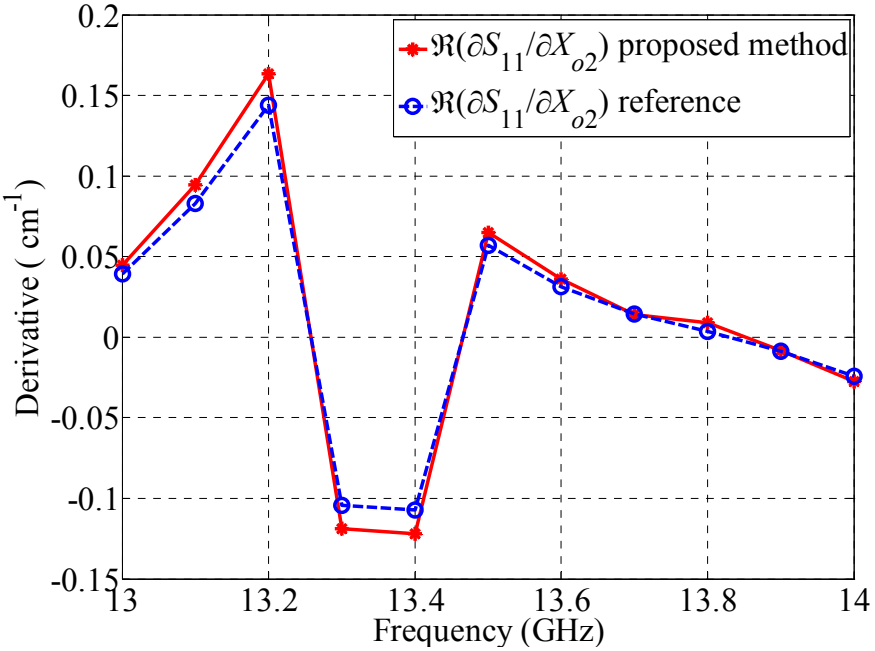

Figure 4.7 Sensitivity curves for the real part of S_{11} with respect to X_{o2} in the cylindrical waveguide filter example.

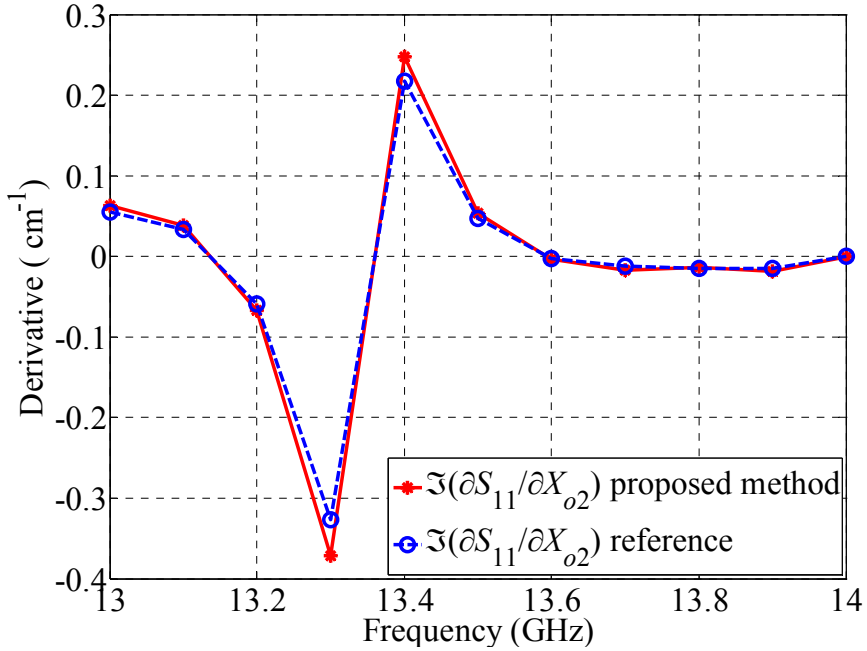

Figure 4.8 Sensitivity curves for the imaginary part of S_{11} with respect to X_{o2} in the cylindrical waveguide filter example.

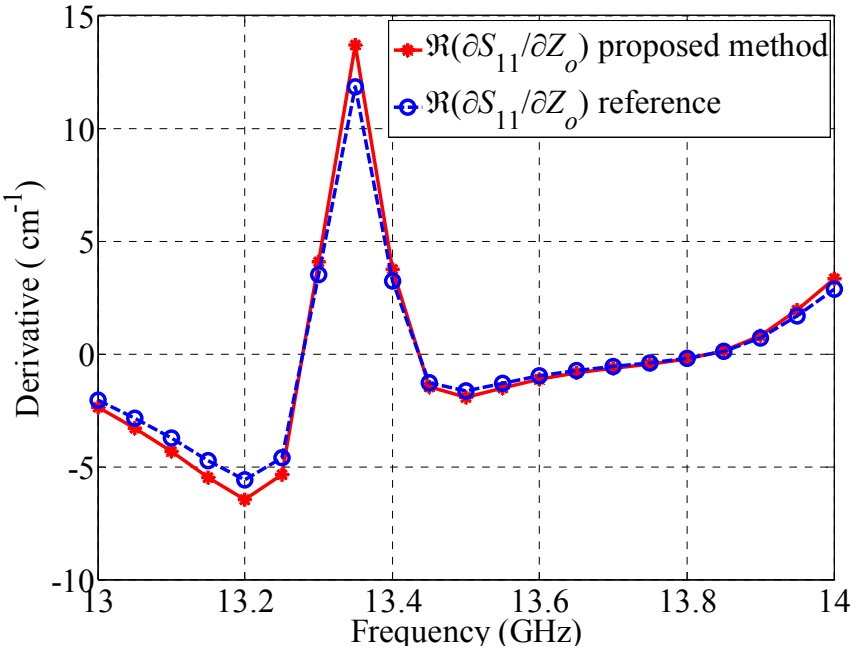

Figure 4.9 Sensitivity curves for the real part of S_{11} with respect to Z_o in the cylindrical waveguide filter example.

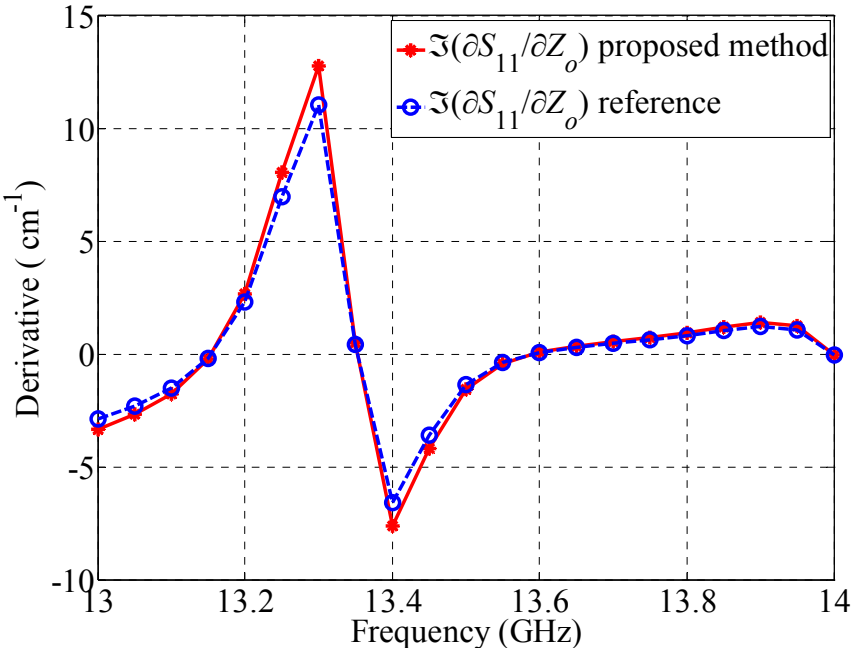

Figure 4.10 Sensitivity curves for the imaginary part of S_{11} with respect to Z_o in the cylindrical waveguide filter example.

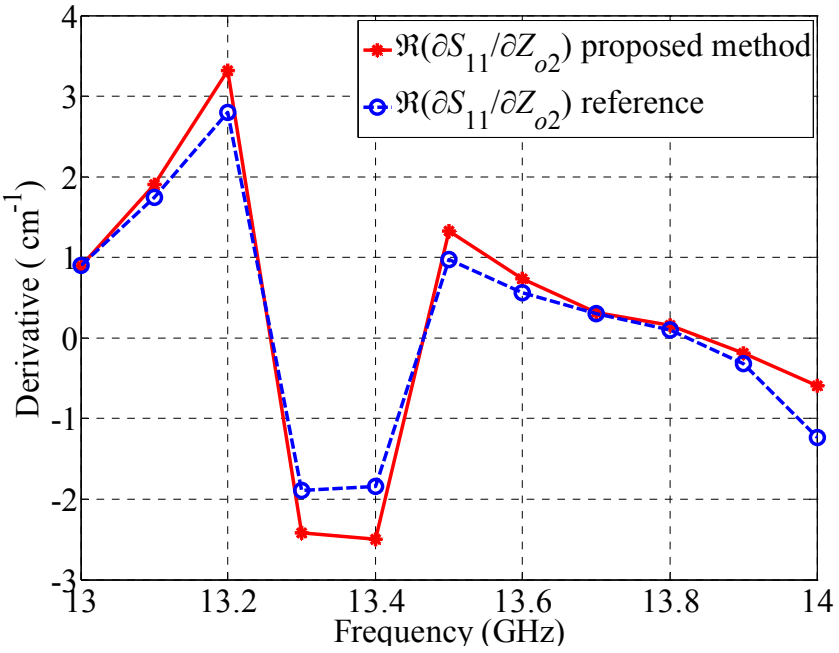

Figure 4.11 Sensitivity curves for the real part of S_{11} with respect to Z_{o2} in the cylindrical waveguide filter example.

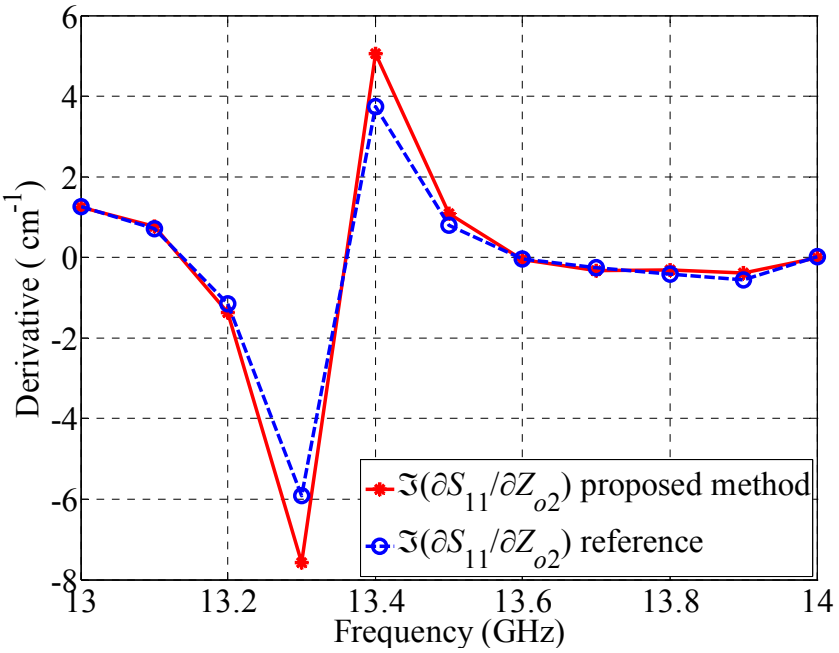

Figure 4.12 Sensitivity curves for the imaginary part of S_{11} with respect to Z_{o2} in the cylindrical waveguide filter example.

References

[1] K. L. Wu and R. H. MacPhie, "A rigorous analysis of a cross waveguide to large circular waveguide junction and its application in waveguide filter design," *IEEE Trans. Microwave Theory Tech.*, vol. 45, pp. 153–157, Jan. 1997.

[2] J. Van Bladel, *Singular Electromagnetic Fields and Sources*, New York: Oxford University Press, 1991.

[3] C. A Balanis, *Advanced Engineering Electromagnetics*. New York: Wiley, 1989.

Chapter 5

CONCLUSION

In this thesis, a new analytical self-adjoint sensitivity analysis (SASA) formulation to compute the *S*-parameter Jacobian for metallic shape parameters is proposed. This method is independent of the numerical full-wave analysis and the respective system matrix. The theory works for the both volumetric and infinitesimally thin metallic shapes. However, the latter one is in the first stage of development and needs further investigation.

The proposed method needs only the field solution at the surface or around the edges of the metallic structure to calculate the gradients of the *S*-parameters with respect to all designable parameters. The advantage of this method over the previous method of FDFD-SASA is the fact that it does not employ any approximations in the field solution of the adjoint problem. It operates as a post-process for commercial simulators based on volumetric partial differential equations (PDE).

This method opens the possibility for exact sensitivity analysis with all

electromagnetic high-frequency simulators whose system matrices are not differentiable with respect to shape parameters, e.g., the FDTD method and the MoM.

First, we briefly explained the methodology of FDFD-SASA. Since, the focus of this thesis is on the metallic shape parameters, the implementation of the FDFD-SASA method for metallic shape parameters is reviewed.

Then, we investigated our new frequency-domain sensitivity analysis approach for metallic shapes. It has the same high efficiency as the SASA but eliminates the requirement to access the system matrix generated by the simulator. The proposed method is validated for three microwave examples including an H-plane waveguide filter, a two-section impedance transformer, and a cylindrical waveguide filter. The field solutions are exported from the EM simulator Ansoft HFSS [1] are used in MATLAB® [2] to calculate the sensitivity information. The calculated derivatives are in a very good agreement with the reference sensitivity curves.

From the experience and knowledge gained in the above work, the following topics for further research are suggested.

1) Improving the theory of the exact sensitivity analysis for infinitesimally thin metallic structures.
2) Developing the theory of the exact sensitivity analysis for dielectric shape parameters.
3) Implementation of the above with various full-wave EM simulators.

References

[1] Ansoft HFSS ver. 13, Ansoft Corporation, 225 West Station Square Drive, Suite 200, Pittsburgh, PA 15219, USA, 2011, www.ansoft.com.

[2] Matlab, ver. 7.1, The MathWorks Inc., Natick, MA, USA, 2010, www.mathworks.com.

COMPLETE REFERENCE LIST

Chapter 1

[1] D. D. G. Cacuci, *Sensitivity & Uncertainty Analysis, Volume 1: Theory*. Boca Raton, FL: Chaman & Hall/CRC, 2003.

[2] A. D. Belegundu and T. R. Chandrupatla, *Optimization Concepts and Applications in Engineering*. Upper Saddle River, NJ: Prentice-Hall, 1999.

[3] E. J. Haug, K. K. Choi, and V. Komkov, *Design Sensitivity Analysis of Structural Systems.* Orlando, FL: Academic, 1986.

[4] S. W. Director and R. A. Roher, "The generalized adjoint network and network sensitivities," *IEEE Trans. Circuit Theory*, vol. CT-16, pp. 318-323, Aug. 1969.

[5] S. W. Director and R. A. Rohrer, "Automated network design—The frequency-domain case," *IEEE Trans. Circuit Theory*, vol. CT-16, pp. 330-337, Aug. 1969.

[6] B. D. H. Tellegen, "A general network theorem with applications," *Philips Res. Rep.*, vol. 7, pp. 259-269, 1952.

[7] P. Penfield, Jr., R. Spence, and S. Duinker, "A generalized form of Tellegen's theorem," *IEEE Trans. Circuit Theory*, vol. CT-17, pp. 302-305, Aug. 1970.

[8] F. H. Branin, Jr., "Network sensitivity and noise analysis simplified," *IEEE Trans. Circuit Theory*, vol. CT-20, pp. 285-288, May 1973.

[9] S. W. Director, " *LU* factorization in network sensitivity computations," *IEEE Trans. Circuit Theory*, vol. CT-18, pp. 14-185 Jan. 1971.

[10] J. W. Bandler, Q. J. Zhang, and R. M. Biernacki, "A unified theory for frequency-domain simulation and sensitivity analysis of linear and nonlinear circuits, *IEEE Trans. Microwave Theory Tech*, vol. 36, pp. 1661-1669, Dec. 1988.

[11] J. W. Bandler and R. E. Seviora, "Wave sensitivities of networks, " *IEEE Trans. Microwave Theory Tech*, vol. 20, pp. 138-147, Feb. 1972.

[12] V. A. Monaco and P. Tiberio, "Computer-aided analysis of microwave circuits," *IEEE Trans. Microwave Theory Tech*, vol. 7, MTT-22, pp. 249-263, Mar. 1974.

[13] N. K. Georgieva, S. Glavic, M. H. Bakr, and J. W. Bandler, "Feasible adjoint sensitivity technique for EM design optimization," *IEEE Trans. Microwave Theory Tech*, vol. 50, pp. 2751-2758, Dec. 2002.

[14] M. H. Bakr and N. K. Nikolova, "An adjoint variable method for time domain TLM with wide-band Johns matrix boundaries," *IEEE Trans. Microwave Theory Tech.,* vol. 52, pp. 678-685, Feb. 2004.

[15] N. K. Nikolova, H. W. Tam, and M. H. Bakr, "Sensitivity analysis with the FDTD method on structured grids," *IEEE Trans. Microwave Theory Tech.,* vol. 52, pp. 1207-1216, Apr. 2004.

[16] M. H. Bakr and N. K. Nikolova, "An adjoint variable method for frequency domain TLM problems with conducting boundaries," *IEEE Microwave and Wireless Components Letters*, vol. 13, pp. 408-410, Sep. 2003.

[17] S. M. Ali, N. K. Nikolova, and M. H. Bakr, "Central adjoint variable method for sensitivity analysis with structured grid electromagnetic solvers," *IEEE Trans. Magnetics*, vol. 40, pp. 1969-1971, Jul. 2004.

[18] N. K. Nikolova, J. Zhu, D. Li, M. Bakr, and J. Bandler, "Sensitivities analysis of network parameters with electromagnetic frequency domain simulators," *IEEE Trans. Microwave Theory Tech*., vol. 54, pp. 670-681, Feb. 2006.

[19] R. Safian, N. K. Nikolova, M. H. Bakr, and J.W. Bandler, "Feasible adjoint sensitivity technique for EM design exploiting Broyden's update," in *IEEE MTT-S Int. Microwave Symp. Dig.*, Philadelphia, PA, Jun. 2003, pp. 299-302.

[20] H. Akel and J. P. Webb, "Design sensitivities for scattering-matrix calculation with tetrahedral edge elements," *IEEE Trans. Magnetics*, vol. 36, pp. 1043-1046, Jul. 2000.

[21] J. P. Webb, "Design sensitivities using high-order tetrahedral vector

elements," *IEEE. Trans. Magn*., vol 37, pp. 3600-3603, Sep. 2001.

[22] L. Vardapetyan, J. Manges, and Z. Cendes, "Sensitivity analysis of *S*-parameters including port variations using transfinite element method," *IEEE MTT-S Int. Microwave Symp. Dig.*, pp. 527-530, Jun. 2008.

[23] M. K. Bakr, N. K. Nikolova, and P. A. W. Basl, "Self-adjoint *S*-parameter sensitivities for lossless homogeneous TLM problems, *Int. J. Numer. Modeling*, vol. 18, no. 6, pp. 441–455, Nov. 2005.

[24] N. K. Nikolova, Ying Li, Yan Li, and M. H. Bakr, "Sensitivity analysis of scattering parameters with electromagnetic time-domain simulators," *IEEE Trans. Microwave Theory Tech.*, vol. 54, pp. 1589-1610, Apr. 2006.

[25] N. K. Nikolova, X. Zhu, Y. Song, A. Hasib, and M. H. Bakr, "*S*-parameter sensitivities for electromagnetic optimization based on volume field solutions," *IEEE Trans. Microwave Theory Tech.*, vol. 57, pp. 1526-1538, Jun. 2009.

[26] X. Zhu, A. Hasib, N.K. Nikolova, and M.H. Bakr, "Efficient electromagnetic optimization using self-adjoint Jacobian computation based on a central-node FDFD method," in *IEEE MTT-S Int. Microw. Symp. Dig.*, Atlanta, GA, Jun. 2008, pp. 979-982.

[27] X. Zhu, A. Hasib, and N. K. Nikolova, "Electromagnetic sensitivity analysis of scattering parameters based on the FDFD method," in *Int. Signals, Syst., Electron. Symp*., Montreal, QC, Canada, Jul.-Aug. 2007, pp. 165-168.

[28] N. K. Nikolova, A. Hasib, and X. Zhu, "Independent sensitivity solver based on the frequency domain finite difference method," *The 24th Int. Review of Progress in Applied Computational Electromagnetics (ACES 2008)*, pp. 1024-1029, Mar.-Apr. 2008.

[29] A. Hasib, *Sensitivity Analysis for Design Optimization of Metallic Microwave Structures with the Finite-difference Frequency-domain Method*, M.A.Sc., Dept. Elect. Comput. Eng., McMaster Univ, Hamilton, ON, Canada, 2008.

[30] X. Zhu, *Frequency-domain Self-adjoint S-parameter Sensitivity Analysis for Microwave Design*, M.A.Sc thesis, Dept. Elect. Comput. Eng., McMaster Univ., Hamilton, ON, Canada, 2008.

[31] P. A. W. Basl, M. H. Bakr, N. K. Nikolova, "Efficient TLM sensitivity analysis exploiting rubber cells, in *IEEE MTT-S Int. Microwave Symp. Dig.*, Jun. 2008, pp. 53-56.

[32] D. Huilian, S. Poman, and W. 1. R. Hoefer, "Cells with tensor properties for conformal TLM boundary modeling, *2006 IEEE MTT-S International Microwave Symposium*, San Francisco, CA, USA, 2006, vol. 11, pp. 157-160.

[33] Y. S. Chung, C. Cheon, I. H. Park, and S. Y. Hahn, "Optimal design method for microwave device using time domain method and design sensitivity analysis—Part I: FETD case," *IEEE Trans. Magn.*, vol. 37, pp. 3289-3293, Sep. 2001.

[34] , "Optimal design method for microwave device using time domain method and design sensitivity analysis—Part II: FDTD case," *IEEE Trans. Magn.*, vol. 37, pp. 3255-3259, Sep. 2001.

[35] M. S. Dadash, K. Moussakhani, N. K. Nikolova, and L. Liu, " New method for exact self-adjoint sensitivity analysis of metallic shapes, presented at the *IEEE MTT-S Int. Microwave Symp.*, Jun. 2011.

[36] S. Amari, "Sensitivity analysis of coupled resonator filters," *IEEE Trans. Circuits Syst. II*, vol. 47, pp. 1017-1022, Oct. 2000.

[37] P. Harscher, S. Amari, and R. Vahldieck, "A fast finite-element-based field optimizer using analytically alculated gradients," *IEEE Trans. Microwave Theory Tech.*, vol. 50, pp. 433-439, Feb. 2002.

[38] Ansoft HFSS ver. 12.1, Ansoft Corporation, 225 West Station Square Drive, Suite 200, Pittsburgh, PA 15219, USA, 2010, www.ansoft.com.

[39] Ansoft HFSS ver. 13, Ansoft Corporation, 225 West Station Square Drive, Suite 200, Pittsburgh, PA 15219, USA, 2011, www.ansoft.com.

[40] CST Studio Suite ver. 2010.06, Computer Simulation Technology, Bad Nauheimer Str. 19, 64289 Darmstadt, Germany, www.cst.com.

[41] Matlab, ver. 7.1, The MathWorks Inc., USA, 2010, www.mathworks.com.

Chapter 2

[1] D. G. Cacuci, *Sensitivity & Uncertainty Analysis, Volume 1: Theory*. Boca Raton, FL: Chaman & Hall/CRC, 2003.

[2] A. D. Belegundu and T. R. Chandrupatla, *Optimization Concepts and Applications in Engineering*. Upper Saddle River, NJ: Prentice-Hall, 1999.

[3] E. J. Haug, K. K. Choi, and V. Komkov, *Design Sensitivity Analysis of Structural Systems.* Orlando, FL: Academic, 1986.

[4] M. H. Bakr and N. K. Nikolova, "An adjoint variable method for time domain TLM with wide-band Johns matrix boundaries," *IEEE Trans. Microwave Theory Tech.,* vol. 52, pp. 678-685, Feb. 2004.

[5] N. K. Nikolova, H. W. Tam, and M. H. Bakr, "Sensitivity analysis with the FDTD method on structured grids," *IEEE Trans. Microwave Theory Tech.,* vol. 52, pp. 1207-1216, Apr. 2004.

[6] M. H. Bakr and N. K. Nikolova, "An adjoint variable method for frequency domain TLM problems with conducting boundaries," *IEEE Microwave and Wireless Components Letters*, vol. 13, pp. 408-410, Sep. 2003.

[7] S. M. Ali, N. K. Nikolova, and M. H. Bakr, "Central adjoint variable method for sensitivity analysis with structured grid electromagnetic solvers," *IEEE Trans. Magnetics,* vol. 40, pp. 1969-1971, Jul. 2004.

[8] N. K. Nikolova, J. Zhu, D. Li, M. Bakr, and J. W. Bandler, "Sensitivities analysis of network parameters with electromagnetic frequency domain simulators," *IEEE Trans. Microwave Theory Tech.*, vol. 54, pp. 670-681, Feb. 2006.

[9] M. K. Bakr, N. K. Nikolova, and P. A. W. Basl, "Self-adjoint *S*-parameter sensitivities for lossless homogeneous TLM problems, *Int. J. Numer. Modeling*, vol. 18, no. 6, pp. 441–455, Nov. 2005.

[10] N. K. Nikolova, Ying Li, Yan Li, and M. H. Bakr, "Sensitivity analysis of scattering parameters with electromagnetic time-domain simulators," *IEEE Trans. Microwave Theory Tech.*, vol. 54, pp. 1589-1610, Apr. 2006.

[11] N. K. Nikolova, X. Zhu, Y. Song, A. Hasib, and M. H. Bakr, "*S*-parameter sensitivities for electromagnetic optimization based on volume field solutions," *IEEE Trans. Microwave Theory Tech.*, vol. 57, pp. 1526-1538, Jun. 2009.

[12] X. Zhu, A. Hasib, N.K. Nikolova, and M. H. Bakr, "Efficient electromagnetic optimization using self-adjoint Jacobian computation based on a central-node FDFD method," in *IEEE MTT-S Int. Microw. Symp. Dig.*, Atlanta, GA, Jun. 2008, pp. 979-982.

[13] X. Zhu, A. Hasib, and N. K. Nikolova, "Electromagnetic sensitivity analysis of scattering parameters based on the FDFD method," in *Int. Signals, Syst., Electron. Symp.*, Montreal, QC, Canada, Jul.-Aug. 2007, pp. 165-168.

[14] N. K. Nikolova, A. Hasib, and X. Zhu, "Independent sensitivity solver based on the frequency domain finite difference method," *The 24th Int. Review of Progress in Applied Computational Electromagnetics (ACES 2008)*, pp. 1024-1029, Mar.-Apr. 2008.

[15] A. Hasib, *Sensitivity Analysis for Design Optimization of Metallic Microwave Structures with the Finite-difference Frequency-domain Method*, M.A.Sc., Dept. Elect. Comput. Eng., McMaster Univ, Hamilton, ON, Canada, 2008.

[16] X. Zhu, *Frequency-domain Self-adjoint S-parameter Sensitivity Analysis for Microwave Design*, M.A.Sc thesis, Dept. Elect. Comput. Eng., McMaster Univ., Hamilton, ON, Canada, 2008.

[17] M. Salazar-Palma, T. K. Sarkar, L.-E. García-Castillo, T. Roy, and A. Djordjevic, *Iterative and Self-Adaptive Finite-Elements in Electro-magnetic Modeling*. Norwood, MA: Artech House, 1998, pp. 462–463, 465–466.

[18] M. H. Bakr and N. K. Nikolova, "An adjoint variable method for time domain TLM with fixed structured grids," *IEEE Trans. Microwave Theory Tech.*, vol. 52, pp. 554-559, Feb. 2004.

Chapter 3

[1] Ansoft HFSS ver. 13, Ansoft Corporation, 225 West Station Square Drive, Suite 200, Pittsburgh, PA 15219, USA, 2011, www.ansoft.com.

[2] CST Studio Suite ver. 2010.06, Computer Simulation Technology, Bad Nauheimer Str. 19, 64289 Darmstadt, Germany, www.cst.com.

[3] N. K. Nikolova, X. Zhu, Y. Song, A. Hasib, and M. H. Bakr, "*S*-parameter sensitivities for electromagnetic optimization based on volume field

solutions," *IEEE Trans. Microw. Theory Tech.*, vol. 57, pp. 1526–1538, Jun. 2009.

[4] H. Akel and J.P. Webb, "Design sensitivities for scattering-matrix calculation with tetrahedral edge elements," *IEEE Trans. Magnetics*, vol. 36, pp. 1043–1046, Jul. 2000.

[5] L. Vardapetyan, J. Manges, and Z. Cendes, "Sensitivity analysis of *S*-parameters including port variations using transfinite element method," *IEEE MTT-S Int. Microwave Symp. Dig.*, pp. 527–530, Jun. 2008.

[6] N. K. Nikolova, H. W. Tam, and M. H. Bakr, "Sensitivity analysis with the FDTD method on structured grids," *IEEE Trans. Microw. Theory Tech.*, vol. 52, pp. 1207–1216, Apr. 2004.

[7] Y. S. Chung, C. Cheon, I. H. Park, and S. Y. Hahn, "Optimal shape design of microwave device using FDTD and design sensitivity analysis," *IEEE Trans. Microw. Theory Tech.*, vol. 48, pp. 2289–2296, Dec. 2000.

[8] Matlab, ver. 7.1, The MathWorks Inc., Natick, MA, USA, 2010, www.mathworks.com.

[9] G. Matthaei, L. Young, and E. M. T. Jones, *Microwave Filters, Impedance-Matching Networks, and Coupling Structures*. Norwood, MA: Artech House, 1980, pp. 545–547.

[10] L. Young, "Inhomogeneous quarter-wave transformers of two sections," *IRE Trans. Microwave Theory Tech.*, vol. MTT-8, pp. 645–649, Nov. 1960.

[11] N. K. Nikolova, J. Zhu, D. Li, M. Bakr, and J. W. Bandler, "Sensitivities analysis of network parameters with electromagnetic frequency domain simulators," *IEEE Trans. Microwave Theory Tech.*, vol. 54, pp. 670-681, Feb. 2006.

[12] M. S. Dadash, K. Moussakhani, N. K. Nikolova, and L. Liu, " New method for exact self-adjoint sensitivity analysis of metallic shapes, presented at the *IEEE MTT-S Int. Microwave Symp.*, Jun. 2011.

Chapter 4

[1] K. L. Wu and R. H. MacPhie, "A rigorous analysis of a cross waveguide to large circular waveguide junction and its application in waveguide filter design," *IEEE Trans. Microwave Theory Tech.*, vol. 45, pp. 153–157, Jan. 1997.

[2] J. Van Bladel, *Singular Electromagnetic Fields and Sources*, New York: Oxford University Press, 1991.

[3] C. A Balanis, *Advanced Engineering Electromagnetics*. New York: Wiley, 1989.

Chapter 5

[42] Ansoft HFSS ver. 13, Ansoft Corporation, 225 West Station Square Drive, Suite 200, Pittsburgh, PA 15219, USA, 2011, www.ansoft.com.

[43] Matlab, ver. 7.1, The MathWorks Inc., Natick, MA, USA, 2010, www.mathworks.com.